Alternative alkali resistant deNOx technologies. Appendix-I

PSO Project 7318

Putluru, Siva Sankar Reddy; Jensen, Anker Degn

Publication date:
2011

Document Version
Publisher's PDF, also known as Version of record

Appendix-I

PSO Project 7318

2007-2010

Putluru Siva Sankar Reddy

Anker Degn Jensen

CHEC Research Centre

Department of Chemical and Biochemical Engineering

Technical University of Denmark

Preface

This is the appendix to the final report for the PSO project 7318 “Alternative alkali resistant deNO$_x$ technologies” funded by Energinet.dk, 2007-2010.
We are grateful to the technical staff of the CHEC group, in particular Carsten Nørby, for having always been very helpful.
Haldor Topsøe is gratefully acknowledged for catalysts supply and SEM analysis.

Table of Contents

Abstract

The increased use of biomass as fuel has created some new challenges to establish SCR flue gas treatment technology. One of these challenges comes from biomass complex chemical composition, which includes potassium shown to have a negative impact on the SCR catalyst. Studies have shown that potassium deactivates SCR catalyst and reduces its ability to reduce NO to N_2. An attempt was made to protect the SCR catalyst from alkali poisoning by the imposition of a coating on the catalyst surface. Various compounds were coated on a commercial catalyst supplied by Haldor Topsøe A/S and tested for alkali poisoning resistance. These materials were broadly divided as metal oxides, zeolites and other materials. The coated catalysts were exposed to potassium chloride aerosols at 350°C for 650-1200 h. SCR activity, SEM and EDX measurements were performed to analyze the coated catalysts resistance to potassium poisoning. Coated catalysts (Mg, Mg containing compounds and Zeolites) showed appreciable alkali resistivity compared to the uncoated reference catalyst. Coated catalysts showed high potassium concentration at the surface of the coating and low potassium concentration across the cross section when compared to the uncoated reference catalyst. Thus, it is assumed that the coating layer accumulates the potassium at the surface and prevents to penetrate through the catalyst. The overall assessment is that it is possible to protect an SCR catalyst from potassium poisoning by the imposition of coating layer.

Chapter 1

Introduction

1.1 Background

Generally, nitrogen oxides are generated from stationary sources such as, e.g. industrial boilers, gas turbines, steam power plants, waste incinerators, marine engines, and petrochemical plants. The selective catalytic reduction (SCR) is the most widely used technology for removing nitrogen oxides generated from stationary sources due to economic and technological efficiency. SCR may thus be deemed a well-proven technology as regards its application with conventional, non-renewable fuels. However, over the past two decades there has been an increasing interest globally and particularly in Denmark the utilization of non-conventional fuels like biomass for energy production. Biomass such as wood and straw are CO_2 neutral fuels which may help to reduce the greenhouse effect. According to the latest official estimate [1], Denmark has approximately 165 PJ (petajoule) of residual biomass resources including waste, of which only half are currently used. However, the potential of biomass fuels from a change of crops is huge. Such reorganisation of the farming areas together with a few other options may lead to a total biomass fuel potential as high as 400 PJ.

Biomass provides about 14% of world energy resources or about 25 million barrels of oil equivalent per day (Mboe/day) [2]. It is the most important source of energy in developing countries. In general, it is rather difficult to estimate biomass resources because it strongly depends on the natural vegetation. It is reported that nearly 66% of renewable energy production in the EU in 2004 was based on biomass, and the demand for biomass will increase rapidly during near future. The same trend is observed in the US, where biomass sources provide a small but growing percentage of all energy consumed [2]. In 2002, biomass supplied about 47 percent of all renewable energy consumed in the United States. Electricity generation from biomass (excluding municipal solid waste) represented about 11 percent of all generation from renewable sources in the United States. In fact, biomass supplied more energy to the US in 2002 than any other form of renewable energy, including hydroelectric power. Biomass supplied almost six times the energy of geothermal, solar and wind energy sources combined. Globally, biomass meets about 14 percent of the world´s energy needs. Thus, the worldwide use of biomass for production of energy is expected to keep an ascendant trend. The main pollutants resulting from biofuels are nitrogen oxides and hydrogen chlorine, the main emission being NOx, which may be reduced significantly by applying SCR technology. However, even if SCR is a well-proven technology, its application with non-conventional fuels like biomass brings specific challenges. In particular, deactivation of the catalyst by biomass containing alkali metals and subsequent activity reduction is problematic. Flue gases stemming from the incineration of biomass fuel typically contain about 200-1000 mg KCl/Nm^3 whereas incineration of coal only leads to ppm levels of KCl.

Naturally, the SCR catalyst is exposed to many different gaseous species, depending on the type of fuel combusted in the power plant. Natural gas comprise a relatively clean combustion gas, whereas combustion of e.g. municipal waste or straw often contain species that can lead to possible deactivating of traditional vanadia-titania-based SCR catalysts. The composition of various species of both fuel and ash associated with commercial or pilot plants currently combusting or co-combusting biomass have recently been reported [3-5]. All studies show a significant increase in the quantity of alkali and alkaline-earth elements (K, Na, Mg, Ca), phosphorous and chlorine in the

biomass-based fuels compared to coal. The quantity of potassium and chlorine in the straw can be more than an order of magnitude higher than that of coal (Table 1.1).

Table 1.1 Fuel composition, Moisture, volatiles and ash-concentration are given on a wet basis, all other elements on dry basis [2].

	COPRIB*	SAKLEI**	Lignite	Straw
	(wt%)			
Moisture	2.00	2.00	2.00	6.70
Volatiles	39.53	24.07	51.85	68.76
Ash	5.00	14.49	5.28	7.37
C	76.14	71.51	62.70	44.80
O	11.59	6.55	-----	-----
N	1.41	1.75	0.71	1.10
S	0.81	0.63	0.40	0.20
Cl	0.01	0.01	0.05	0.73
P	0.004	0.11	0.02	0.14
Ca	0.06	0.93	1.17	0.42
Mg	0.03	0.16	0.19	0.10
Na	0.01	0.02	0.01	0.02
K	0.07	0.08	0.01	1.90

*Columbia high volatile bituminous coal
**South Africa medium volatile bituminous coal

Especially the high content of potassium in e.g. wood and straw is of major concern. On the other hand, the sulfur content in biomass is typically lower in biomass than in coal. Zheng et al. [4] showed a clear relationship between sulfur in fuel and SO_2 emission. Thus, by firing or co-firing with biomass a reduction of SO_2 in the flue gas is expected. There are several practical concerns when these constituents enter the boiler in higher concentrations: high-temperature corrosion due to chlorine; accelerated slagging; and fouling [5]. A major problem regarding the application of SCR catalysts has been their deactivation by different components in the flue gas.

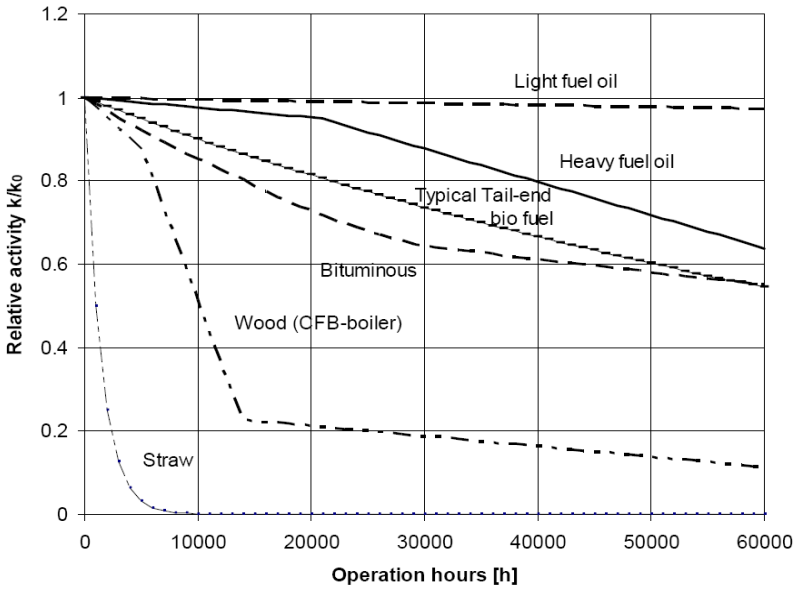

Figure 1.1 Expected deactivation of SCR catalyst for various fuel source [5].

Figure 1.1 shows the deactivation trend for various fuel types as activity relative to fresh-catalyst activity (V_2O_5-WO_3/TiO_2) versus operating time. The activity curves have been calculated using a deactivation model developed by Haldor Topsøe that considers ash deposition rate, pore plugging development and chemical impact on active sites [5]. For straw and wood firing the SCR catalyst deactivation rate is significantly higher. It is quite challenging to improve the SCR catalyst life for biomass fired applications.

1.2 Objectives

There were several strategies to limit the alkali deactivation [5]. 10-20% biomass co-firing with coal, fly ash recirculation to capture the potassium and modified super acidic supports to host the alkali poisons are some of the promising approaches. Biomass co-firing and modified super acidic support approaches were part of our previous efforts to decrease the intensity of deactivation. Protective coating technique to counteract the alkali deactivation was novel and untried approach. The objective of the present work has been to contribute to the knowledge about alternative alkali-resistant technologies for the removal of NO, with focus on protective coating technique. The attention has been on various coating materials like metal oxides and zeolites. Coated vanadia-based commercial SCR catalysts were exposed to potassium aerosols under realistic conditions. Fresh commercial and coated catalysts were exposed to alkali aerosols and tested their SCR activity. Based on the coating material composition, SCR relative activity, SEM analysis, acidic and basic character of the materials one of the most promising material (Mg) was selected for detailed investigation.

The project was initiated by two students Per Donskov Rams and Jannik B. Pedersen for fulfillment of their Bachelor Project. The results of their investigations are reported in Chapter 4. Based on the initial observations various coating materials were further tested and reported in Chapter 5-8. Finally, all the coating materials were classified depending on the acidic and basic nature. Intellectual protection of the investigation has been initiated through patent application entitled ‘Protective surface coating for DeNO$_x$ catalyst’ and the innovation is successfully transferred to Haldor Topsøe A/S.

Chapter 2

Literature Study

2.1 Introduction

Nitrogen oxides (NO_x) are simple molecules that are naturally present in the atmosphere. NO_x typically consist of a mixture of 95% NO and 5% NO_2. The natural sources of these oxides include nitrogen fixation by lightening, volcanic activity, and microbial activity. For a long time, there was little concern about these nitrogen oxides. However, the levels of NO_x have now increased to an extent that they have become an extremely important family of air polluting compounds [6]. The increase in NO_x emissions is due to the significant rise in anthropogenic (human) activities. The increasing level of human industrial activity continuously requires improved environmental technologies to prevent uncontrolled pollution of our common environment. Catalytic flue gas cleaning plays a major role worldwide for ensuring a sustainable environment. Pollutants are emitted continuously from both mobile and stationary sources worldwide. The stationary sources for gaseous emissions range from private homes over small industries and waste incineration facilities to large coal-fired power plants. The trends of making industry – and in particular power plants – more fuel flexible also pushes forward the development of new flue gas cleaning technologies. In addition, the increased operating efficiency will generally result in lower emission rates.

2.2 Sources of NOx and control technologies

The largest source of NO_x emissions is from combustion processes [6]. Nitrogen oxides are emitted when fossil fuels are burned to produce steam for electric power or when gasoline is used to power automobiles. In fact, automobiles and other mobile sources are responsible for 54% of the NO_x emitted from anthropogenic sources in Europe in 2000. Over 40% comes from stationary sources such as power plants, industrial boilers, petroleum refineries, etc. A small percentage of emissions result from industrial processes (e.g., chemical production and metal production), agriculture (soil and agricultural residues) and waste incineration [6].

There are three mechanisms of NO_x formation during combustion — thermal, prompt, and fuel NO_x. An understanding of these mechanisms is vital when designing technologies for NO_x emission reduction.

Thermal NO_x: This method of NO_x formation was first proposed by Zeldovich [7] and involves the reaction of gaseous N_2 and gaseous O_2 at combustion conditions. Both thermodynamics and kinetics are important to the formation of thermal NO_x, so concentration, temperature, and residence time influence the amount of NO_x produced. Therefore, the formation of NO_x can be limited by reducing the flame temperature (<1300°C) and reducing the residence time.

Prompt NO_x: Prompt NO_x is formed when molecular nitrogen (N_2) in the air reacts with hydrocarbon free radicals. Prompt NO_x occurs in fuel-rich regions where the hydrocarbon free radicals are more likely to be found. In general, considerably more NO is formed by thermal fixation than by the generation of prompt NO_x. Prompt NO_x can be reduced by operating at lower temperatures and highly oxidizing combustion conditions.

Fuel NO_x: Some fuels may contain compounds possessing N-H or N-C bonds. Examples include pyridine, quinoline, and amine type compounds. During the combustion process these nitrogen-

containing organics decompose into compounds such as HCN, NH_3, or free radicals such as NH^* and CN^*. All of these compounds ultimately form NO_x [8]. Fuel NO_x is independent of the flame temperature at normal combustion temperatures and is insensitive to the nature of the organic nitrogen compound. The amount of fuel NO_x formed will therefore depend on the amount of nitrogen-containing compounds in the original fuel. Fuel oil typically contains 0.1% to 0.5% nitrogen while coal could contain up to 1.6% nitrogen. Fuel NO_x typically falls in the range of 20% to 50% of the total NO_x emissions depending on the combustion conditions [9]. Fuel NO_x can be limited by decreasing the concentration of bound nitrogen in the fuel or by operating the burner in fuel-rich conditions.
There are two primary categories of control techniques for NO_x emissions. These are

1. Combustion control
2. Flue gas treatment

Combustion control is a primary treatment method for controlling NO_x emissions since efforts are made to minimize the level of NO_x formation during the combustion process. Flue gas treatment is a secondary treatment method whereby the flue gas, containing the produced NO_x, is treated using an add-on technology. Some characteristics and efficiencies of these combustion control NO_x reduction technologies are summarized in Table 2.1. The NO_x reduction efficiencies vary depending on the technique. However, with strict laws demanding ever-lower levels of emitted NO_x, frequently combustion modification is not sufficient to meet the demands of these stringent emission laws. Flue gas treatment, in many cases, is the only technology that meets legislation requirements. One of the most successful technologies used for the abatement of NO_x in flue gas streams is the Selective Catalytic Reduction (SCR) process. NO_x is selectively reduced (using a reductant such as ammonia) to nitrogen and water using a catalyst.

Table 2.1 Characteristics of NO_x abatement techniques [10].

NO_x Abatement Technique	**Mode of Operation**	**Efficiency**
Water injection	Reduced peak temperature	40–70%
Flue gas recirculation	Reduced peak temperature	40–80%
Reduced air pretreat	Reduced peak temperature	25–65%
Less excess air	Reduced peak temperature	1–15%
Burner out of service	Reduced peak temperature	30–60%
Low NO_x burners	Reduced residence time at peak temperature	30–50%
Selective catalytic reduction	Chemical reduction of NO_x	70–90%
Selective noncatalytic reduction	Chemical reduction of NO_x	25–50%
Catalytic absorption	Chemical reduction of NO_x and SO_2	60–90%
Catalytic combustion	Low temperature combustion	>90%

2.3 Selective Catalytic Reduction

Among flue gas treatment methods the Selective Catalytic Reduction (SCR) is the most world-wide used for controlling NO_x emissions from stationary combustion sources. It was first installed in Japan in the late 1970s on industrial and utility plants, whereas in Europe, the first commercial SCR process appeared in 1985. Based on the Japanese and European experience, the process was then adopted in the USA during the 1990s where it was first confined to gas turbines primarily located in California. [11–13]. The commercial use of the SCR process in the years has followed the introduction of stringent limits to regulate NO_x emissions in each country. In 2001, SCR

commercial installations were in operation in the Japanese and European power companies for an estimated overall capacity close to 100 000 and 60 000 MW, respectively [13]. However, in the last years the use of the SCR process has further increased due to its introduction to processes such as industrial and municipal waste incinerators, chemical plants and cement industries among the others. Moreover, SCR catalysts are also increasingly employed in biomass fired boilers, stationary and non-stationary diesel and gas engines (i.e marine propulsion engines and locomotive engines) [13, 14].

The process of SCR is based on chemical reaction, which involves the reaction of NO_x and ammonia in the presence of oxygen to form nitrogen and water. The technology involves the injection of ammonia into the NO_x containing flue gas. This flue gas then passes through a catalyst, which facilitates the reaction of ammonia with NO_x forming harmless nitrogen and water. The operating temperature is typically ranging between 300°C to 400°C. In practice, several reactions are known to occur but the SCR of NO_x is best represented by the following two equations, Equations (2.1) and (2.2). Since the concentration of NO_2 in combustion flue gasses is relatively low, the dominant reaction is represented by Equation (2.1).

$$4NO + 4NH_3 + O_2 \rightarrow 4N_2 + 6H_2O \quad (2.1)$$

$$2NO_2 + 4NH_3 + O_2 \rightarrow 3N_2 + 6H_2O \quad (2.2)$$

In general, the reaction requires temperatures between 200°C and 450°C in the presence of oxygen. The term ‘‘selective’’ describes the ability of ammonia to react selectively with NO_x, instead of being oxidized by oxygen.

A simplified diagram of the SCR system is presented in Figure 2.1. The composition of a flue gas is very much dependent on the fuel. For example, a typical flue gas from a coal-fired utility plant would be composed of 150–1000 ppm NO_x, 5% O_2, 8% H_2O, 13% CO_2, 200–2000 ppm SO_2, dust, and trace amounts of other components such as alkali metals. The flue gas from a natural gas fired plant would contain more oxygen, less NO_x, and significantly lower amounts of SO_2 and dust. Ammonia is injected into this flue gas before it passes through the catalyst. While in contact with the catalyst, NO_x is converted into harmless nitrogen and water. It is important that the catalyst does not oxidize the SO_2 in the flue gas to SO_3 as this would lead to the subsequent formation of ammonium sulfate salts. These sulfate salts may deposit onto the catalyst, if the temperature is not high enough, or deposit on the equipment downstream of the catalytic reactor where the temperature is cooler. In addition, SO_3 may result in the formation of sulfuric acid, which would cause corrosion problems downstream of the reactor.

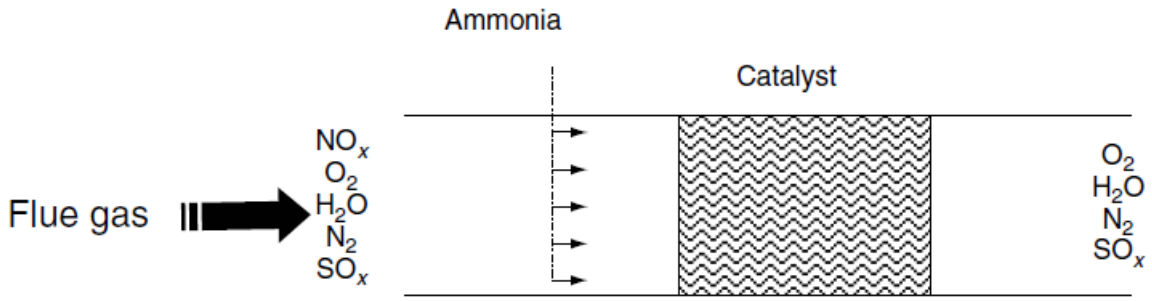

Figure 2.1 Simple schematic of SCR reactor.

2.4 Commercial SCR catalyst

Several catalysts are reported to be active for the SCR of NO_x with ammonia. The most well known and most commonly used catalyst is vanadia well dispersed on a titania support (V_2O_5/TiO_2) with tungsten oxide or molybdenum oxide. Vanadia (V_2O_5) is the active ingredient and is responsible for converting NO_x into nitrogen. However, it is also responsible for the undesired oxidation of SO_2 to SO_3. Therefore, the vanadia content of the catalyst is generally kept low (0.3–1.5%) especially in the presence of high SO_2 concentrations. The titania (anatase) support is very stable and weakly and reversibly sulfated in the presence of SO_2. WO_3 (10 wt%) is added to increase acidity, increase activity, increase the thermal stability of the catalyst, and limit the oxidation of SO_2. Catalysts containing MoO_3 (6 wt%) instead of WO_3 are also available. These catalysts, although less active than the analogous V_2O_5–WO_3/TiO_2 samples, are more tolerant to arsenic, a common catalyst poison [13]. V_2O_5/ TiO_2 operates best at temperatures between 300°C and 400°C.

A typical SCR reactor is sketched in Figure 2.2. The plate or honeycomb elements containing the catalytic material are placed side by side and built into modules. A module can consist of 8 to 81 elements depending on the catalyst type. These modules are then placed into the reactor to form catalysts layers [13]. The reactor usually has more than one layer of catalyst modules therefore the flue gas passes through the layers in stages. Ammonia, either as an aqueous solution or gas is injected into the flue gas stream. A dummy layer is installed upstream of the catalyst layers for flow straightening and uniform distribution.

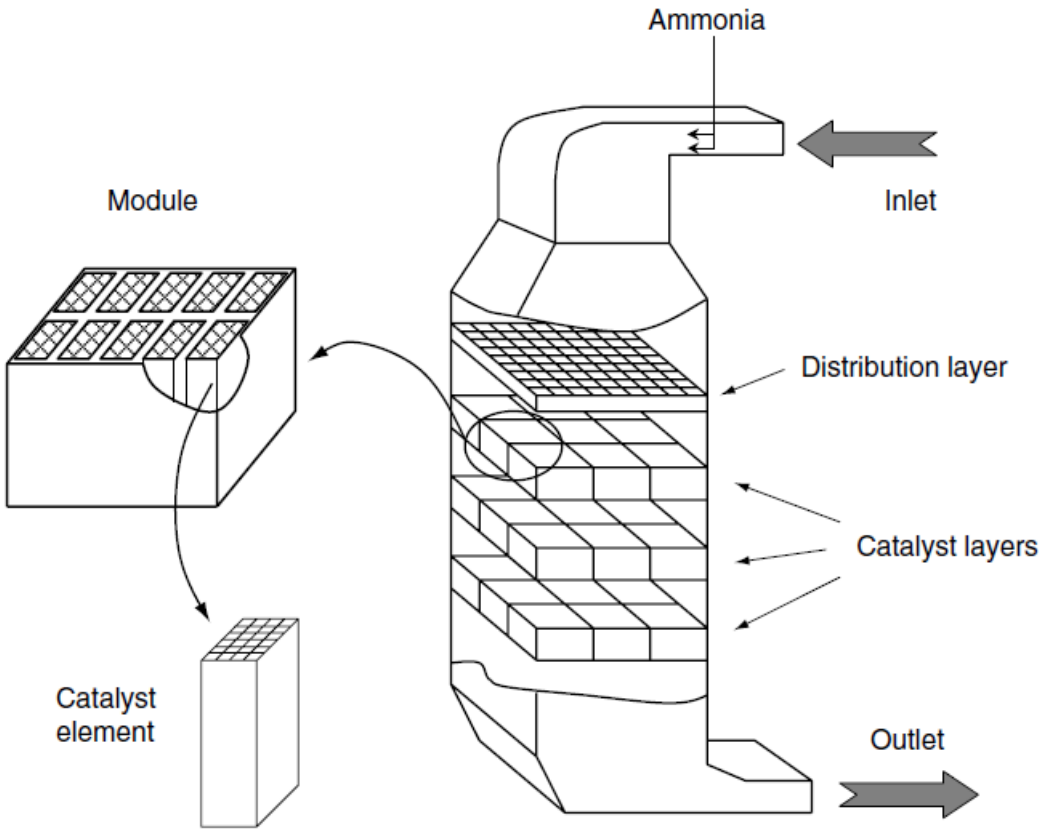

Figure 2.2 The SCR reactor and catalyst layer distribution [13].

2.5 Surface Reaction Studies

Numerous studies have been published related to catalytic activity, reaction mechanism, effects of vanadia loading, effects of active phase composition, and other pertinent topics; these have been summarized in several recent reviews [15, 16]. Three types of vanadium containing species are present at the surface of the vanadia on titania catalysts. Monomeric vanadyl, polymeric vanadates and crystalline vanadia depending on the vanadia loading. Moreover, Brønsted acid sites and Lewis sites are present at the surface of vanadia on titania catalysts. All species were needed to explain the mechanism of the SCR reaction. Despite the number of works concerning the development of active catalysts for SCR, a lack of knowledge about the mechanism of the process exists. There are two popular mechanisms in the literature namely Eley-Rideal and Topsøe.

Eley-Rideal mechanism: In 1979 Inomata et al. [15] proposed a mechanism for the SCR reaction on vanadium oxides. The authors suggested that the reaction proceeds by an Eley-Rideal mechanism, in which NO reacts directly from the gas phase with an absorbed ammonium ion throughout an H-bonded 'activated complex', shown in Figure 2.3 [15]. In spite of the electronic structure, the interactions of the intermediate and the movements of electrons have not been specified; the mechanism in Figure 2.3 is still very popular.

A different mechanism has been proposed by Ramis and co-workers [16] referred as the "amide–nitrosamide" mechanism, these authors suggested that ammonia is adsorbed over a Lewis acid site and is activated to form an amide species. However, recently published results of DFT calculations on a $V_2O_9H_8$ cluster showed that the adsorption of NH_3 on Lewis acid sites is highly unfavorable [17]. The Langmuir-Hinshelwood mechanism proposed is, however, electronically unbalanced as well as site-unbalanced [15].

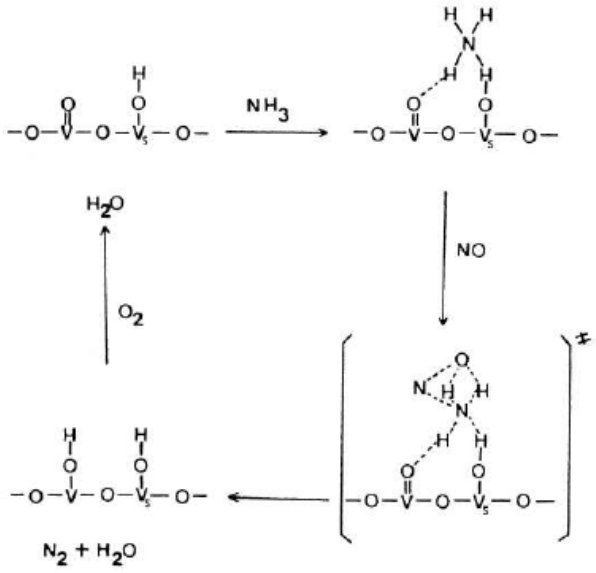

Figure 2.3 Eley-Rideal mechanism of the NO-NH_3 reaction on vanadium oxide proposed by Inomata et al. [15].

Topsøe mechanism: Based on in situ on-line FTIR studies under steady-state conditions, Topsøe et al. [18-22] proposed the mechanistic scheme shown in Figure. 2.4. Herein it was suggested that both the Eley-Rideal and Langmuir-Hinshelwood are possible mechanisms, but that NO more likely reacts as a weakly adsorbed species. They considered that vanadia-titania catalysts exhibit two separate catalytic functions, i.e. acid and redox functions, in a dual-mechanistic fashion. Turco et al. [23] also agree with this scheme. Although the overall reaction not has been equalized (i.e. all

components reacts in the stoichiometry of 1 to 1), it gives a good idea of the possible reaction mechanism.

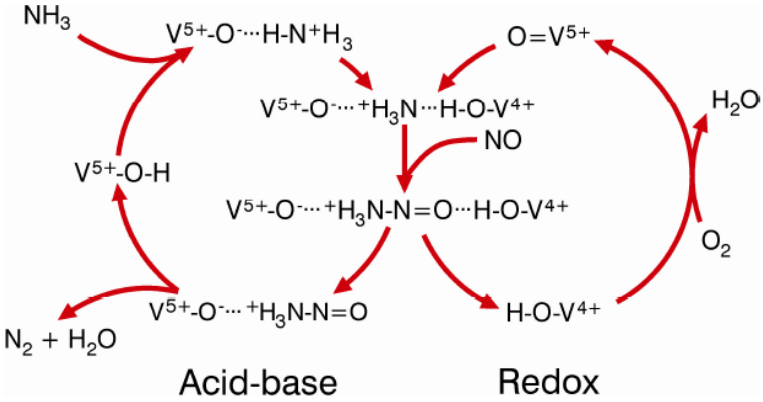

Figure 2.4 The acid-redox catalytic cycle of the SCR reaction over the vanadia-titania catalyst in the presence of oxygen, proposed by Topsøe [18].

The key and rate-determining step in this mechanism is assumed to be the activated adsorption of ammonia on the V^{5+}-OH Brøndsted acid site, which reduces a nearby V^{5+}=O redox site to V^{4+}. This activated intermediate V^{4+}–OH, is very reactive toward gaseous NO, leading to the products, N_2 and H_2O, which desorb from the surface. Dumesic et al. [19, 24] proposed the following simplified reaction scheme to describe the NO conversion and the ammonia slip behavior for vanadia/titania catalysts under industrial SCR conditions

$$NH_3 + M \rightarrow M\text{-}NH_3 \text{ (fast)} \quad (2.3)$$
$$M\text{-}NH_3 + S \rightarrow S\text{-}NH_3 + M \text{ (slow)} \quad (2.4)$$
$$NO + S\text{-}NH_3 \rightarrow \text{Products} + S \text{ (slow)} \quad (2.5)$$

Where M represents an ammonia adsorption site and S represents a reactive site on which ammonia is activated. These three steps (2.3)-(2.5) are some of the steps in the catalytic cycle proposed by Topsøe in Figure. 2.4. Combining the reaction scheme with Figure. 2.4, it is seen that M in the steps (2.3) and (2.4) are V^{5+}-OH and the S sites in the steps (2.4) and (2.5) can be identified as V^{5+}=O surface groups.

Went et al. [25] used TPD and laser Raman spectroscopy to determine the structure of the catalyst and of the adsorbed species. It was found that the specific activity of polymeric vanadate species was 10 times greater than that of monomeric vanadyls at 500 K. Monomeric species produce N_2 both in the presence and in the absence of oxygen, where as polymeric species produce both N_2 and N_2O. The selectivity towards N_2O increases with increasing O_2 concentration in the feed. Chen and Yang [26] concluded from their studies that the active sites from SCR reaction over sulfated titania are Brønsted sites and the mechanism is Eley-Rideal; 52% of the chemisorbed ammonia was active in the SCR reaction while 48% of the chemisorbed ammonia was inactive. They also concluded that the Brønsted acid sites of the V-OH groups (and specifically terminal V-OH) were the active sites for the reaction.

So far no exclusive reaction mechanism is found for the SCR reaction over vanadia on titania catalysts which can explain all experimental observations. The Eley-Rideal mechanism, however, is favored by many investigators. Finally, it is concluded that the SCR reaction is most favorable on polymeric vanadate species with more Brønsted acid sites such as vanadium hydroxyl groups (V-OH).

2.6 SCR catalyst deactivation

Generally speaking, the catalyst deactivates if the intrinsic activity is reduced, if transport of reagents to the active sites is inhibited, or if adsorption/desorption is hindered. Consequently, deactivation of SCR catalysts takes place by several mechanisms, which are also known for other catalyst systems [27-29]:

- Chemical poisoning (e.g., by alkali)
- Surface fouling and/or pore clogging (e.g., by fly ash compounds)
- Loss of surface area by thermal ageing/sintering.

Chemical poisoning: Loss of SCR activity is commonly observed by an increase in the NH_3-slip at a given NO_x removal rate [27, 30]. An increase of the NH_3-slip has several implications, for example in a coal-fired boiler: (i) the formation of ammonium sulfate salts, which causes corrosion and fouling of the air preheater; (ii) an increase of the NH_3 content in the fly ash, which may make it unsellable; and (iii) an increase of NH_3 in waste water from a wet SO_2 scrubber. Knowledge of the deactivation mechanism and the rate of catalyst degradation is instrumental for the SCR technology. For example, the overall economics is determined by catalyst lifetime; furthermore, the plant operator may risk severe economic penalties, or the operation of the plant may even be prohibited, if the emission limits for NO_x are exceeded.

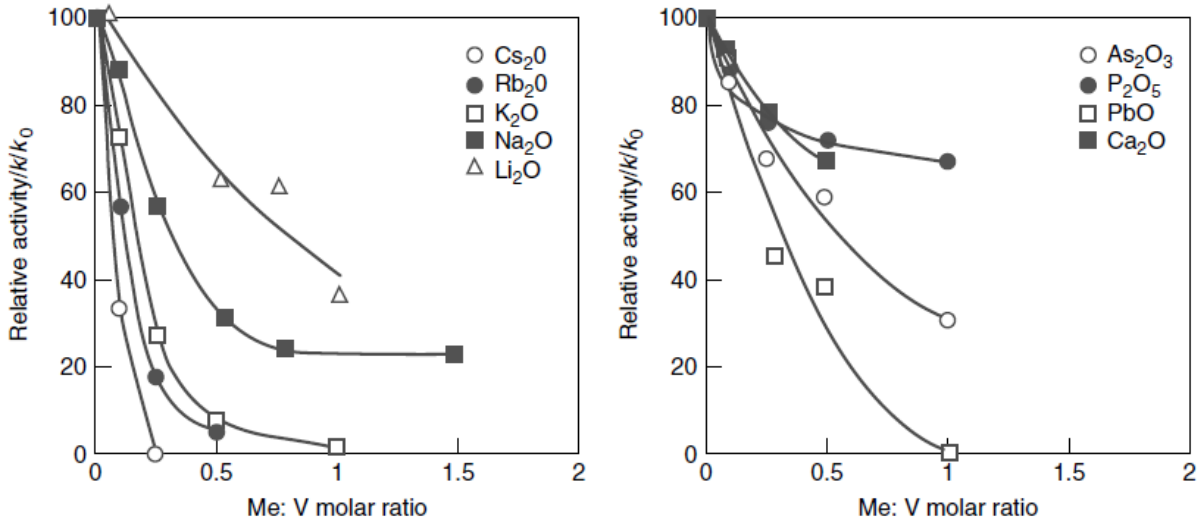

Figure 2.5 Effect of loading of different poisons on the activity of vanadia-titania catalysts [31].

Poisoning is the loss of activity due to strong chemisorption on the active sites of impurities present in the flue gas. The poison may act by simply blocking an active site, or it may alter the adsorption properties of reactants and products by an electronic effect. As noted above, different poisons act with different strengths on catalyst deactivation. Chen et al. [31] investigated the quantitative effect of poisoning with different compounds by impregnation of V/TiO_2 catalyst samples with aqueous solutions, followed by calcinations. The data in Figure 2.5 show that alkali metals deactivate the catalysts in the order of their basicity: Cs > Rb > K > Na > Li. This difference between the effect of Na and K was confirmed in a later study [32].Whilst P and Ca are only mild poisons (weaker bases), Pb is a moderate poison, lying between K and Na on a molar basis.
A direct correlation between the amount of chemisorbed NH_3 and the activity of the poison-doped catalyst was found [33]. This provided supporting evidence for the proposed mechanism that NO

reacts on the catalyst surface from the gas phase, or a weakly adsorbed state, with strongly adsorbed and activated ammonia molecules. Alkali will irreversibly bind to the ammonia adsorption sites and cause a permanent loss in activity (see Figure 2.6), and this has been confirmed in a number of later studies [32–37]. Kamata et al. [32] also found that large additions of K_2O to the vanadia-based catalysts resulted in the formation of KVO_3. Chen and Yang [34] found that the addition of WO_3 to V_2O_5/TiO_2 catalysts improved the resistance towards alkali poisoning. SO_2 was found to reduce the deactivating effect of especially alkali due to its acidity; most likely Brønsted acid sites are regenerated [33]. This promoting effect of SO_2 requires its presence in the flue gas (i.e., stable sites are not formed) [35]. Catalysts with better resistance towards alkali have been proposed to contain a higher content of vanadia on titania [36] or vanadia on more acidic supports, for example sulfated zirconia [35].

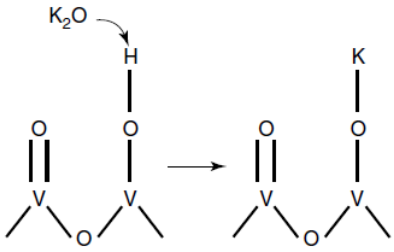

Figure 2.6 Proposed mechanism for deactivation of vanadia SCR catalysts by alkali.

In the combustion of biofuels, alkali is present as aerosols as the flue gas cools to the SCR temperature [37]. Furthermore, alkali is present at much higher concentrations as compared to coal combustion. Alkali in the ash from biofuels (and in waste incineration plants) causes problems for both the heat exchanger steel and SCR catalysts, and has so far proved to be prohibitive for SCR installation in the high-dust position on purely biofired units. The co-combustion of 7% (on an energy basis) straw with bituminous coal did not appear to alter the deactivation rate of a corrugated plate-type catalyst [38].

Several authors have proposed a reason for the decreased activity after doping with potassium. Figure. 2.7 shows the effect of a gradual potassium-poisoning of a V_2O_5-WO_3/TiO_2 SCR-catalyst. A monolayer deposition of potassium was calculated to a K-loading at approximately 11%, thus no (or only negligible) physical blocking could occur on the active sites in the poisoned catalysts with loadings up until about 2% K_2O. Odenbrandt et al. [39] showed that there was a chemical interaction between K_2O and V_2O_5-WO_3/TiO_2 and not due to plugging by precipitated K_2O by means of spectroscopic studies. Furthermore, they found that potassium preferentially coordinated to the specific sites on the catalyst surface, namely the hydroxyl groups on V_2O_5, and probably on WO_3, together with a decrease in both number and strength of Brønsted acid sites.

Lietti et al. [40] also found that potassium deactivated the 3.56 wt% V_2O_5/TiO_2-catalyst significantly when adding more than 0.5 wt% potassium. By applying FTIR spectroscopy, is was found that the nature of the surface vanadium oxides species does not change in wet conditions when adding potassium, but a shift in vanadyl stretching frequencies was detected from 1035 cm^{-1} to 1013 and 1002 cm^{-1} due to formation of strong basic anions on the catalyst surface acting as ligand for vanadyl complexes, reducing Lewis acidity of vanadium ions. The results of IR and TPD results also indicated a reduction of ammonia coverage (both molecular chemisorbed ammonia and ammonium ions) upon potassium doping, along with the formation of strong basic sites, to which ammonia can adsorb in form of weakly H-bonded species.

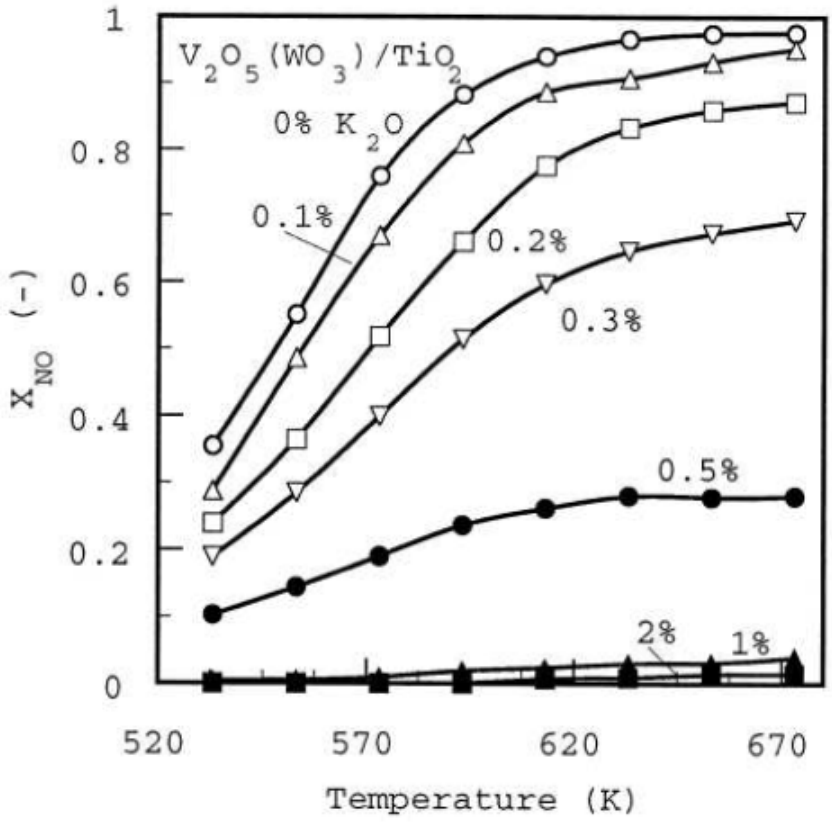

Figure 2.7 Temperature dependence of NO conversion, for V_2O5-WO_3/TiO_2 catalysts with different K_2O contents [39].

The strong deactivation of $V_2O_5/WO_3–TiO_2$ SCR catalysts by alkali and alkaline earth metals was exemplified in detail for K and Ca [41]. The poisoning element occupies the non-atomic hole sites of the (0 1 0) V_2O_5 surface, such that both Brønsted acid and V^{5+} = O sites are blocked. Indeed, these sites play a crucial role in the SCR mechanism, because the former stabilize NH_3 on the surface for the reduction of NO with consequent formation of a nitrosamide (NH_2NO) specie, and the latter favors the fast decomposition of NH_2NO. Upon reaction between the catalytic surface and the poisoning element, these sites are inaccessible to the substrate, thus causing a strong decrease of the SCR catalytic activity.
Zheng et al. [37, 42] suggested the following reactions for the proton exchange on the catalytic Brønsted acid site with KCl and K_2SO_4 in reaction (2.6)-(2.8).

$$V{-}OH + KCl \rightarrow V{-}O{-}K + HCl \quad (2.6)$$
$$V{-}OH + K_2SO_4 \rightarrow V{-}O{-}K + KH_SO_4 \quad (2.7)$$
$$V{-}OH + KHSO_4 \rightarrow V{-}O{-}K + H_2SO_4 \quad (2.8)$$

Once the V-OH sites have reacted with potassium, they are no longer active in the ammonia adsorption, and thus no reduction of NO takes place. The above reactions both deactivate the active SCR sites, although the KCl is slightly more poisonous for the V_2O_5-WO_3/TiO_2 catalyst than the K_2SO_4 [42], which is left unexplained. The authors also found that particle deposition and pore blocking promoted the deactivation by decreasing the diffusion rate of NO and NH_3 into the catalyst. The mechanism of which potassium in aerosol form penetrated the catalyst to the active sites is not known, but several mechanisms were suggested, most relevant being the possibility of mobile surface potassium species on the catalyst surface. It was suggested that the finest fraction of

the aerosols is deposited, due to their high diffusion coefficient, by diffusing directly into the catalyst structure. The process may be similar to the catalyst calcination process, where the active species of the catalyst are dispersed over the support surface by heat treatment.
To validate this mechanism, mobility of the deactivating species, KCl and K_2SO_4, is required, which can be estimated from the Tamman and Hüttig temperatures. They indicate the temperatures (measured in Kelvin) at which a surface specie becomes mobile are estimated from the following semi-empirical correlations [43]

$$T_{Hüttig} = 0.3T_{melting} \quad (2.9)$$
$$T_{Tamman} = 0.5T_{melting} \quad (2.10)$$

When the Hüttig temperature is reached, atoms at defects will become mobile, and at the Tamman temperature, atoms from the bulk will exhibit mobility. For KCl (melting point at 771°C) the $T_{Hüttig}$ and T_{Tamman} temperatures are 40 and 249°C. For K_2SO_4 (melting point 1069°C) the temperatures are 129 and 397°C, respectively. KCl and K_2SO_4 may thus be expected to be mobile at normal SCR operating temperatures. Zheng et al. [37, 42] tested the deactivation of the V_2O_5-WO_3/TiO_2 catalysts at both 250 and 350°C under biomass combustion, where fast deactivation was observed at both temperatures compared to coal firing. This correlate well with proposed deactivation mechanism of mobile surface species, since the lowest temperature tested of 250°C is above the Tamman temperature for KCl. This indicates, if flue gas aerosols of potassium chloride or sulfate is present, that the deactivation is caused by surface diffusion of potassium deposited from the finest fraction of aerosol particles.
Surface fouling and/or pore clogging: Undesired deposits on the surface of the catalyst walls or in the pores will deactivate the catalyst, either by covering the active sites or by restricting diffusion to the interior of the catalyst wall. For industrial SCR units, fouling or clogging is observed by an increase in the pressure drop over the reactor. Plugging of catalyst channels with fly ash results in an increased pressure drop and a higher effective space velocity and, consequently, also the possibility of lower NO_x conversion [27]. The catalyst in high-dust installations is kept clean by frequent soot blowing (usually steam nozzles or sonic horns). Fused slag-like ash particles termed ‘‘pop-corn’’ may be so large that one single particle may clog a catalyst channel.
Sintering: High-temperature ageing of vanadia-based SCR catalysts has several impacts on the catalyst properties. Nova et al. [29] reported a significant loss in the BET surface area of commercial V_2O_5/WO_3/TiO_2 catalysts aged at 500 to 900°C. Above 850°C, the formation of rutile TiO_2 is observed from X-ray diffraction (XRD) patterns with the phase transformation from anatase to rutile being accompanied by a significant loss in surface area. The loss of selectivity was supposed to arise from the formation of polymeric vanadia species and even bulk phase V_2O_5 in all cases [29].

2.7 Alkali deactivation and its influence on reaction mechanism

Alkali is believed to act mainly as a combined chemical and physical poison in biomass. Potassium, in particular, is present as sub-micron particles mainly as chlorides and sulphates. Sub-micron aerosols adhere to the catalyst surface or diffuse into the macro pores. The aerosols cannot diffuse into the clusters of primary TiO_2 support particles, which appear as islands at the catalyst surface. However, the alkalis are very mobile and are readily transported by surface diffusion into the clusters and react with the active sites (Figure 2.8). The reaction is not reversible: when an active site has reacted with K it is lost for the rest of the lifetime of the catalyst. There are reports that the effect of alkali is stronger at higher temperatures [37, 42], which could have to do with a temperature dependence of the mobility.

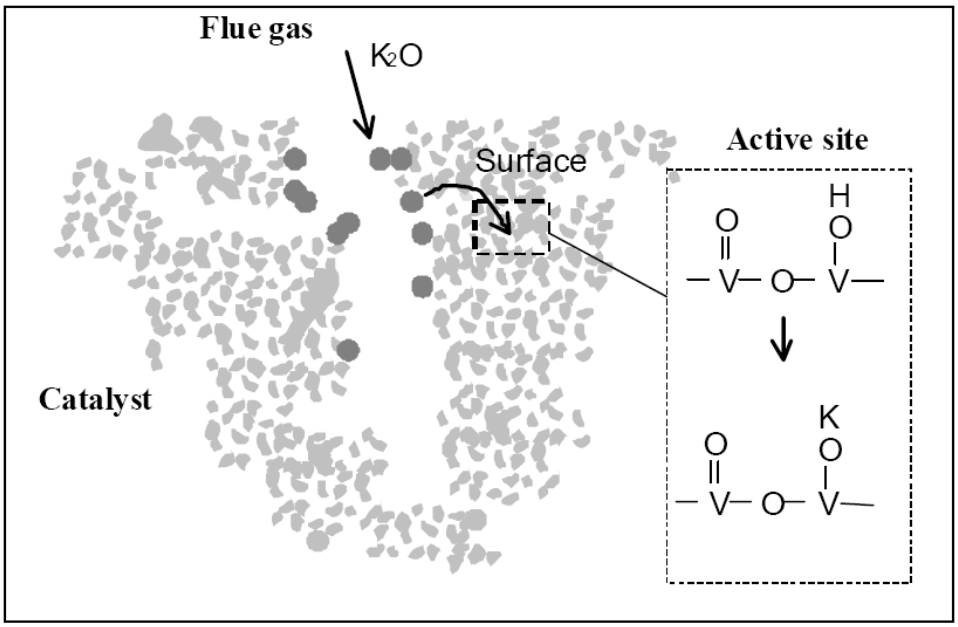

Figure 2.8 Diffusion and poisoning mechanism of alkali [44].

Alkali-metal aerosols formed during combustion of biomaterial are well known to be able to severely impact the performance of SCR catalysts. The sub-micron particles adhere to the surface of the catalyst and are readily transported to the active sites by surface diffusion. Spectroscopic studies suggest that the poisoning mechanism occurs via chemical bonding of the alkali metal to the crucial –V-OH sites, the so-called Brønsted-acid sites which also adsorb and "activate" the ammonia, forming –V-OM (M being K or Na) and thereby blocking the catalytic cycle (Figure 2.9). Exposure to alkali-metal aerosols can at worst cause complete loss of activity of the catalyst within a few thousand hours of operation.

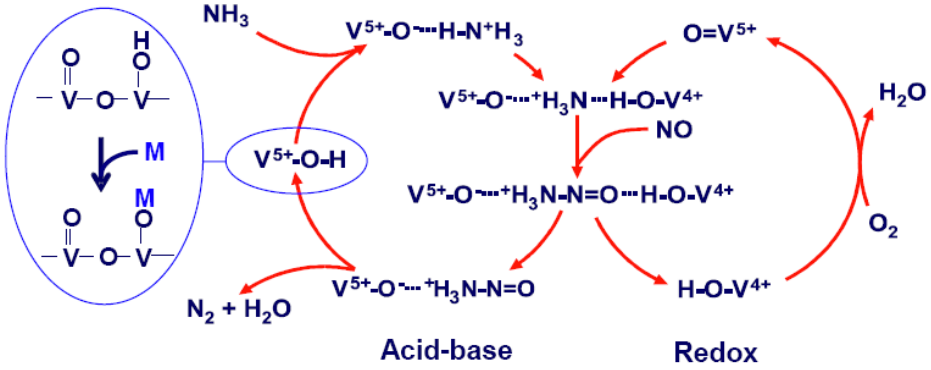

Figure 2.9 Topsøe deactivation mechanism [5].

2.8. Alkali resistant SCR catalysts

There are some general process based approaches to overcome the deactivation due to poisons resulted in loss of catalytic surface sites [5].

(1) Purify feed and/or use guard bed to adsorb poison;
(2) Employ additives that selectively adsorb poison;
(3) Choose right biomass fired boiler that lower the alkali-metal aerosols release;
(5) Co-firing of up to 10-20% biomass can be done without causing extraordinary deactivation of the catalyst compared to 100% biomass firing;
(6) The use of SCR on 100% biomass-fired boilers may be done as a tail-end installation to minimise the amount of poisoning species entering the SCR;
(7) Injection of coal fly ash in a wood-fuel oil co-fired boiler can reduce problems with deposits in the convective part of the boiler in the air-preheater and significantly reduce catalyst deactivation rate by capturing poisonous constituent of the wood ash.

There exist different strategies to regenerate deactivated catalysts, for example, washing with a solution of diluted sulfuric acid, which enables complete restoration of the initial activity of the catalyst [37, 45]. The major disadvantage of such procedures is that in most cases, the power plant has to be stopped in order to remove the deactivated catalyst. Instead of changing/modifying the existing process alkali resistant catalyst design is more challenging and demanding. There are some catalytic approaches to increase the life of the catalyst from the alkali metal poisons.

Super acidic supports: An efficient way to resist the deactivation problem could be to use an alternative catalyst, which is more resistant towards poisoning with potassium. Since deactivation with alkali additives generally occurs due to strong acid-base interaction with the V–OH sites responsible for the activated ammonia adsorption, one possible way to increase catalyst resistance to alkaline poisons is to use supports with high or even super-acidic properties, which would interact stronger with potassium than the catalytic vanadium species. Vanadia supported on sulphated-ZrO_2 and WO_3-ZrO_2 catalysts showed better activity even in the presence of potassium K/V=0.4 [46]. V_2O_5/ sulphated-ZrO_2, V_2O_5/ WO_3-ZrO_2 and commercial V_2O_5-WO_3/TiO_2 catalyst showed relative value of 40%, 35% and 23%, respectively. The authors reported that part of vanadium is still poisoned by potassium that is accounted for the loss in activity. Based on the above results it was clear that the rate of deactivation is less compared to commercial catalyst, but still it is not enough from the commercial point of view.

Chemical deactivation of Fe-zeolites and Cu-zeolite has been close to phenomena observed with vanadia-based SCR catalysts [47, 48], thus said alkaline metals being strong poisons to the catalyst. While alkaline metals and alkaline earths exhibit deactivating potential towards Fe–zeolite and Cu-zeolite catalysts, their resistance towards these poisons was shown to be much higher than that of a standard V_2O_5–WO_3/TiO_2-SCR catalyst as currently used for NO_x abatement applications. If high alkaline metal contents are to be expected in an exhaust stream (use of biomass), the use of Fe–zeolite and Cu-zeolite catalysts instead of vanadia-based materials is to be recommended and need more commercial evidences [47, 48]. While the observed deactivation of Fe–zeolite and Cu-zeolite catalysts by alkaline metals are influenced by the reduced acidity and ammonia storage capacity of the material. Such a high alkali resistivity of zeolites was due to unique properties like high surface area, pore structure, pure Brønsted acidity. Commercial use of these zeolites is limited by economic factor when compared to TiO_2.

Nano catalysts: Comprehensive studies of the activity of nano-VO_X/TiO_2 catalysts for both oxidation reactions and SCR of NO_X in flue-gases by NH_3 have been initiated [49, 50]. Preliminary results indicate a superior activity compared to traditional SCR catalysts, thus suggesting that the nano materials might prove useful where small catalyst bed volumes or SCR catalysts with prolonged life on stream are desired. In these investigations an optimum content of 15% V_2O_5 is reported with high surface area of 227 m^2/g. These studies are still ongoing for further clarification in terms of SO_2 oxidation, thermal and mechanical resistance aspects.

Protective coating techniques: Coating of vanadium supported TiO_2 catalyst to counteract the deactivation due to poisoning is an untried approach. The ultimate success criterion for the coating is minimal loss of activity. Since the coating must bind to the catalyst material loss of activity cannot be avoided unless the coating itself is SCR active. Two possible solutions could be interesting for selecting coating materials.

1. One would be to create a coating which acts as a physical barrier for aerosols only, allows reactant gases to reach the catalyst surface.
2. The second would be to create a coating that may be included in a reaction with potassium poison.

Table 2.2 shows the some of the process parameters to be considered while selecting the coating materials.

Table 2.2 Coating materials parameters which influence activity.

Parameter	Effects
1. Optimum thickness	Eliminates the diffusion problems.
2. Adherence	A strong pairing prevents the coating falls off.
3. Durability	Should withstand at 300-400°C for long time in the presence of fly ash.
4. Pressure drop	Should be minimum for high efficiency of power plant.
5. Reactivity to potassium	These materials can interact with potassium forming non-poisonous neutral product, thereby protecting active vanadium.
6. Pore structure	For higher effective diffusion coefficient, improved poison resistance, etc.
7. Relative activity	Drop in initial activity after coating is expected, due to additional coating layer which acts as a resistant layer or blocks the some of the active site

Coating materials based on physical blocking: A linear correlation between the alkali content in the ultra fine particles and the alkali accumulation on the catalyst samples has been reported [3]. The linear correlation between the accumulation of alkali accumulation on the samples and the amount of alkali in the flue gas decreases with increased particles sizes. The results clearly imply that large amounts of alkali in ultra fine particles (<100 nm) in the flue gas increased the alkali accumulation on the catalyst. Based on the above evidence, if the catalyst is protected or covered by fine particles which are less than (<100 nm) the potassium particles will deposit and accumulate on the surface, but not further penetrate into the catalyst. The promising materials are nano-metal oxides, zeolites, micoporous and mesoporous materials.

Use of slightly basic materials can also prevent the alkali poisons to reach until the active vanadium species. The slightly basic nature of the coating does not attract the alkali poisons because of basic-basic nature of the two substances. The promising materials are Mg and Mg containing materials.

Coating materials based on chemically reactive compounds to potassium: Instead of using super acid catalysts as a support materiel for SCR to resist the poisoning effect, if it is used as a coating layer on the surface of vanadium supported TiO_2 seems to be more practical approach. The alkali metal has to cross the coating layer before it reaches the active vanadium species there by the direct alkali attack can be minimized. The promising super acid materials are sulphated ZrO_2, WO_3-ZrO_2 and zeolites with optimum Si/Al ratio.

2.9 Conclusions

Despite extensive contributions to the literature since 1975 regarding selective catalytic reduction (SCR) catalysis with ammonia for NO_x removal from combustion gases, there is still on-going, controversial discussion in academia concerning both catalytically active sites in the SCR mechanism and deactivation phenomena with regard to practical SCR applications. In the present

report, most popular reaction mechanisms were considered and related to the deactivation phenomena of alkali metals. Finally, all the latest approaches were considered to overcome the alkali deactivation. An innovative and promising approach based on a coating technique is also visioned to improve the drawbacks of the previous approaches.

Chapter 3

Experimental

This chapter provides detailed information about experimental approaches and methods used in the report.

3.1 Commercial catalyst composition

Vanadium based catalyst plates were supplied by Haldor Topsøe A/S. The composition of the catalyst mass base is approx. 1.2-3% V_2O_5, 7% WO_3 dispersed on a fibre reinforced TiO_2 carrier. Fibre material consists of primarily SiO_2 and alumina and calcium to a lesser extent. The monoliths had a size of 75 mm x 75 mm x 500 mm. The hydraulic diameter of the channels was about 6.5mmand the wall thickness was 1.0 mm.

3.2 Catalyst coating

V_2O_5/WO_3-TiO_2 catalyst plates were coated by spray coating technique with 5-30 wt% of the coating material in water solution. The particle size of the suspension was measured by HYDRO2000G (laser sensor). Average particle size of the coating materials were adjusted (less than 15 μm) by shaking the solution with 3-4 mm glass beads for 5-10 min. Finally coated catalysts plates were dried in the oven for 10 h and calcined at 450°C for 5 h at a heating rate of 5°C /min.

3.3 SCR catalyst deactivation

To expose the catalyst to alkali poisons under more realistic conditions plate type catalysts were placed in a pilot plant reactor shown in Figure 3.1 and exposed to well-defined aerosols of KCl. Hot flue gas was produced by a natural gas burner and a solution of the salt in distilled water (7.4 g/l KCl) was prepared and mixed several days before being added to the system. An aerosol of the salt was then generated by injecting the solution through a fluid nozzle into the flue gas close to the burner where the temperature was 1050–1100°C. A bayonet heat exchanger was inserted into the main duct downstream the formation of the desired aerosol particles to cool down the flue gas to avoid accelerated corrosion caused by the potassium compounds.

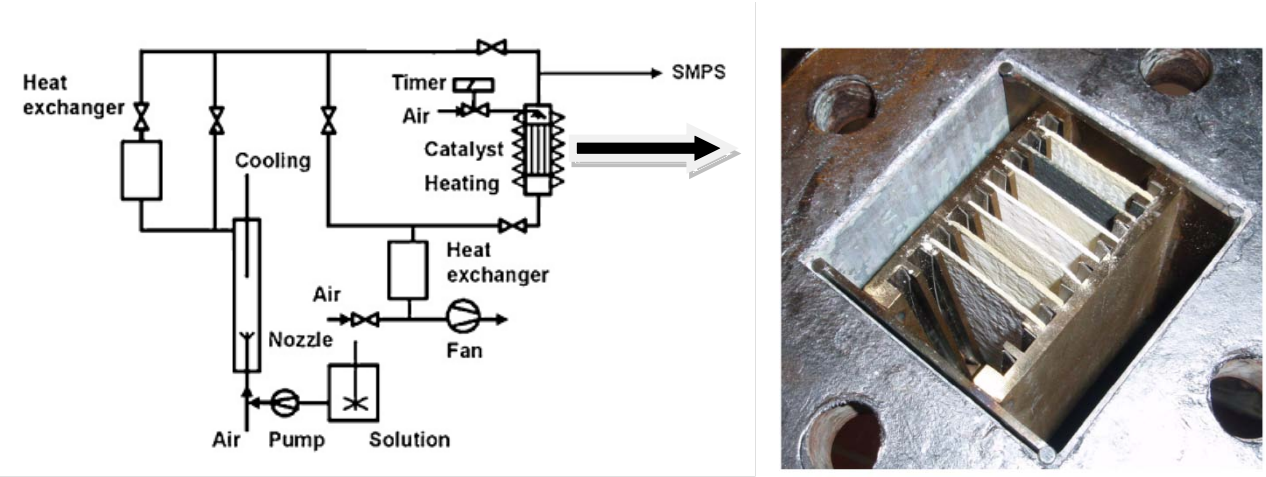

Figure 3.1 Potassium chloride aerosol exposure pilot plant experimental setup.

The catalyst box was well insulated and heated by an electrical heating wire. The exposure temperature was kept at 350°C and the temperature difference over the cross section of the catalyst box at the catalyst inlet was within 4°C and the temperature difference between the catalyst inlet and outlet was kept less than 5°C. A soot blower and a steel grid were installed 20 cm and 5 cm, respectively, above the catalyst to minimize plugging problems. The soot blower consists of a steel pipe with a diameter of 16 mm and a hole of 10 mm, a time controller and connects to compressed air at a pressure of 5 bar. Two additional soot blowers were placed just above the steel grid to blow away the particles deposited on the mesh. Soot blowing was carried out by 3–5 s of blowing with compressed air at an interval of 30 min. The total flow rate at the outlet of the burner was about 60 N m^3/h and the flow rate through the catalyst was kept at 40-45 N m^3/h by adjusting the bypass valve, which corresponds to a channel velocity of 6 m/s at 350°C. The experiment was conducted for 650-1200 h continuously. After exposed time catalyst monolith plates were removed immediately to avoid further deactivation.

3.4 SCR activity measurements

In the laboratory, the activities of the catalysts were measured by means of the setup shown in Figure 3.2. This mainly consisted of three sections: a gas metering and mixing section, a reactor, and an analyser section. The flow rates of the individual gases were controlled by mass flow controllers providing a constant flow, and measured by a bubble flowmeter. Mixing was then performed with a flow panel. Normally, two different gas streams were made and directed to the reactor. Water was added by passing part of the nitrogen gas through an evaporator consisting of a Permapure tube placed in a thermostated water bath.

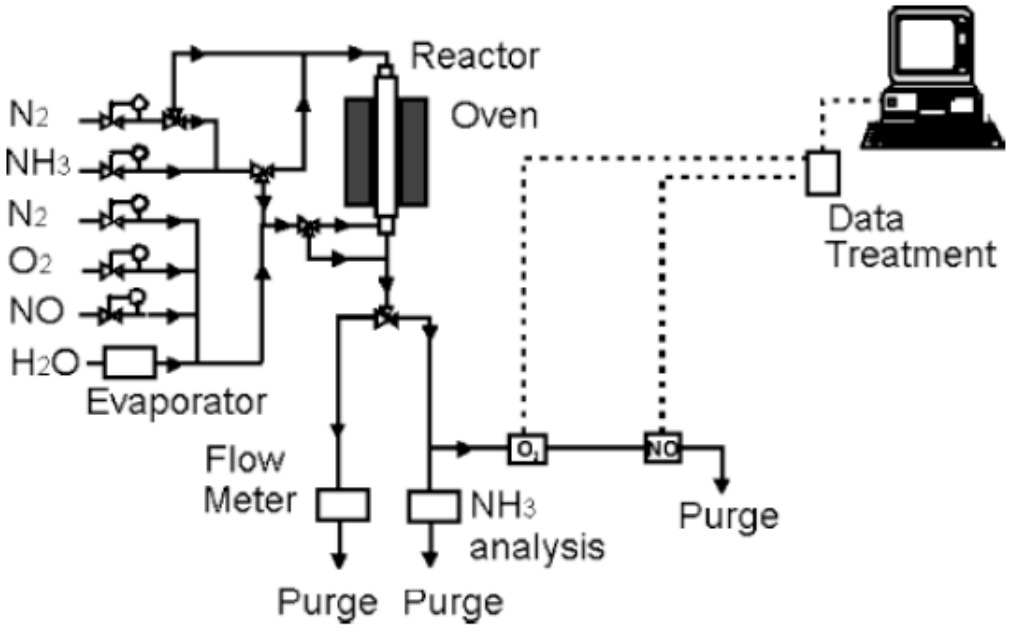

Figure 3.2 The laboratory gas flow setup.

The reactor was a fixed-bed reactor made of quartz shown in Figure 3.3. The inner and bottom tubes of the reactor were removable. Ammonia, O_2, H_2O, and half of N_2 were added through the bottom (1 in Figure 3.3), which functions as a preheating section, whereas NO and the other half of N_2 were added from the top of the reactor inlet (2 in Figure 3.3). With this arrangement, reactive gases could be kept separated until they were mixed, just above the catalysts placed on the porous

quartz plate. This minimises homogeneous and wall catalysed reactions in the pre-heating section, which, in any case, were negligible at the temperatures used here. The reactor temperature was measured below the porous quartz plate by a thermocouple shielded in a quartz tube. The reactor was placed in a three-zone oven for effective temperature control. Nitric oxide was analysed by a conventional UV analyser. No NH_3 measurements have been performed.

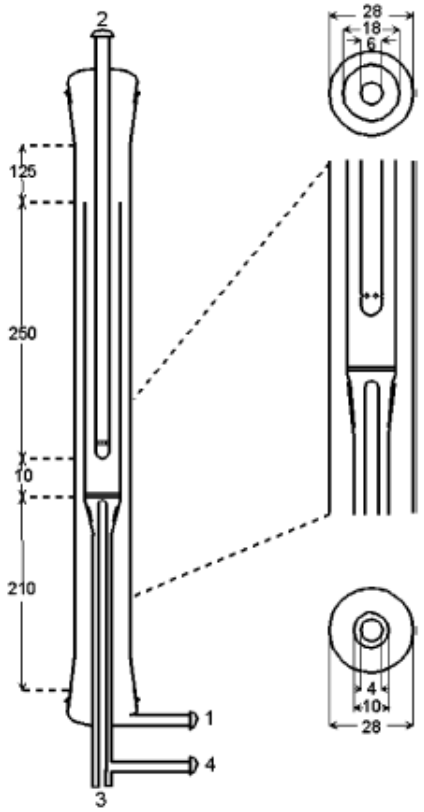

Figure 3.3 Sketch of the laboratory reactor. All shown measures are in millimeters. (1) Bottom gas inlet. (2) Top gas inlet. (3) Thermocouple. (4) Gas outlet.

The activity was measured on catalyst plates (1.7 x 1.7 cm^2) with a total flow rate of 3 l / min. The composition of the feed gas was 400 ppm NO, 500 ppm NH_3, 5 vol% O_2 and 1.4 vol% H_2O. Activities of the catalysts were typically measured in situ at 350 ^oC after attaining steady state values of temperature and conversion values. Steady state conversion values of NO and NH_3 gases were measured from online analyzers. As NH_3 is in excess, the observed reaction rate can be regarded as pseudo first order with respect to NO and zero order with respect to NH_3. The observed catalyst activity can be approximated by an observed rate constant *K* (m/s) with first order in NO as[42, 51]:

$$K=-SV*ln\ (1-X)/A_p \qquad (3.1)$$

Where SV is the space velocity which represents the flow rate of the flue gas per unit volume of the catalyst element, A_p is the geometric surface area per unit volume, and X is the fractional NO conversion. To compare the deactivation levels of different catalysts, the relative activity were used (Equation 3.2), which was defined in stage wise as shown in Figure 3.4.

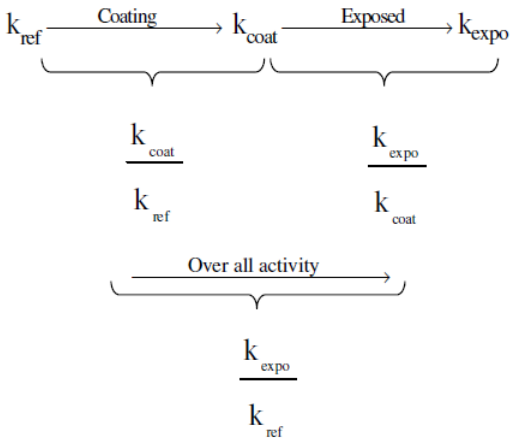

Figure 3.4 Relative activity determined for reference, coated and aerosol exposed catalyst plates.

Relative activity = K_{expo}/K_{ref} or K_{coat}/K_{ref} or K_{expo}/K_{coat} (3.2)

3.5 SEM and EDX analysis

The distributions of potassium in the exposed catalysts were investigated at the Centre for Microstructure and Surface Analysis, Danish Technological Institute by SEM-EDX on a LEO 440 microscope and Haldor Topsøe A/S. The samples were analyzed on the surface and on the cross section. To analyze the surfaces, the samples were attached on Al-stubs with carbon tape. The sample surfaces were analyzed in wet mode with water vapor in the microscope chamber. The samples were not coated. To analyze the cross sections, the samples were embedded and then polished (without water present) with SiC paper. To conduct the embeddings, they were coated with a thin layer of carbon. The embedded samples were operated in high vacuum. To improve the detection limit of the peaks in the X-ray analysis, WDX analysis is used in the microprobe.

Used instruments:

- Light Optical Microscope (LOM) for structure analysis.
- Quanta-SEM for structure analysis of the surface (operated at 20kV, 0.8mbar (wet mode)).
- Quanta-SEM for standard Energy Dispersive X-ray Spectrometry (EDX)-analysis (chemical analysis, operated at 20kV).
- Microprobe-SEM for Wavelength Dispersive X-ray Spectrometry (WDX)-analysis (chemical analysis, operated at 20kV).

Chapter 4

Initial screening tests

4.1 Coating materials

Possible coating materials could be metal oxides like Al_2O_3, MnO_x, MgO, TiO_2, $Zr(SO_4)_2$ as they showed good corrosion resistance to alkali substances [51]. Studies have shown that acidic carrier material has a beneficial influence on resistance to alkali poisons [52]. It must therefore be presumed that an acidic coating can increase deactivation resistance. In the present work various coating materials like manganese oxide, sulphated-ZrO_2, silica gel, titanium dioxide, aluminum oxide and magnesium oxide were tested, as discussed below.

Manganese oxide: Manganese (Mn)-based catalysts have been reported to be active for low temperature SCR of NO_x with NH_3. Unsupported Mn exhibited excellent activity for SCR of NO_x with NH_3 in the temperature range of 75-200°C [53]. Supported Mn catalysts, such as Mn/TiO_2 [54-56] and Mn/Al_2O_3 [57] were also active for low-temperature SCR of NO_x with NH_3.

Sulphated-ZrO_2: One of the possible ways to increase catalyst resistance to alkaline poisons is the use of materials, revealing high or super-acidic properties which would interact stronger with potassium than vanadium species. Arata et al. has identified a range of active sulphated oxides, i.e. ZrO_2, Fe_2O_3, SmO_2, TiO_2, etc. whose surface properties and mainly surface acidity significantly vary with sulphation [58]. Among these oxides, which can be used as support, zirconia is one of the most attractive, because it reveals the highest acidity with $H_0 \leq -16$, where H_0 is the Hammet acidity function.

Silica gel: High surface area (300-1000 m^2/g) material like SiO_2 can disperse the potassium poisons there by active vanadium can be protected.

Titanium Dioxide: As mentioned previously titanium dioxide (TiO_2) is also resistance to catalyst poisons. Since it is also the carrier material within the catalyst one can minimize the adverse effects due to presence of secondary material.

Aluminum oxide: The activated form of aluminum oxide has very high affinity for water. It also has a large specific surface area of between 150 and 500 m^2/g and can be synthesized for various pore size typically between 15 to 60 Å [59]. Since there are many opportunities to produce alumina with a specific meaning pore size and the substance is known to be particularly reactive, it is suitable for coating material blocking properties.

Magnesium oxide: A thin Mg film on a ruthenium (Ru001) surface has shown that potassium oxide reacts with Mg surface and favors the formation of KO complex [60]. This makes it attractive as a coating material which can bind potassium.

4.2 Selection of coating method

To find a suitable method for the coating on the catalyst plates trail experiments were conducted with various coating techniques and densities of aqueous suspensions. Possible coating techniques were dip coating, spray coating and paint brush or roller coating. Dip-coating technique causes water to penetrate into the catalyst plate and leaches the water-soluble catalytically active components like V_2O_5 and WO_3. Brush and paint roller has showed promising coating technique but, requires high viscosity of the suspension. Through this technique well distributed coating can be obtained but, the thickness of coating is very hard to control. Best results were obtained with an

air spray gun (1.5 bar) with a nozzle of diameter of 0.5 mm. This technique requires a lower viscosity. High viscosity can easily clog up the small nozzle. The technique provides very thin layer coating without changing the original structure of the catalyst plate. All the coated catalysts were prepared with air spray coating with 5-30 wt% aqueous suspension.

4.3 Particle size distribution

5-30 wt% aqueous suspensions were made with the powder materials. 3-5 mm glass beads were also used to reduce the particle size in a fluid shaking machine. The volume-based particle size distribution was measured on a HYDRO 2000s (laser sensor). The effect of further shaking with glass beads in the fluid shake machine is illustrated with the particle distribution of Mg coating in Figure 4.1, where the shaking number two is the green graph. Particle size distribution of the other coating materials is reported in Appendix-Chapter 4 (Page 68-72).

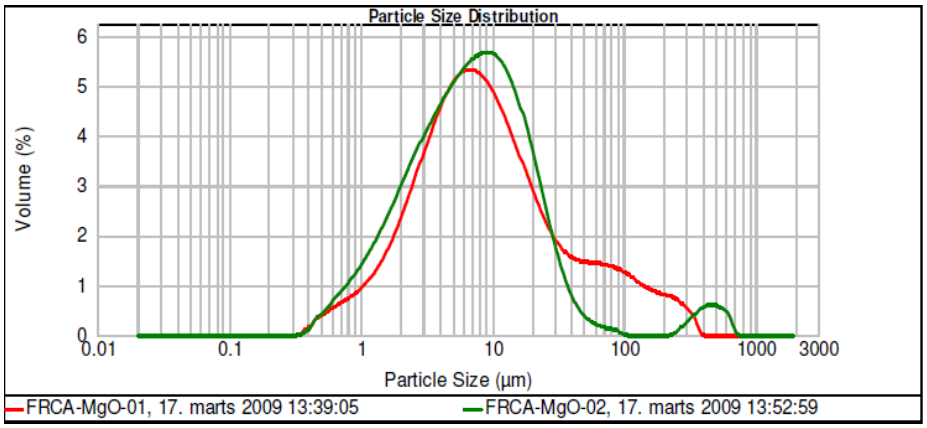

Figure 4.1 Particle size distribution of Mg coating (Vol. Weighted mean = 22.3 µm).

4.4 SEM analysis on fresh catalysts

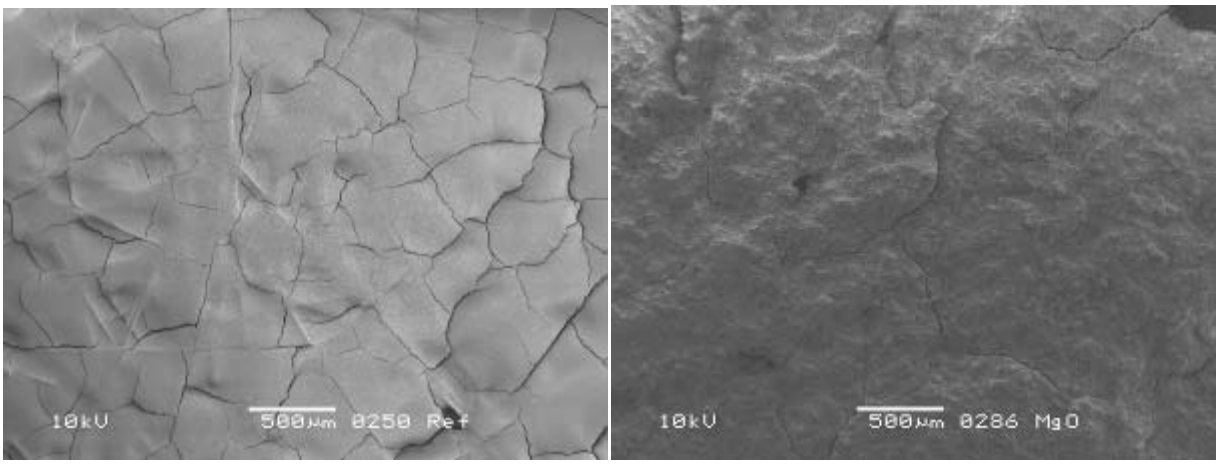

Figure 4.2 Reference (left) and Mg coated (right) catalyst SEM images (x35).

SEM images of surface and cross sections of the catalyst plates were recorded, with the aim to find out how the coating on the catalyst surface appeared. The coated catalyst plates were compared with uncoated coated plate (Reference). Several SEM images for both exposed and unexposed catalyst plates are listed in Appendix-Chapter 4 (Page 68-72). Surface and cross sectional SEM images can

be analyzed by taking Mg as an example. The SEM image of low magnification (x35) is shown in Figure 4.2. Rough surface of Mg coated catalyst can be observed with naked eye after calcination. It can also be seen that the surface seems uneven when compared to the reference plate. To find out the particle size in the coating, the SEM image was magnified 1000 times. As seen on the right in Figure 4.3, it was not evenly coated which was also evident in x35 magnification. It can also be observed that Mg particles appear to be varying shape with a tendency to form rounded edges.

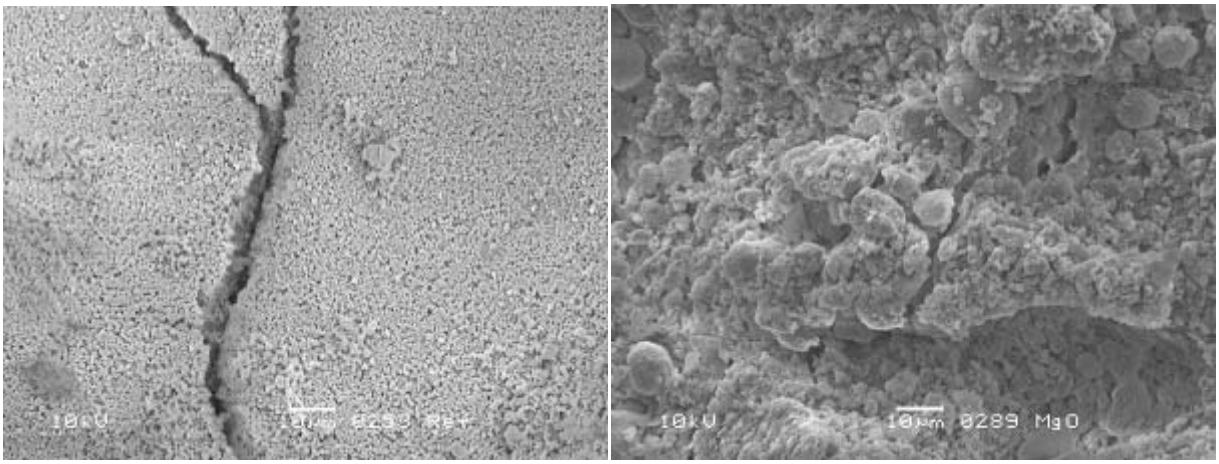

Figure 4.3 Reference catalyst (left) in conjunction with Mg coated catalyst (right) magnified images.

SEM cross section images were used to estimate the thickness of the coating. Since the thickness of the coating varies on the surface of the catalyst an average thickness value was estimated for the various coatings applied by taking an average of 7 arbitrary locations on a SEM picture. It is clear from Figure 4.4 that the Mg coating having problems with adhesion to the catalyst surface. It can also be observed that the thickness of coating vary about a factor of two from the thinnest to thickest. An estimate of an average thickness is 64 µm based on Figure 4.4 left. In close-up of the coating it is clear that there is non-uniformity in size or shape of particles, which is consistent with the measurement of particle distribution and surface pictures.

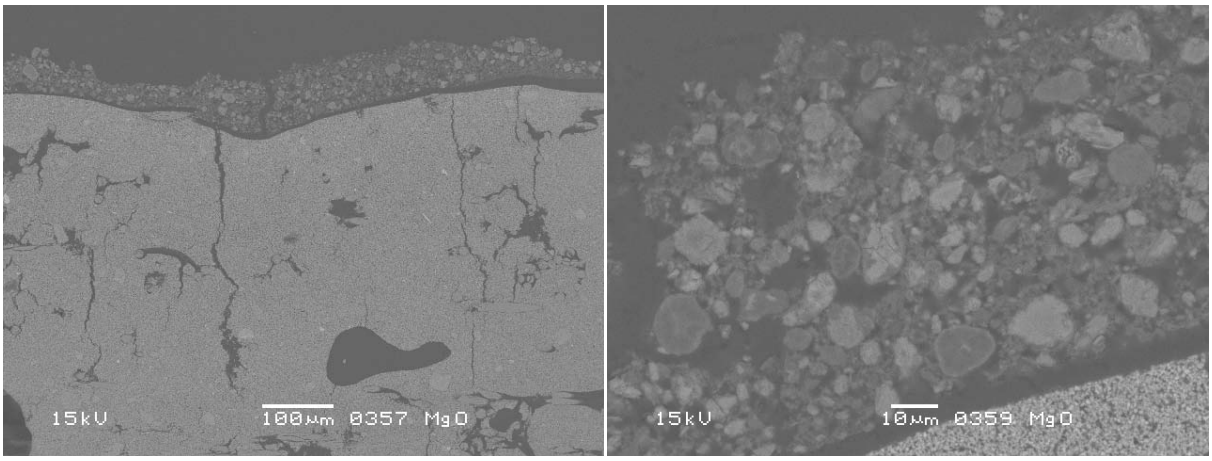

Figure 4.4 Mg coated cross sectional images (x150 and x1000); Estimated coating thickness = 64 µm.

In the similar way all the coated materials were analyzed with mean particle size, thickness of coating and adhesion as listed Table 4.1. All the materials showed an average particle size well

below 10 µm (except Mg = 22.30 µm) with these numbers one can expect very fine coat on the catalyst surface.

Table 4.1 Summary of coating results; particle size diameters (Vol. weighted mean), thickness (average of 7 arbitrary locations on the SEM image at 150 x magnification) and adhesion.

Coating material	particle size (µm)	thickness (µm)	adhesion
Manganese oxide (Mn)	6.40	16	ok
Sulphated-ZrO_2 (Sul-Zr)	3.00	19	ok
Silica gel (Si)	7.32	7	ok
Titanium dioxide (Ti)	2.30	11	ok
Aluminum oxide (Al)	9.10	60	not good
Magnesium oxide (Mg)	22.30	64	not good

4.5 SCR activity results

Catalytic activity of reference, coated and exposed catalysts are presented in Figure 4.5. From figure it is clear that the coated catalysts are showing less relative activity compared to that of reference catalyst. By coating the catalyst plates it seems reasonable to expect a decrease in activity because an additional film resistance is added. In some cases coating material may also be responsible for the NO reduction. Compared to the high activity of V_2O_5-WO_3/TiO_2 catalyst, coating contribution for enhancing the reaction can be neglected. Except Al and Mg, all the coated catalysts showed relative activity values (K_{coat}/K_{ref}) around 0.85 impaling that there is a thin coating on the catalyst which is responsible for the slight decrease in activity. That of Al and Mg catalysts showed relative values of 0.68 and 0.78 implying that the coating layer thickness is comparatively high. Coated catalysts activity trend is in accordance with the SEM cross sectional measurements (Table 4.1).

The relative activity (K_{expo}/K_{coat}) of the aerosol exposed catalysts to the corresponding fresh coated catalyst is shown in Figure 4.5. The reference catalyst showed a relative activity of 0.23 indicating severe deactivation of the catalyst. Similar deactivation patterns were also reported on reference catalysts by Zheng et al. [37, 61]. Among the coated catalysts Mg containing catalyst showed high alkali resistivity as compared to uncoated reference catalyst. Relative activity (K_{expo}/K_{coat}) of Mg coated catalyst is 0.75. Rest of the coated catalysts like Mn (0.40), Sul-Zr (0.35), Si (0.29) and Ti (0.39) catalysts showed less alkali resistivity compared to Mg coated catalyst. Al coated catalyst showed a relative value of 0.10 only, when compared to uncoated reference catalyst the level of deactivation is very high. All the measurements are taken based on the average values of 2 or 3 experimental runs to predict the accurate values by minimizing the experimental errors. There were no reports available in the literature to compare the SCR activity on protective coating DeNOx catalysts for alkali containing flue gases.

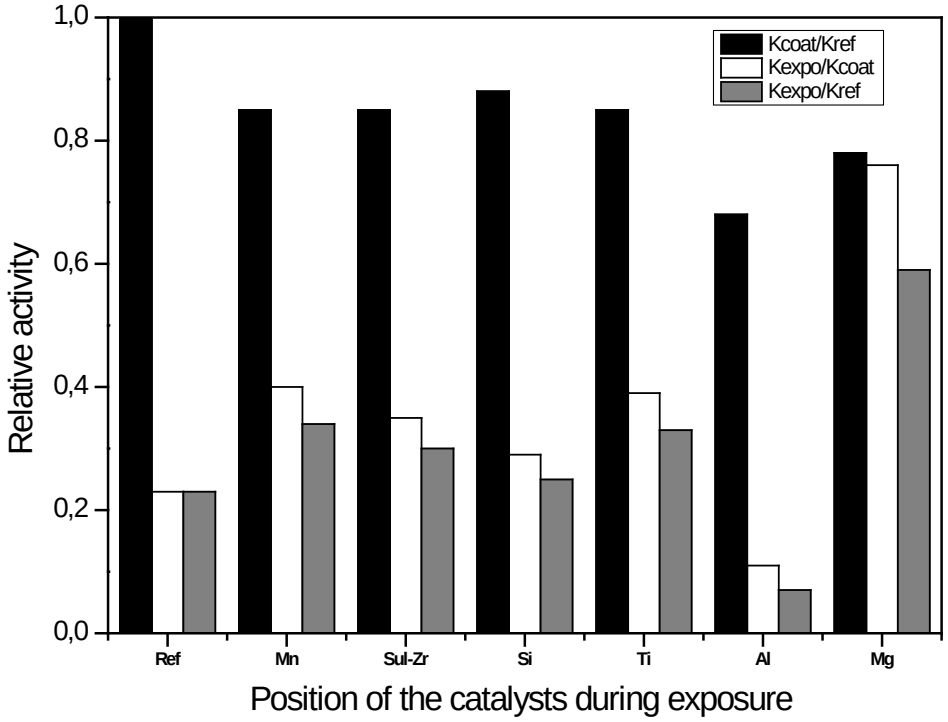

Figure 4.5 Relative activity of reference, coated and aerosol exposed catalysts for 650 h at 350°C.

Overall relative activity (k_{expo}/k_{ref}) of aerosol exposed catalysts to that of fresh or coated catalyst are also shown in Figure 4.5. Irrespective of type of coating and nature of material overall relative activity is a typical comparison to see the alkali resistivity. Among all the catalysts Mg coated catalyst (0.59) is performing better compared to that of uncoated reference catalyst (0.23). Other coated catalysts with overall relative value less than 0.5 are not considered from the commercial point of view.

4.6 SEM and EDX analysis of deactivated catalysts

To compare the intensity of deactivation and to obtain an understanding of the way of working at the different coating on various catalysts SEM images and EDX analysis is used. The aim was to identify the deposited potassium concentration on the surface and the cross section of the catalyst plates. Catalyst plates were primarily tested with two types of images in the following sections:

1. SEM surface images
2. SEM cross-sectional images

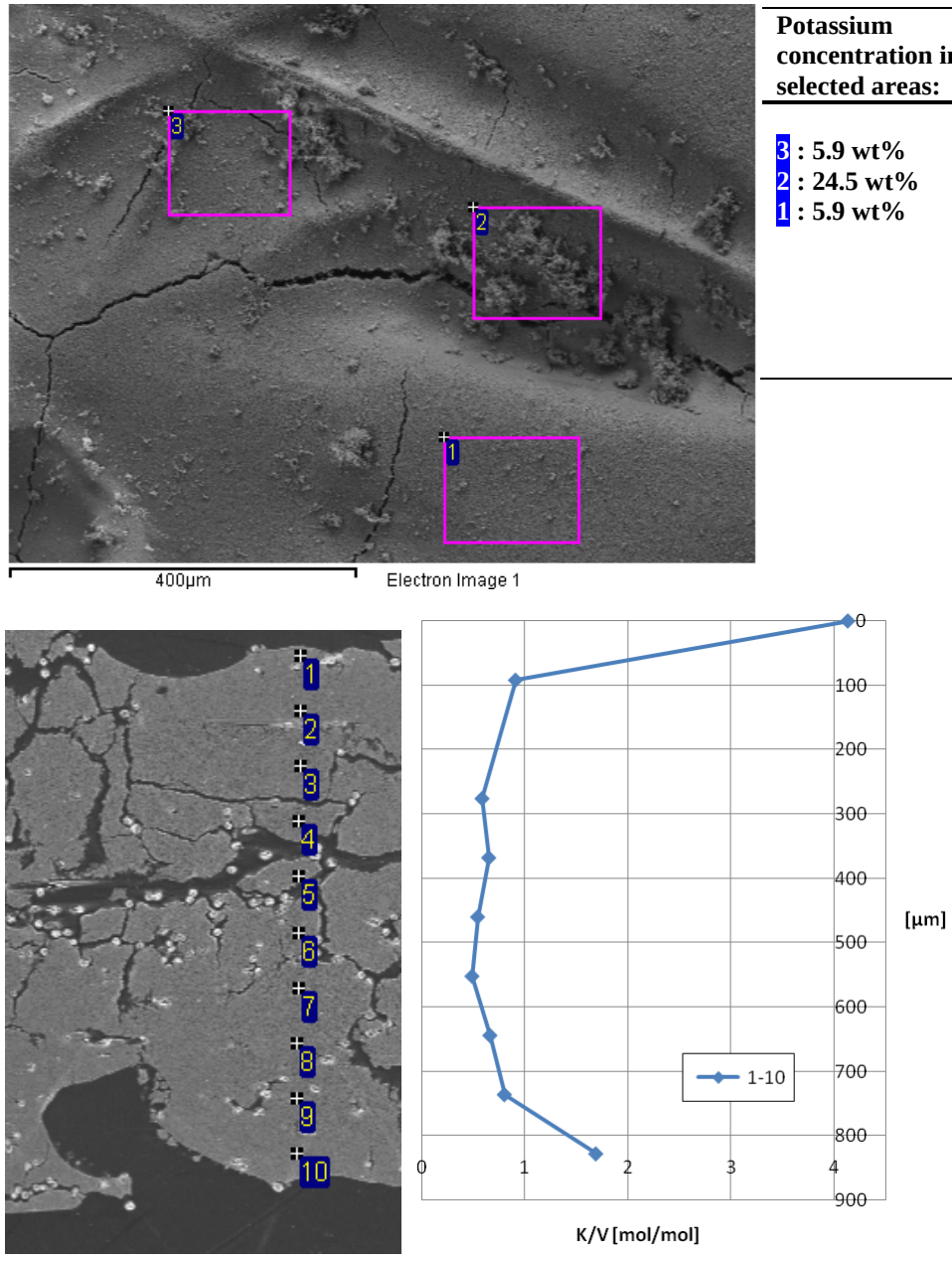

Figure 4.6 Reference catalyst plate exposed for 650 hours with potassium chloride: surface potassium concentration (top), catalyst plate cross section and K/V concentration (bottom).

EDX analysis is used to measure the potassium concentration on the surface and the cross section images of reference and coated catalysts. It can be seen from Figure 4.6 that the potassium concentration on the outer surface is varying from point to point. High concentration may be due to agglomeration of potassium aerosols. Another possible prediction could be the position of the catalyst plate during the aerosol exposure, it is expected that the rate of aerosol deposition could decrease along the length of the catalyst. K/V molar ratio over the cross-section of the reference plate clearly shows that at the surface (K/V=4.2) of the plate there is a high potassium concentration is there and approximately constant ratio is seen along the cross section (K/V = 0.5). It indicates that the potassium aerosols are not only deactivating the surface vanadium active species but also diffusing along the cross section of the plate causing worse deactivation. K/V molar ratio about 0.5

is enough for a significant chemical deactivation according to lab-scale study using the wet impregnation [42] and biomass fired power plant exposure [37, 51].

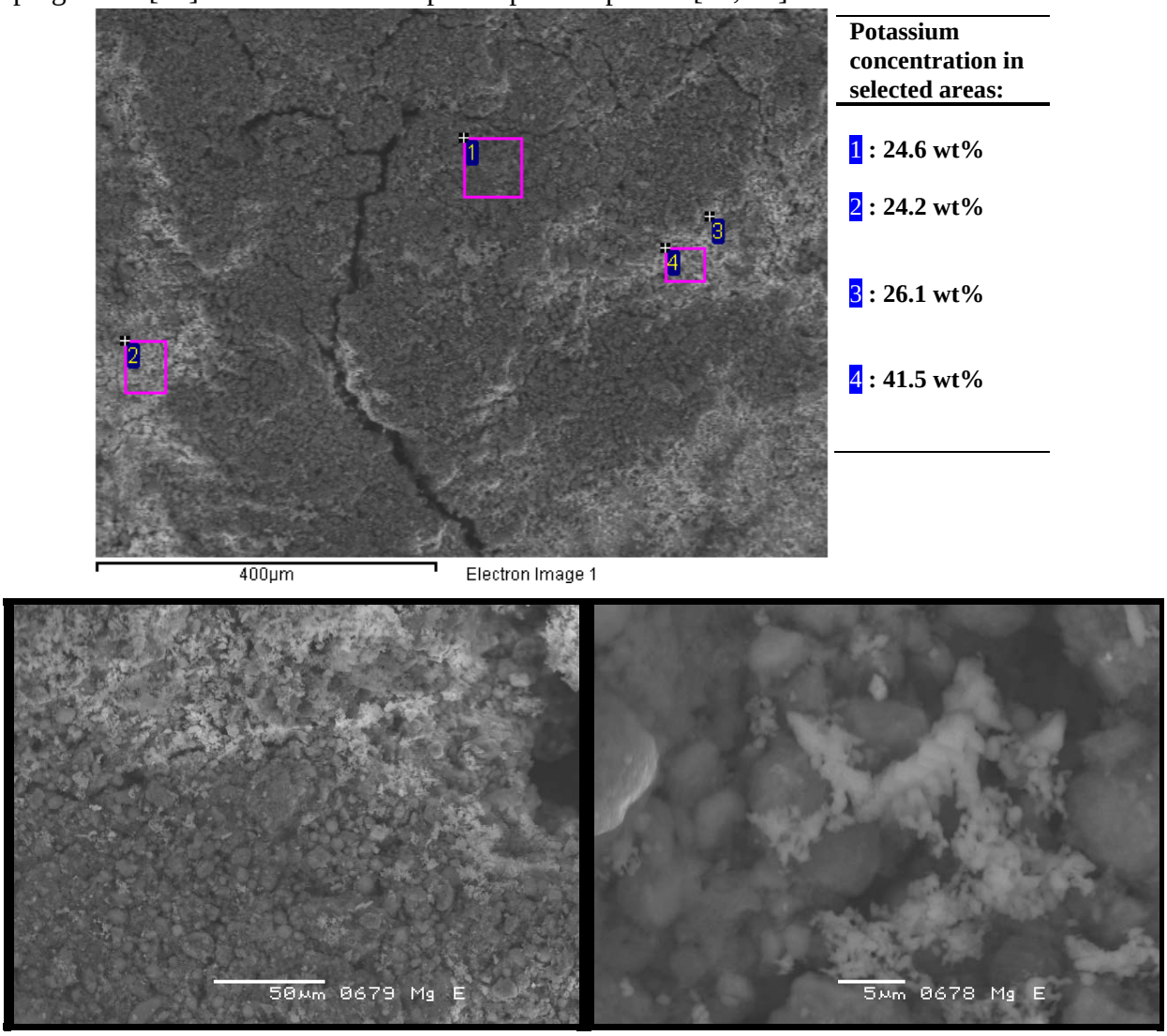

Figure 4.7 Mg coated catalyst plate exposed for 650 hours with potassium chloride: surface potassium concentration (top), magnified images (bottom).

Mg coated catalyst showed high alkali resistivity in the SCR activity measurements. SEM and EDX analysis of the catalyst surfaces coated with Mg is examined with a focus on the surface concentration of potassium and the result shown in Figure 4.7. In addition to that two magnified images were also are displayed (bottom). EDX analysis showed potassium surface concentration of 25.0 mass percent. The surface potassium composition of Mg coated catalyst is generally much higher than the reference catalyst. Figure 4.7 also shows the magnified images of Mg exposed catalyst with potassium chloride accumulation. It can be seen that potassium chloride is gathered closely around the particles of Mg coating. The average particle diameter of Mg particle is reproduced approximately 10-20 µm, and about 0.2 µm for potassium chloride which is also reported by Zheng et al. [37, 61].

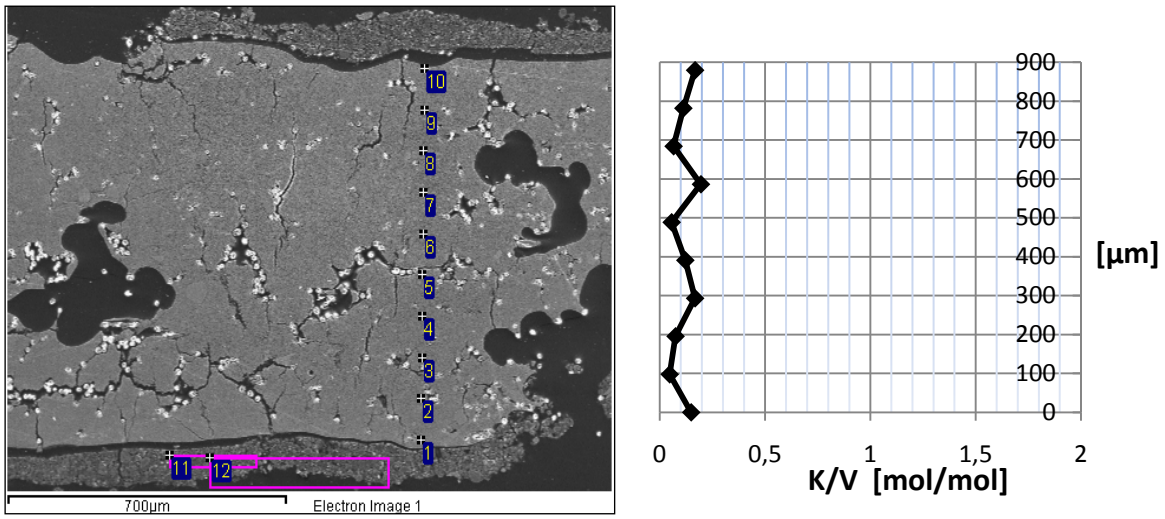

Figure 4.8 EDX analysis for 10 points on the cross section of the Mg catalyst plate.

EDX analysis across the cross section of the Mg coated catalyst plate with a concentration profile of potassium / vanadium ratio is shown in Figure 4.8. It is interesting that the profile of potassium concentration along the cross section is almost constant. Since all potassium concentrations significantly below background noise limit for EDX measurements, it is reasonable to believe that the potassium content is virtually zero. In a similar way all the SEM and EDX measurements were recorded for other coated catalysts (Appendix-Chapter 4, Page 68-72).

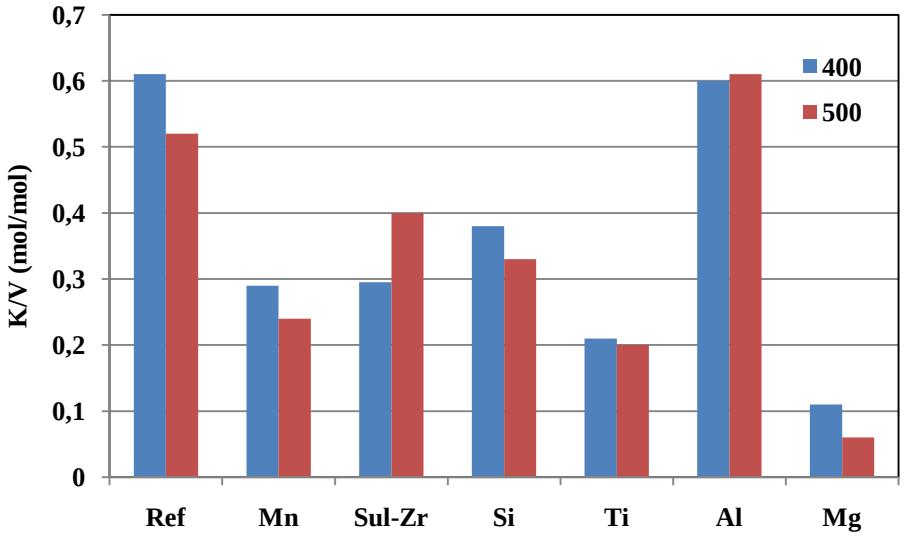

Figure 4.9 K/V molar ratio of catalysts at 400 and 500 µm from the catalyst surface.

On the basis of EDX analysis the K/V molar ratio found for all the exposed plates at 400 and 500 µm from the catalyst surface are shown in Figure 4.9. As mentioned earlier, the ratio between potassium and vanadium on a molar basis vs cross section is considered, to know how many active vanadium sites are occupied by potassium.
For the reference catalyst the K/V ratio at 400 and 500 µm from the catalyst surface is approx. 0.5-0.6. Previous studies have shown a K/V ratio of about 0.7 in the equivalent distance from the catalyst surfaces. Similar experiments were performed and reported by Zheng et al. [37, 61], with a longer exposure time of around 1800 hours, which may explain the somewhat higher K/V ratio. Mg

coated catalyst showing very low K/V ratio at 400 and 500 μm from the catalyst surface is approx. 0.11 and 0.06, respectively. That of other coated catalysts Mn, Zr, Si and Ti catalysts showed K/V ratio 0.2-0.4. It can be said that all the coated catalysts provide a protection against potassium up to certain extent. Coating with Al has not been successful. Overall there is a good relation between the SCR alkali resistivity and K/V ratio across the cross section for all the catalysts mentioned in this batch of the catalysts.

4.7 Conclusions

It was found that the spray gun gives the best coating on the catalyst surface, especially in terms of thin and uniform coating. Various coated catalysts have been analyzed with particle distribution and SEM. In experiments with Mg it was observed that the coating has a tendency to crack on the surface of the catalyst. It is found that the Mg coating has an average thickness of 64 μm and is composed of larger particles with an average diameter of 22.3 μm according to SEM analysis.

Based on activity measurements it can be concluded that catalyst plate coated with Mg showed improved deactivation resistance. The Overall relative SCR activity (k_{expo}/k_{ref}) of the Mg coated catalyst was 0.59 and that of exposed reference plate is measured to be 0.23 i.e. the resistance of the Mg- coated catalyst is 2.5 times better. Surface analysis of the reference plate showed a highly variable potassium concentration of 5-24.5 wt (%). Mg coated catalyst showed even higher surface concentrations of potassium ranging from 19.4 to 41.5 wt (%) indicating that the Mg coating acts as a barrier to the potassium, instead of allowing it to diffuse into the catalyst. Across the cross section the Mg coated catalyst has lowest potassium concentration. The cross section results indicate that Mg coating virtually prevents potassium to reach the catalyst interior. From EDX analysis an average K/V ratio of 0.12 was observed on the catalyst outer surface while reference catalyst showed an average K/V ratio of 0.6.

Based on activity measurements, SEM and EDX analysis it is concluded that Mg coated catalyst has improved alkali deactivation resistance. The overall assessment is that it is possible to protect the SCR catalyst against alkali poisons through the coating technique.

Chapter 5

Zeolite coatings

5.1 Coating materials

In this chapter Mg coating adhesion property is improved by taking dilute aqueous suspensions with single and double coating to control the thickness. Furthermore, additional possible coating materials considered are: Sulphated –ZrO_2, HBETA-150, HBETA-25 and Montmorillonite. It has been reported that zeolites (HBETA) are considered to be highly alkali resistant support materials [48, 62-64]. Some of the properties and supplier data is given below.

Magnesium oxide: Supplier: Sigma Aldrich, Formula: MgO, M.Wt: 40.30 g/mol.

Sulphated-ZrO_2: Supplier: Saint-Gobain, Formula: $Zr(SO_4)_2$, M.Wt: 285.4 g/mol, Surface Area:150 m^2/g.

HBETA-150: Supplier: Zeolyst international, Tetragonal crystal structure with straight 12-membered ring channels (7.6 x 6.4 Å) with crossed 10-membered ring channels (5.5 x 6.5 Å), Si/Al=150.

HBETA-25: Supplier: Zeolyst International, Surface area: 680 m^2/g, Si/Al=25.

Montmorillonite (K-10): Supplier: Sigma Aldrich, Formula:$(Na,Ca)_{0.3}(Al, Mg)_2Si_4O_{10}(OH)_2.n(H_2O)$, M.Wt: 549.07g/mol, Surface area:250 m^2/g.

5.2 Particle size distribution

In the previous batch Mg coated catalyst was prepared with 30% aqueous suspension. In this section 15% aqueous suspension is used in an attempt to make better coating without forming cracks. Other coatings were made with 5% aqueous suspensions. From Figure 5.1 it is interesting to see HBETA-150 coating material showing bimodal particle size distribution with average particle size (D_{50}) of 3.63 μm. With 15% aqueous suspension solution Mg coating showed average particle size of 6.24 μm (Figure 5.1). The average particle size of the coating materials measured from the HYDRO 2000G instrument is listed in Table 5.1.

Table 5.1 Average particle size of coating materials.

Coating material	Average particle size (μm)
Magnesium oxide (Mg)	6.24
Sulphated-ZrO_2 (Sul-Zr)	2.03
HBETA-150	3.63
HBETA-25	5.61
K-10	11.49

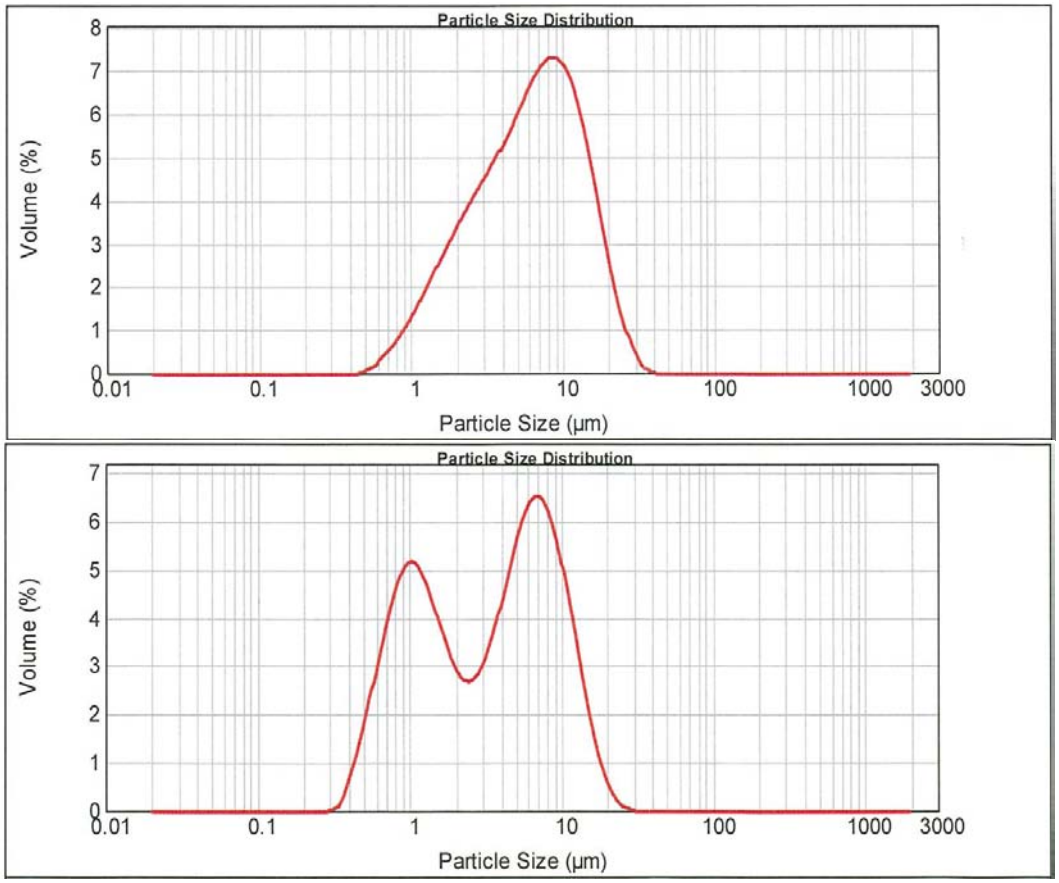

Figure 5.1 Particle size distribution of Mg coating (top) and HBEA-150 (bottom).

5.3 SCR activity results

Catalytic activity of reference, coated and aerosol exposed catalysts are presented in Figure 5.3. From figure it is clear that the coated catalysts are showing less relative activity compared to that of reference catalyst as already seen in Chapter 4. Mg-1 and Mg-2 represent Mg coating with single and double coat, respectively. All the coated catalysts showed relative activity (K_{coat}/K_{ref}) values of 0.7 to 0.9 impaling that the coating is very thin. Mg-2 coated catalyst showed less relative value compared to Mg-1 because of the double coating. HBEA-150, HBEA-25 and K-10 coated catalysts showed relative activity around 0.9 even though they coated with similar concentration and coating method.

The relative activity of the aerosol exposed catalysts to that corresponding fresh coated catalyst is shown in Figure 5.3. The reference catalyst showed a relative activity (K_{expo}/K_{coat}) of 0.25 showing severe deactivation of the catalyst and in good agreement with the result of Chapter 4 for the reference catalyst. Among coated catalysts Mg-1 and HBEA-25 catalysts showed alkali resistivity as compared to the uncoated reference catalyst. The relative activity of Mg-1 and HBEA-25 are 0.34 and 0.48, respectively. The remaining coated catalysts like Mg-2 and Sul-Zr, HBEA-150 and K-10 catalysts did not showed any alkali resistivity, instead they further deactivated the catalysts when compared to uncoated reference catalyst and the reason is not clear, but may involve changes in the coating layer thickness and concentration of the aqueous suspension. In this series Mg coated catalysts did not showed superior performance this was a disappointing result. This will be investigated further.

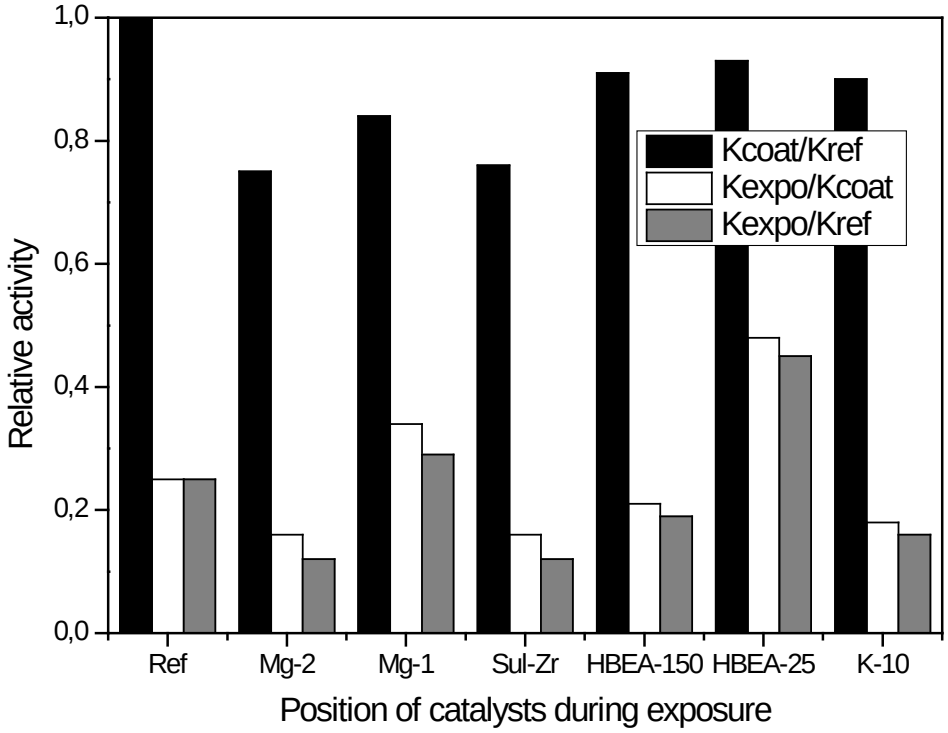

Figure 5.3 Relative activity of reference, coated and aerosol exposed catalysts for 850 h at 350°C.

The Overall relative activity of aerosol exposed catalyst to that of fresh reference (K_{expo}/K_{ref}) is shown in Figure 5.3. Among all the catalysts Mg-1 and HBEA-25 catalysts are performing better compared to that of uncoated reference catalyst. Mg-1 and HBEA-25 catalysts showed relative decrease of 0.29 and 0.45, respectively.

HBEA zeolite with Si/Al ratio around 20-25 is reported active for NH_3-SCR, and is especially preferable for alkali containing flue gases [48, 62, 64]. Cu-Zeolite and Fe-Zeolite catalysts showed high poison resistance when compared to commercial vanadium catalysts [48, 62]. Such a high alkali resistivity is due to high surface area and acidity of the zeolite supports compared to simple metal oxides like TiO_2.

The superior activity of HBEA-25 can be well discussed with the surface composition the catalysts with SEM and EDX analysis. Coating acts as an alkali barrier for there by active vanadium sites can be protected.

From the chapter 4 we identified suitable coating method by studying the surface and cross sectional images of the fresh catalysts. From this section onwards the fresh catalysts are not considered for the SEM and EDX analysis for the faster screening of the coated catalysts. Only promising SCR alkali resistant catalysts are considered for detailed surface analysis.

5.4 SEM and EDX analysis of deactivated catalysts

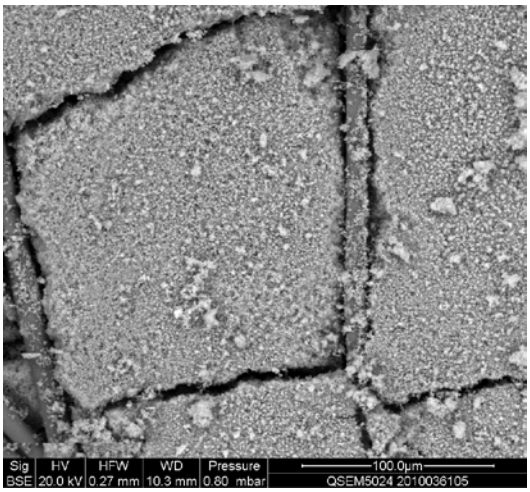

Elements	Scan 1 (wt%)	Scan 2 (wt%)
K	5,7	6,9
Ti	40,3	39,5
V	1	1
W	7,3	7,3

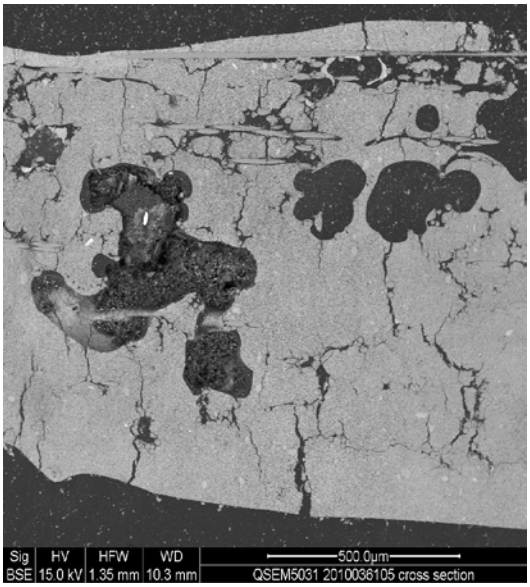

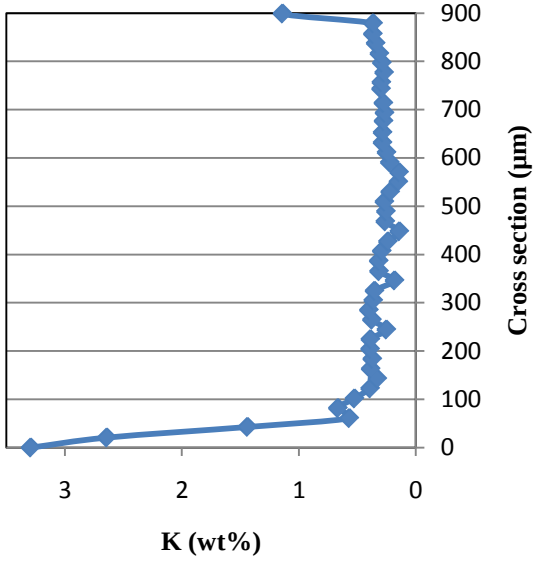

Figure 5.4 Reference catalyst plate exposed for 850 hours with potassium chloride. Surface potassium concentration (top) 6.3 wt%; potassium concentration along the catalyst plate cross section (bottom).

The surface of the reference catalyst with potassium concentration can be seen from Figure 5.4 (top). Average surface composition of potassium observed was 6.3 wt%. Other major catalyst components are Ti, W and V. The content of vanadium is very near to the 1.2 wt% from the EDX analysis. At one end of the plate potassium concentration is 3.4 wt% (Bottom) and approximately constant value is seen along the cross section (K= 0.45 wt%). Potassium concentration is gradually decreasing along the thickness of the plate. It further indicates that the potassium aerosols are not only deactivating the surface vanadium species but, also diffusing along the cross section of the plate causing intense deactivation [37, 61]. In this reference catalyst without any coating protection severe deactivation is observed up to 130 µm thickness with potassium concentration above the average value.

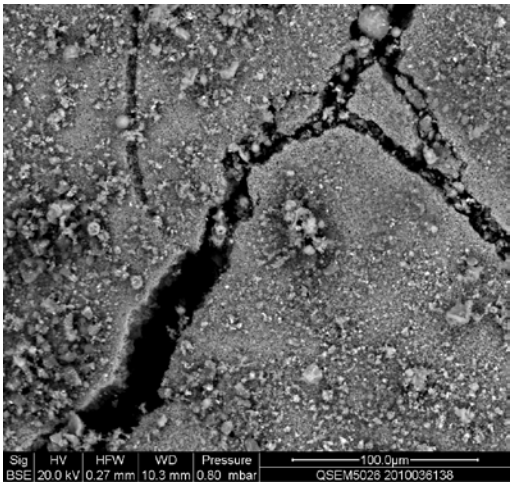

Elements	Scan 1 (wt%)	Scan 2 (wt%)
Al	<1	0
Si	6,9	5,1
K	5,4	4,8
Ti	32,1	36,1
V	1	1
W	7,6	9

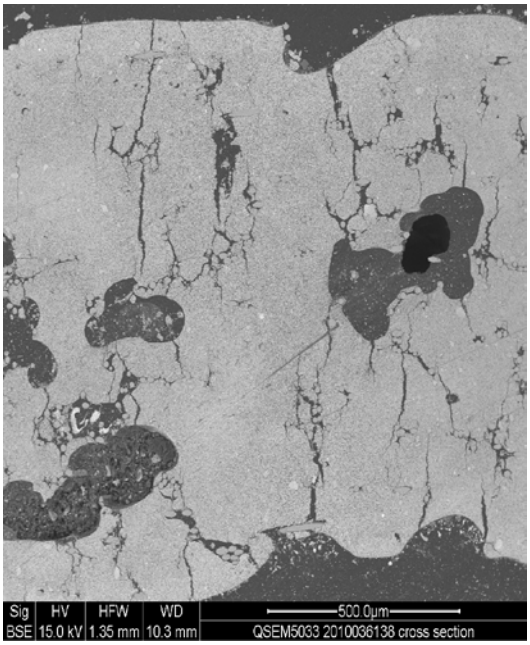

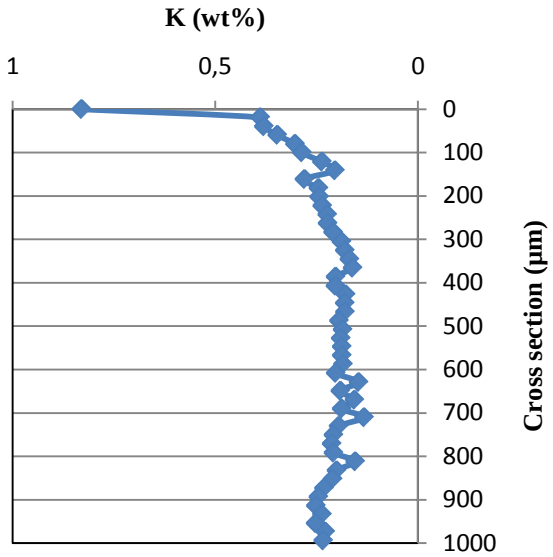

Figure 5.5 HBEA-25 coated catalyst plate exposed for 850 hours with potassium chloride. Surface potassium concentration 5.1 wt% (top); potassium concentration along the catalyst plate cross section (bottom).

A surface image of the HBEA-25 coated catalyst with potassium concentration is shown in Figure 5.5 (top). Average surface composition of potassium observed was 5.1 wt%. The elemental composition indicates that the HBEA-25 coating is present on the surface and is responsible for SCR alkali resistivity. Zeolites are known to be strong acidic materials with Si/Al ratio ranging from 10-40. The potassium concentration at one end of the plate showed a value of 0.75 wt% and approximately constant value is seen along the cross section (K= 0.22 wt%). The potassium concentration is decreasing along the thickness of the plate. Compared to the reference catalyst (K= 0.45 wt%), HBEA-25 coated catalyst showed a lower potassium concentration along the cross section of the plate. It further indicates that the potassium aerosols are only available at the surface, not along the cross section of the catalyst plate. The SCR alkali resistivity and potassium blocking ability is due to the highly acidic nature of the HBEA-25 zeolite.

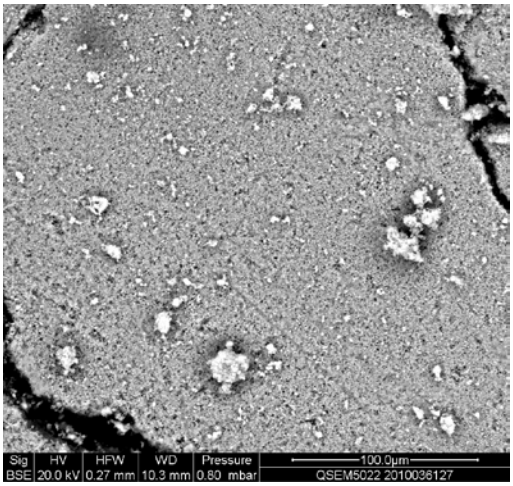

Elements	Scan 1 (wt%)	Scan 2 (wt%)	Scan 3 (wt%)
Si	1,4	1,4	1,6
K	3,1	4,7	3,2
Ti	48,7	46,5	49,9
V	1	1	1
W	6,2	6,3	6

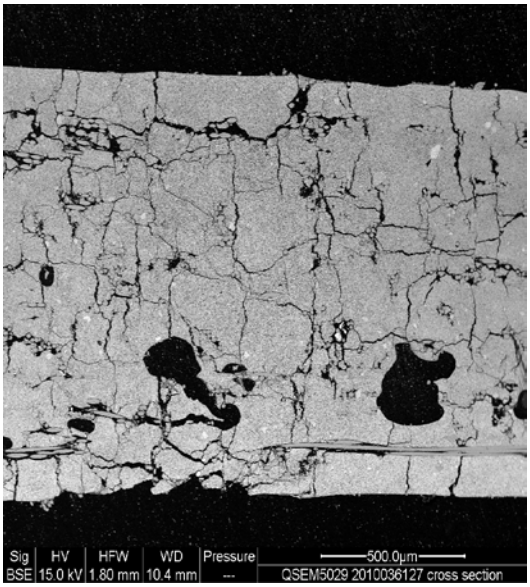

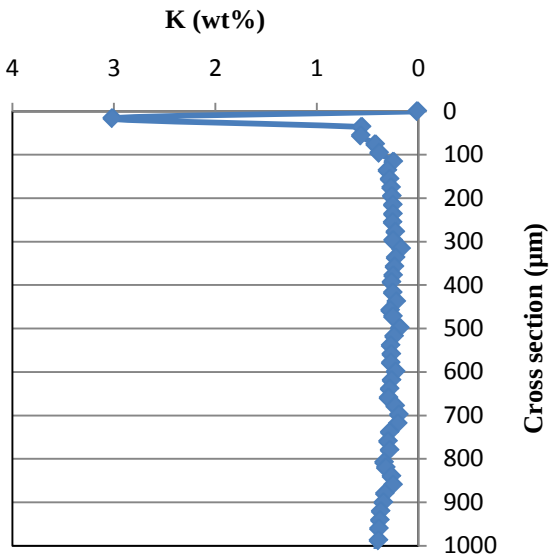

Figure 5.6 HBEA-150 coated catalyst plate exposed for 850 hours with potassium chloride. Surface potassium concentration 3.7 wt% (Top); potassium concentration along the catalyst plate cross section (bottom).

A surface image of the HBEA-150 coated catalyst with potassium concentration is shown in Figure 5.6. Average surface composition of potassium observed was 3.7 wt%. Other catalyst components like Ti, V, W and Si were also seen. There is no or undetectable level of Al in the coating. With the given Si/Al = 150 the HBEA material is considered to be neutral or only slightly acidic. HBEA-150 coating did not show appreciable SCR alkali resistivity because, there is no acidic medium to counteract the potassium. Potassium concentration over the surface of the plate showed a value of 3.2 wt% and an approximately constant value is seen along the cross section (K = 0.3 wt%) after 100 µm. It indicates that the neutral zeolite coating cannot act as a potassium resisting barrier.

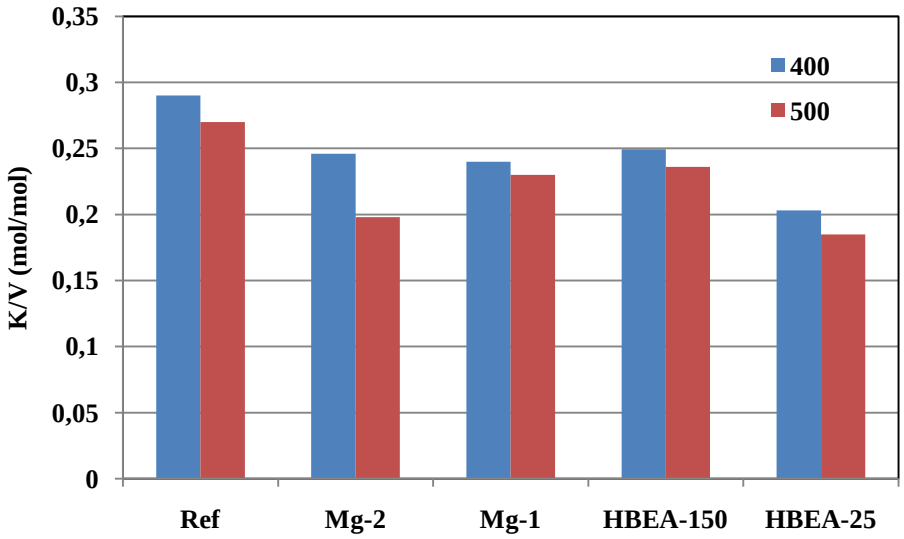

Figure 5.7: Potassium concentration of catalysts at 400 and 500 µm from the catalyst surface.

On the basis of elemental analysis potassium concentrations found for all the exposed plates over 400 and 500 µm from the catalyst surface are shown in Figure 5.7. For the reference catalyst, the potassium concentration at 400 and 500 µm from the catalyst surface is approx. 0.29 and 0.27 wt%, respectively. HBEA-25 catalyst showed a potassium concentration of 0.12 and 0.17 wt% at 400 and 500 µm, respectively from the surface. That of Mg-1, Mg-2 and HBEA-150 catalysts showed potassium concentration around 0.25 wt% i.e. the same on the reference catalyst within the uncertainty. Sul-Zr and K-10 were not considered for surface analysis due to poor SCR alkali resistivity.

5.5 Conclusions

Faster screening of promising materials like zeolites and Mg were tested for SCR alkali resistivity. Based on SCR activity measurements HBEA-25 coatings showed improved deactivation resistance. Overall relative activity (K_{expo}/K_{ref}) of the catalyst plate coated with HBEA-25 is 0.45 and that of reference plate showed to be 0.25.

Surface analysis of the reference plate showed a potassium concentration of 6.3 wt (%). Acidic HBEA-25 coated catalyst showed less potassium 5.1 wt%.

Across the cross section HBEA-25 coated catalyst has lowest potassium concentration compared to that of the reference catalyst. The cross section results indicate that HBEA-25 coating prevent potassium to reach the catalyst surface. Mg coated catalysts are not performed well in the present batch. After examining SEM images of the exposed catalysts there was very thin coating or film on the surface and performing like a reference catalyst without any protection (Check Appendix-5, page 74).

Chapter 6

Improved Mg coating with Si binder

6.1 Coating materials

In the chapter 4 and chapter 5 it was concluded that the Mg and zeolite containing coatings were promising for the SCR of alkali containing flue gases. In the chapter 5 adhesion property of Mg coated catalysts were very poor and resulted with poor alkali resistivity. In this chapter the Mg coating properties were improved by adding Si gel as a binder. In this section the possible coating materials considered are Mg, Mg with Si gel, HZSM5-15, HZSM5-140 and HMordenite-10.

Magnesium oxide: Supplier: Sigma Aldrich, Formula: MgO, M.Wt: 40.30 g/mol.

Magnesium oxide with Silica gel: Silica gel supplier: Haldor Topsøe.

HZSM5-140: Supplier: Zeolyst international, framework of ZSM-5 is composed of straight 10-ring, elliptical channels (pore dimension: 5.3 x 5.6 Å) running along the [0 1 0] direction and sinusoidal 10-ring, elliptical channels (pore dimension: 5.1 x 5.5 Å) along the [1 0 0] direction, Si/Al=140.

HZSM5-15: Supplier: Zeolyst International, Surface area: 500 m^2/g, Si/Al=15.

HMordenite-10: Supplier: Zeolyst International, Orthorhombic crystal structure with straight 12-membered ring channels (6.5 x 7.0 Å) and crossed 8-membered ring channels (2.8 x 5.7 Å), surface area: 400 m^2/g, Si/Al=10.

6.2 Particle size distribution

In this chapter 5 wt% Mg and 15 wt% Mg suspension coatings were tested for better coating. All the other coatings were made with 5 wt % aqueous suspension. From Figure 6.1 it can be observed that the average particle size (D_{50}) of 5 wt % Mg and 15 wt % Mg coatings are 9.96 and 8.21 μm, respectively. The average particle size of the coating materials measured from the HYDRO 2000G instrument is listed in the Table 6.1. Mg-Si coating showed decreased particle size after adding the binder to the Mg. Zeolite based coating (HZSM5-15, HZSM5-140 and HMordenite-10) showed very less particle size around 2 to 3 μm.

Table 6.1 Average particle size of coating materials.

Coating material	Average particle size (μm)
HZSM5-140	2.03
HZSM5-15	3.40
5% Mg-5% Si	6.56
5% Mg-1% Si	8.97
5% Mg	9.96
15% Mg	8.21
HMOR-10	2.42

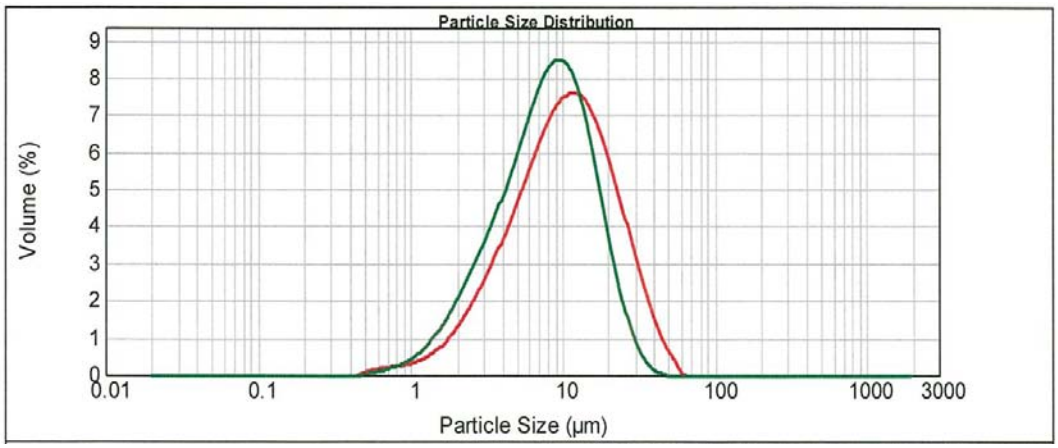

Figure 6.1 Particle size distribution of 5 wt % Mg coating (---) and 15 wt % Mg coating (---).

6.3 SCR activity results

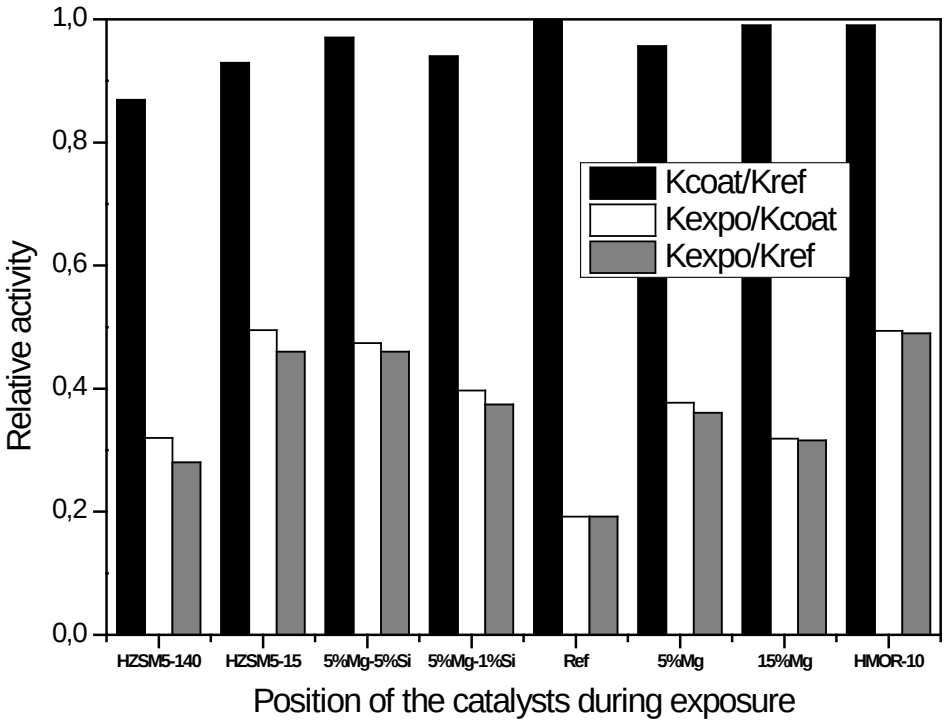

Figure 6.2 Relative activity of reference, coated and aerosol exposed catalysts for 850 h at 350°C.

Catalytic activity of reference, coated and aerosol exposed catalysts are presented in Figure 6.2. From figure it is clear that the coated catalysts are showing less relative activity compared to that of reference catalyst. 5% Mg and 15% Mg represent Mg coating with 5 wt% and 15 wt% aqueous solution, respectively. All the coated catalysts showed relative activity (K_{coat}/K_{ref}) values around 0.9 showing that the coating is providing a low additional resistance to diffusion of the reactants.

The relative activity of the aerosol exposed catalysts to the corresponding fresh coated catalyst is shown in Figure 6.2. The reference catalyst showed a relative activity (K_{expo}/K_{coat}) of 0.192 which indicates that there is severe deactivation of the catalyst once again. All the coated catalysts were performing better than the uncoated reference catalyst. Relative activity of 5% Mg and 15% Mg was 0.377, 0.319, respectively. Mg coating with Si binder showed improved alkali resistivity of 0.474 and 0.397 for 5% Mg-5% Si, 5% Mg-1% Si, respectively. Zeolite based HZSM5-140, HZSM5-15 and HMOR-10 coated catalysts showed relative activity of 0.32, 0.495, and 0.494, respectively. It again proved that zeolite with Si/Al ratio around 10-25 are promising alkali resistant barriers as also observed in chapter 5 with HBEA-25 coating. Overall relative activity (K_{expo}/K_{ref}) of aerosol exposed catalyst to that of fresh reference is shown in Figure 6.2. Coated catalysts showed an activity trend of HZSM5-15 (0.495) > HMOR-10 (0.49) > 5% Mg-5% Si > 5%Mg-1% Si (0.374) > 5% Mg (0.361) > 15% Mg (0.316) > HZSM5-140 (0.28) > Ref (0.192).

6.4 SEM and EDX analysis of deactivated catalysts

	Wt %		
	K	**Ti**	**W**
1	3,6	47,7	9,7
2	4,0	54,6	10,2
3	3,4	45,8	8,0
4	3,7	49,2	9,6

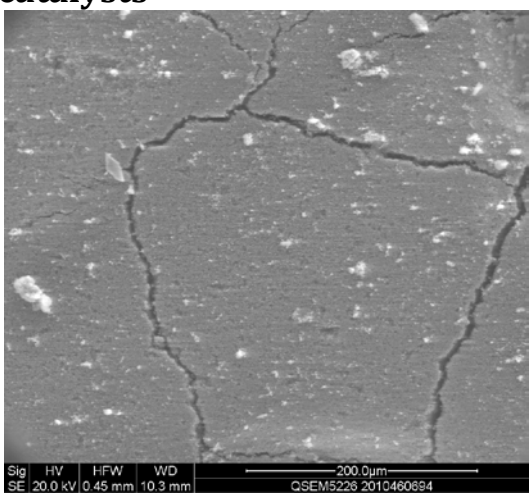

	Wt %		
	K	**Ti**	**W**
1	0,7	52,8	8,9
2	0,8	48,3	8,2
4	0,5	47,5	7,5
6	0,9	49,9	8,1

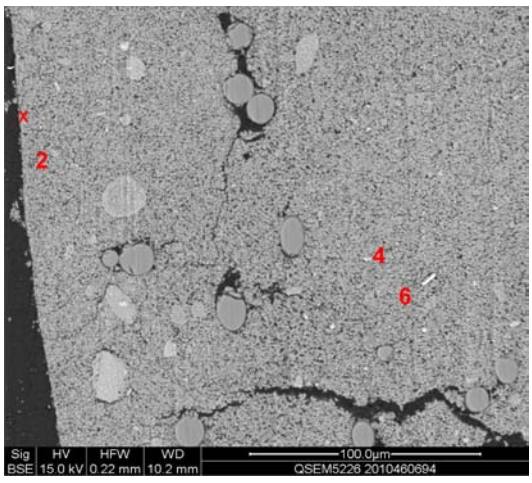

Figure 6.3 Reference catalyst plate exposed for 850 hours with potassium chloride. Surface potassium concentration (top) 3.675 wt%; catalyst plate cross section (bottom).

It can seen from Figure 6.3 (top) that the surface image of the reference catalyst with potassium concentration can be seen. The average surface potassium concentration observed was 3.675 wt%. The surface image reveals that the potassium is deposited evenly in the reference plate. Cross section image showed that the potassium is penetrated through the wall with a concentration of

0.725 wt%. The cross section images showed higher potassium concentration up to a distance of 100-150 µm from the surface, which further indicate that the potassium is penetrating the wall (Appendix- Chapter 6, page 75).

	Wt %			
	K	**Si**	**Ti**	**W**
1	4,1	43,8	2,1	2,1
2	3,5	39,7	0,8	1,4
3	4,3	45,4	1,0	1,5
4	4,4	44,3	0,7	1,8

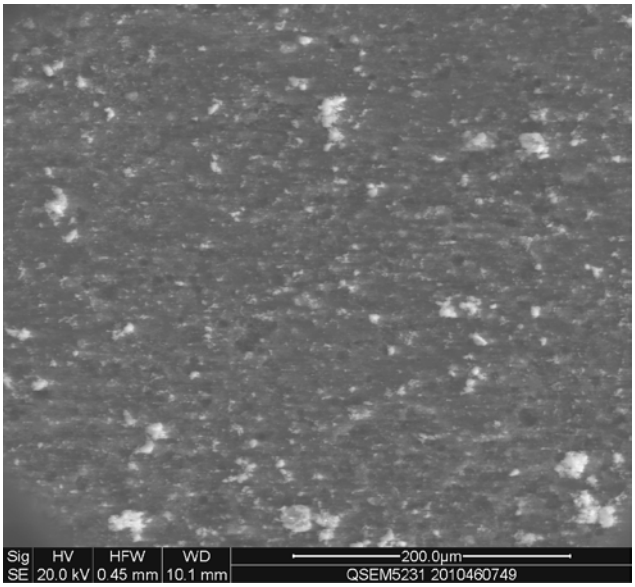

	Wt %			
	Si	**K**	**Ti**	**W**
1	50,1	2,8	0,5	1,9
2	50,6	3,6	0,8	2,8
6	1,4	0,5	52,5	7,4
7	1,8	0,4	48,7	8,9
9	1,4	0,5	50,4	7,9

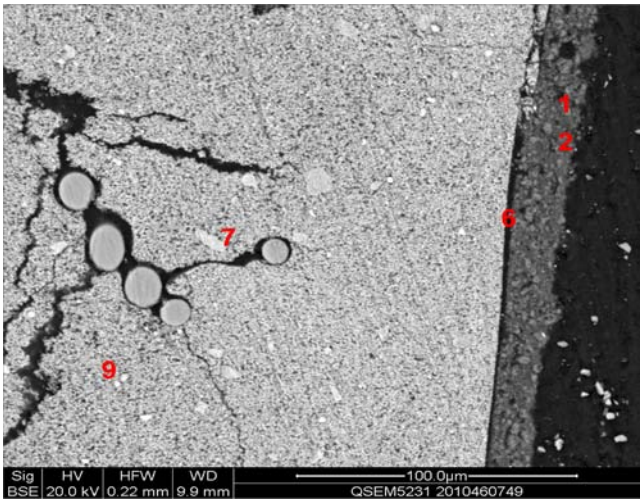

Figure 6.4 HZSM5-15 coated catalyst plate exposed for 850 hours with potassium chloride. Surface potassium concentration 4.075 wt% (top); catalyst plate cross section (bottom).

A surface image of HZSM5-15 coated catalyst with potassium concentration is shown in Figure 6.4. Average surface composition of potassium observed is 4.075 wt%. Other than catalyst components, HZSM5 coating component Si can also observed. Si rich phase is observed in the surface, along the cross section of the plate the Si composition is much lower, showing that the coating material does not penetrate the wall. The concentration of potassium at the inner wall is about 0.5 wt%, which is very near to the detection limit of the EDX analyzer. Through the cross section image it can be observed at the surface (1, 2) there is a rich content of Si and K at the surface, and as it is moved along the thickness of the plate (6,7 and 8) catalyst components Ti and W can be seen with little potassium. Unlike the reference plate the potassium composition is high at the surface and very less inside the plate with an average value of 0.35 wt% (Appendix-Chapter 6, page 77). This further indicates that the HZSM5-15 zeolite can acts as a potassium barrier.

	Wt %			
	K	**Si**	**Ti**	**W**
1	4,9	44,1	1,0	2,3
2	7,0	45,2	1,3	3,8
3	6,7	45,5	1,2	3,2
4	5,0	36,0	0,7	2,6
5	2,7	16,5	22,3	5,2

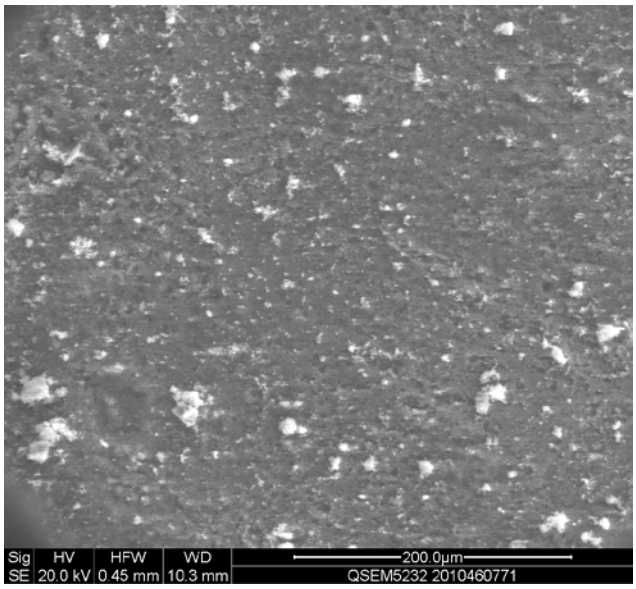

	Wt %			
	Si	**K**	**Ti**	**W**
3	2,0	0,4	52,0	8,6
5	48,9	3,7	2,7	3,9
6	2,4	0,9	40,7	16,2
7	1,9	0,7	47,9	10,4

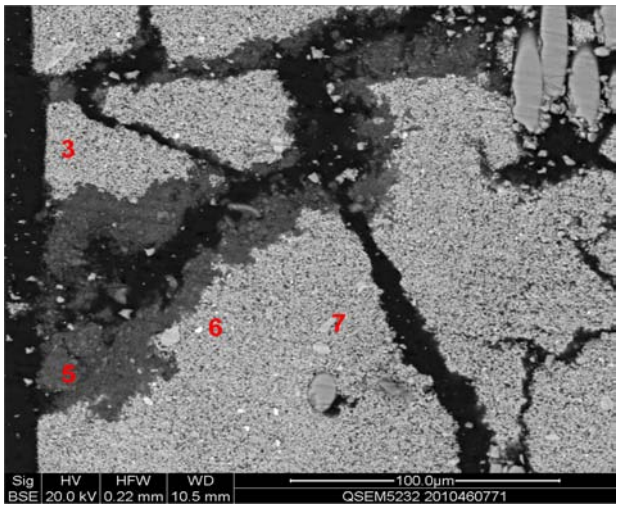

Figure 6.5 HMOR-10 coated catalyst plate exposed for 850 hours with potassium chloride. Surface potassium concentration 5.26 wt% (top); catalyst plate cross section (bottom).

A surface image of the HMOR-10 coated catalyst with potassium concentration is shown in Figure 6.5. Average surface composition of potassium observed was 5.26 wt%. HMOR-10 coating with Si can be observed in the concentration profile. The potassium concentration on Si rich areas (1-4 spots) is high and that of Ti rich area (5th spot) is much lower, it further indicates that the acidic centers are protecting the active vanadium species by hosting the potassium poisons. Cross section images reveal that potassium concentration near the coating layer maximum up to 0.5 wt%. Along the inner cross section the average potassium concentration is about 0.25 wt% (Appendix-Chapter 6, page 80).

	Wt %		
	K	**Ti**	**W**
1	3,5	52,0	8,2
2	2,9	39,5	6,7
3	3,6	44,0	8,9
4	3,7	48,9	8,2

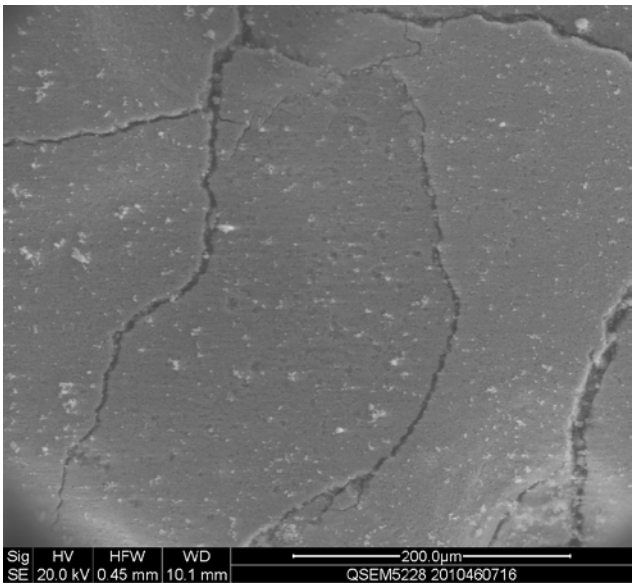

	Wt %		
	K	**Ti**	**W**
1	1,4	22,2	3,8
2	0,8	50,4	8,7
3	0,1	50,1	6,2
6	0,2	54,1	7,4
7	0,1	8,4	2,6

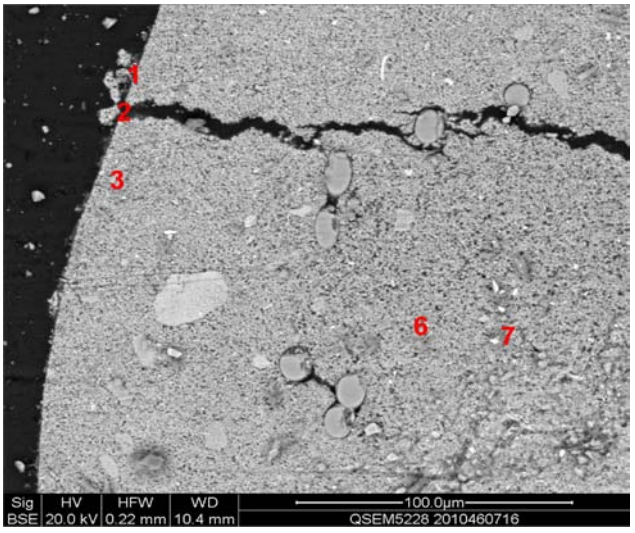

Figure 6.6 5%Mg–5%Si coated catalyst plate exposed for 850 hours with potassium chloride. Surface potassium concentration 3.425 wt% (top); catalyst plate cross section (bottom).

A surface image of the 5%Mg–5%Si coated catalyst is shown in Figure 6.6. Average surface composition of potassium concentration observed is 3.425 wt%. Cross section images reveal that potassium concentration at outer surface of one side, up to 1.4 wt%. In the inner of the wall there is about 0.2 wt% of potassium can be seen (Appendix-chapter 6, page 79).

6.5 Conclusions

Promising materials like zeolites (HZSM5 and HMOR) and Mg with Si binder were tested for SCR alkali resistivity. Based on activity measurements all the coated elements showed improved deactivation resistance.

Irrespective of the surface concentration of the potassium, best coating can be concluded with potassium accumulation across the plate. Uncoated reference catalyst showed comparatively high potassium (0.725 wt%) across the cross section of the plate. Among all the catalysts 5 %wt Mg - 5 wt% Si coated catalyst showed the lowest potassium concentration (≈0.2 wt%) across the plate, while that of HMOR-10 showed 0.25 wt%. HZSM5-15 coated catalyst showed potassium

concentration of 0.35 wt%, respectively. The cross section results indicate that coatings (5%Mg–5%Si, zeolites) significantly prevent potassium to reach the catalyst surface, by up to a factor of three or more.

Chapter 7

Confidential coatings

7.1 Coating materials

Coating materials considered in this section are secret because of the possible patent scope in the near future.

7.2 Particle size distribution

In this chapter coating was prepared with 5% aqueous suspension. The average particle size of the coating materials measured from the HYDRO 2000G instrument is listed in Table 7.1. Among all the catalysts coat 1 and coat 3 showed large average particle size (D_{50})with 14.79 and 18.77 μm, respectively. Figure 7.1 showing particle size distribution of Coat 2 with average particle size (D_{50}) of 3.69 μm.

Table 7.1 Average particle size of coating materials.

Coating material	Average particle size (μm)
Coat 1	14.79
Coat 2	3.69
Coat 3	18.77
Coat 4	5.85

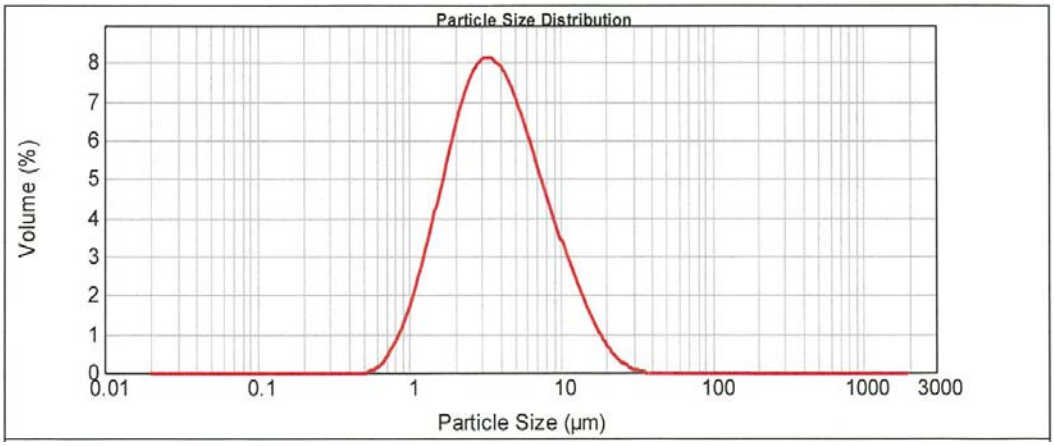

Figure 7.1 Particle size distribution of Coat 2.

7.3 SCR activity results

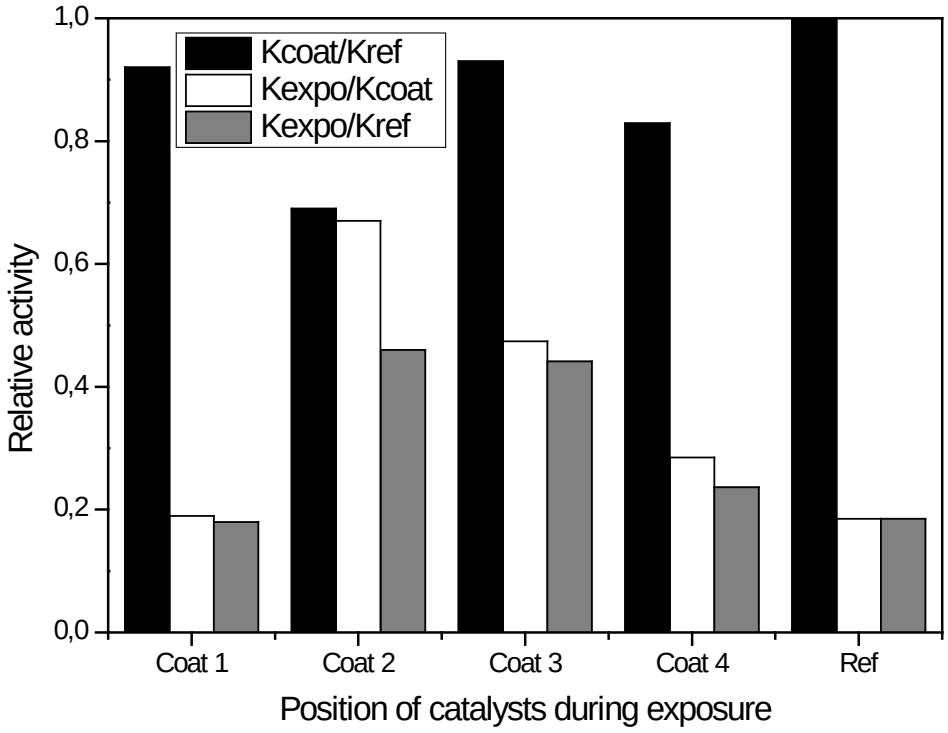

Figure 7.2 Relative activity of reference, coated and aerosol exposed catalysts for 850 h at 350°C.

Catalytic activity of reference, coated and aerosol exposed catalysts are presented in Figure 7.2. From figure it is clear that the coated catalysts are showing less relative activity compared to that of reference catalyst as already seen in previous chapters. All the coated catalysts showed relative activity (K_{coat}/K_{ref}) values of 0.7 to 0.9 impaling that the coating is very thin. The relative activity of the aerosol exposed catalysts to that corresponding fresh coated catalyst is shown in Figure 7.2. The reference catalyst showed a relative activity (K_{expo}/K_{coat}) of 0.185 showing severe deactivation of the catalyst and in good agreement with the results of Chapter 4-6 for the reference catalyst. Among coated catalysts except Coat 1 rest of the 3 catalysts showed alkali resistivity as compared to the uncoated reference catalyst. The relative activity of Coat 1, Coat 2, Coat 3 and Coat 4 are 0.19, 0.67, 0,474 and 0.285, respectively.

The Overall relative activity of aerosol exposed catalyst to that of fresh reference (K_{expo}/K_{ref}) is shown in Figure 7.2. Among all the catalysts Coat 2, Coat 3 and coat 4 catalysts are performing better compared to that of uncoated reference catalyst. Coat 1, Coat 2, Coat 3 and coat 4 catalysts showed relative decrease of 0.18, 0.46, 0.44 and 0.24, respectively.

Because of the confidentiality we are not revealing the chemical composition of the coatings in this chapter, only potassium concentration at the surface and cross section are measured and discussed accordingly on Coat 2 and Coat 3 catalysts.

7.4 SEM and EDX analysis of deactivated catalysts

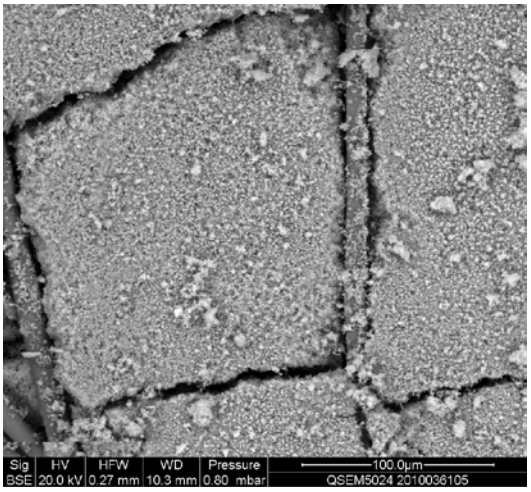

Elements	Scan 1 (wt%)	Scan 2 (wt%)
K	5,6	6,9
Ti	40,3	39,5
V	1	1
W	7,3	7,3

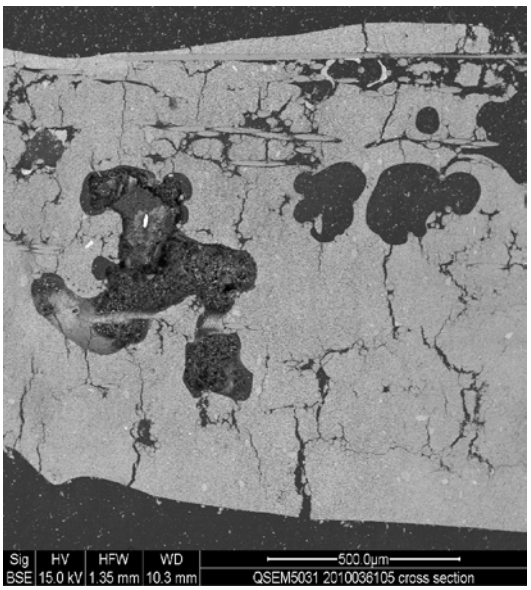

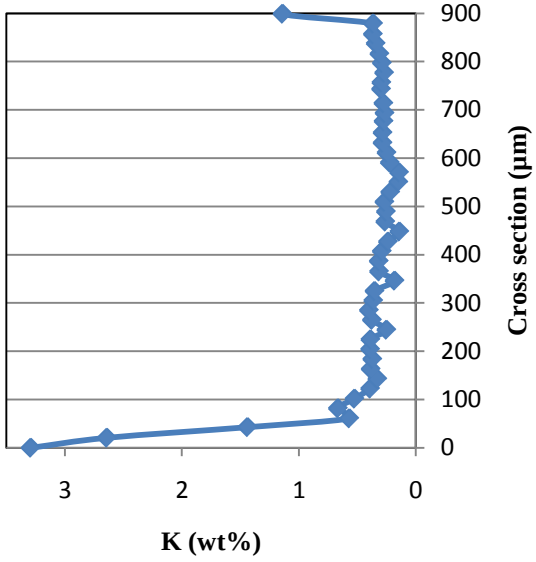

Figure 7.3 Reference catalyst plate exposed for 850 hours with potassium chloride. Surface potassium concentration (top) 6.2 wt%; potassium concentration along the catalyst plate cross section (bottom).

The surface of the reference catalyst with potassium concentration can be seen from Figure 7.3 (top). Average surface composition of potassium observed was 6.2 wt%. Other major catalyst components are Ti, W and V. The content of vanadium is very near to the 1.2 wt% from the EDX analysis. At one end of the plate potassium concentration is 3.4 wt% (Bottom) and approximately constant value is seen along the cross section (K= 0.455 wt%). Potassium concentration is gradually decreasing along the thickness of the plate. It further indicates that the potassium aerosols are not only deactivating the surface vanadium species but, also diffusing along the cross section of the plate causing intense deactivation [37, 61]. In this reference catalyst without any coating protection severe deactivation is observed up to 130 µm thickness with potassium concentration above the average value.

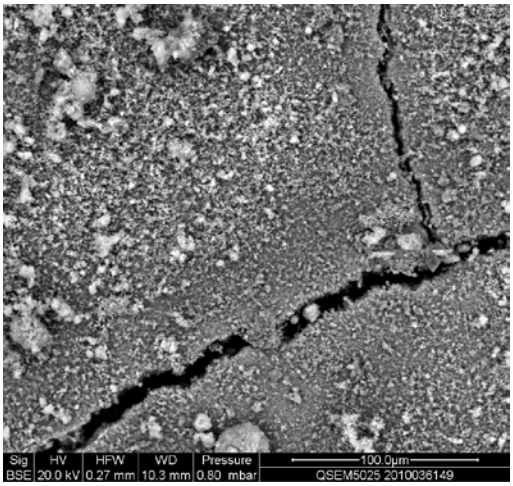

Elements	Scan 1 (wt%)	Scan 2 (wt%)
K	9,4	7,1
Ti	19,6	28,8
V	1	1
W	4	5,9

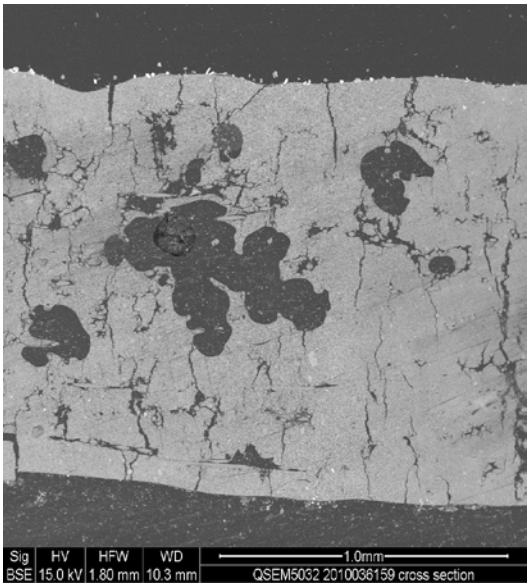

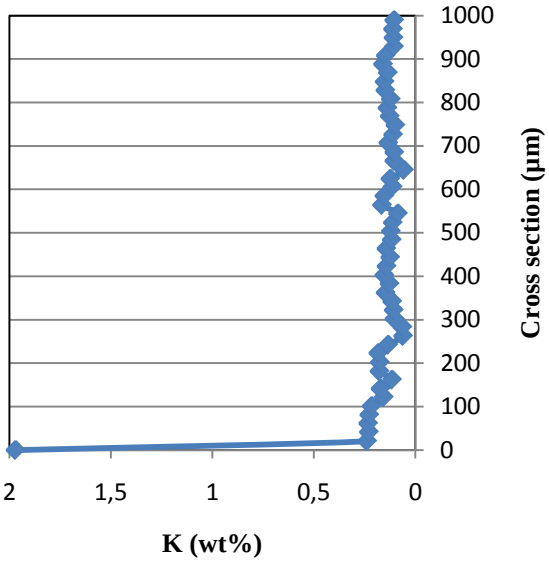

Figure 7.4 Coat 2 catalyst plate exposed for 850 hours with potassium chloride. Surface potassium concentration 8.25 wt% (top); potassium concentration along the catalyst plate cross section (bottom).

A surface image of the Coat 2 catalyst is shown in Figure 7.4 (top). The average surface composition of potassium concentration observed was 8.25 wt%. The elemental composition indicates that the Coat 2 coating is there on the surface which is responsible for SCR alkali resistivity (not shown other elements in table). Observed potassium surface composition value is higher than the uncoated reference catalyst. Similar results were also seen in Chapter 4 with Mg coated catalyst i.e. it inhibits the penetration of potassium into the catalyst. The potassium concentration at one end of the plate showed a value of 1.9 wt% (bottom) and approximately constant value is seen along the cross section (K = 0.20 wt%). The potassium concentration is decreasing along the thickness of the plate. Coat 2 catalyst showed no influence of potassium along the cross section of the plate. It indicates that the potassium aerosols are available at the surface. Such a SCR alkali resistivity and potassium blocking ability is due to the typical composition of the Coat 2.

	Wt %		
	K	**Ti**	**W**
1	5,1	51,3	12,2
2	5,1	41,9	11,0
3	4,6	41,8	11,7
4	3,6	47,5	10,6

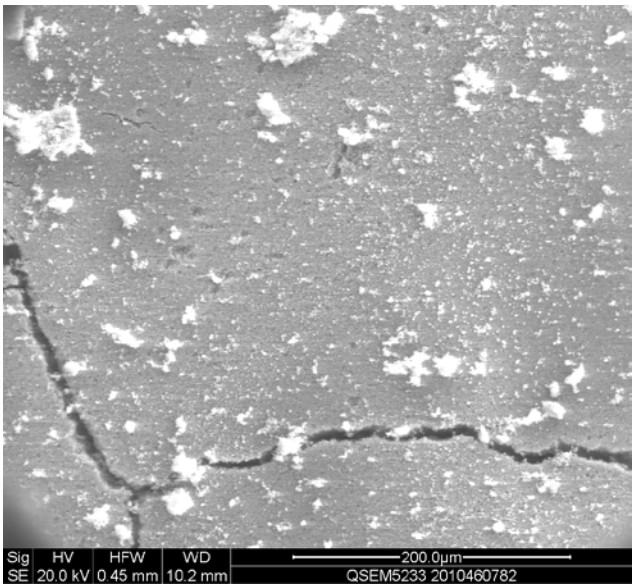

	Wt %		
	K	**Ti**	**W**
1	0,6	44,5	8,3
2	0,7	43,4	8,4
3	0,7	42,3	7,4
7	0,9	47,5	9,3
8	0,8	51,8	7,9

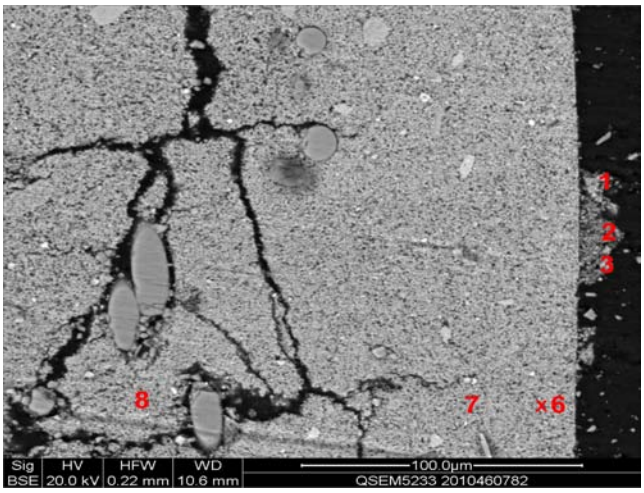

Figure 7.5 Coat 3 catalyst plate exposed for 850 hours with potassium chloride. Surface potassium concentration 4.6 wt% (top); catalyst plate cross section (bottom).

A surface image of Coat 3 catalyst with potassium concentration is shown in Figure 7.5. Average surface composition of potassium observed is 4.6 wt%. From the cross section images it can be seen that the potassium concentration close to one end of the surface is up to 0.7 wt%. Further into the catalyst wall the average potassium concentration is about 0.3 wt% (Appendix-Chapter 7, page 81).

7.5 Conclusions

Confidential coating materials are tested for SCR alkali resistivity. Based on SCR activity measurements Coat 2 and Coat 3 coatings showed improved deactivation resistance. Overall relative activity (K_{expo}/K_{ref}) of the catalyst plate coated with Coat 2 and Coat 3, are 0.46 and 0.44, respectively and that of reference plate showed to be 0.185. Surface analysis of the reference plate showed a potassium concentration of 6.2 wt (%). Coat 2 and Coat 3 catalysts showed surface composition of 8.25 and 4.6 wt%, respectively. Across the cross section Coat 2 and Coat-3 catalysts have lowest potassium concentration compared to that of the reference catalyst. The cross section results indicate that Coat 2 and coat 3 coatings prevent potassium to reach the catalyst surface.

Chapter 8

Metal oxide and zeolite coatings

8.1 Coating materials

Possible coating materials considered are 15%Mg-5%Si, HY-12, HY-60, Fly ash, Nb_2O_5, calcium phosphate and WO_3-ZrO_2.

Magnesium oxide with Silica gel: Mg Supplier**:** Sigma Aldrich; Formula: MgO; M.Wt: 40.30 g/mol; Silica gel supplier: Haldor Topsøe.

Fly ash: Supplier: Dong Energy; Fly ash contains substantial amounts of SiO_2 (both amorphous and crystalline) and calcium oxide (CaO).

HY-60: Supplier: Zeolyst International; Surface area: 720 m^2/g; Si/Al=60.

HY-12: Supplier: Zeolyst International; Surface area: 730 m^2/g; Si/Al=12.

Niobium pentoxide: Supplier: Sigma Aldrich; Formula: Nb_2O_5.

Calcium phosphate: Supplier**:** Sigma Aldrich; Formula: $CaHPO_4.2H_2O$

WO_3-ZrO_2: Supplier**:** Saint-Gobain; Surface area: 125 m^2/g.

8.2 Particle size distribution

In this chapter Mg-Si coating was prepared with 15% Mg-5% Si aqueous suspension to see the influence of thick suspension and rest of the coatings were made with 5% aqueous suspension. The average particle size of the coatings measured from the HYDRO 2000G instrument is shown in Figure 8.1. It can be observed that the particle size of 15%Mg-5%Si coating is 8.25 μm. Zeolite based coating (HY-12, HY-60) showed the smallest particle size among all the coatings around 4 μm. Fly ash and calcium phosphate coatings showed comparatively large particle size 16.09 and 11.97 μm, respectively. Except, WO_3-ZrO_2 coating (Figure 8.1) with broad and two stage particle size distribution, all the coatings showed a single and narrow particle size distribution (Appendix-Chapter 8, page 83-84).

Table 8.1 Average particle size of coating materials.

Coating material	Average particle size (μm)
Fly ash	16.09
HY-60	4.75
Nb_2O_5 (Nb)	5.42
15%Mg-5%Si	8.25
Calcium Phosphate	11.97
WO_3-ZrO_2 (W-Zr)	4.21
HY-12	4.09

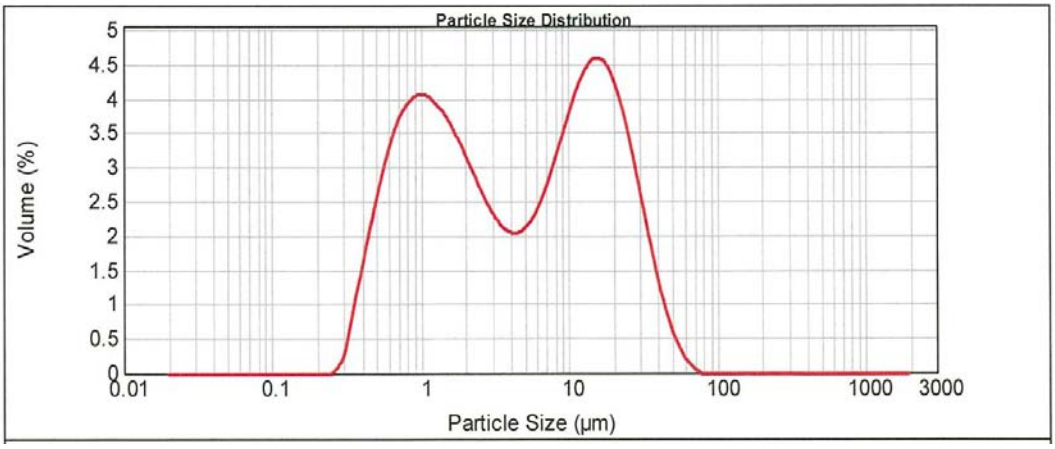

Figure 8.1 Particle size distribution of WO_3-ZrO_2.

8.3 SCR activity results

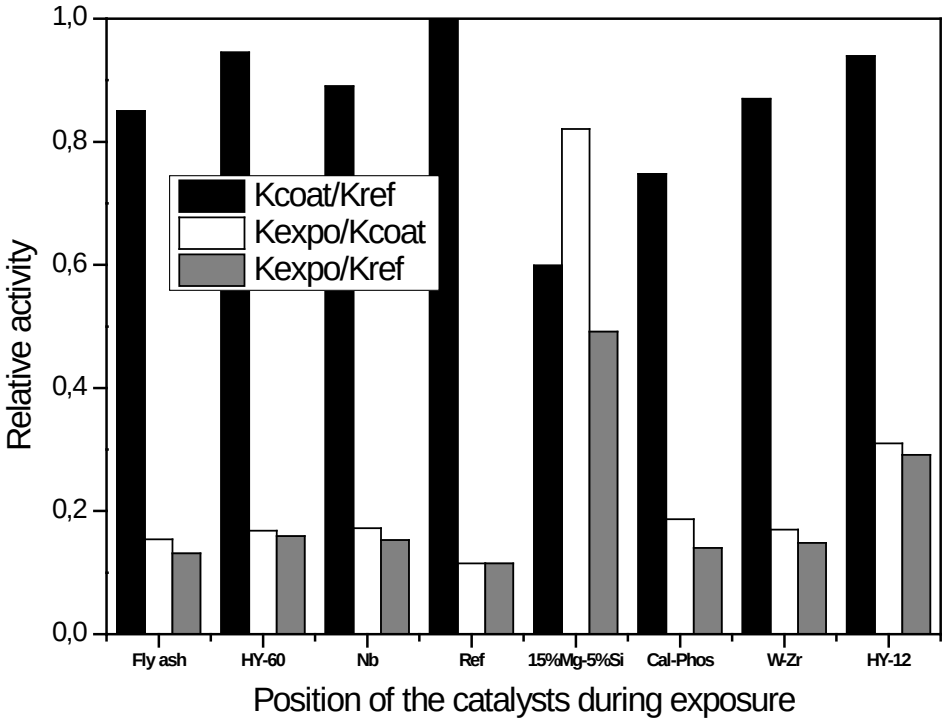

Figure 8.2 Relative activity of reference, coated and aerosol exposed catalysts for 850 h at 350°C.

Catalytic activity of reference, coated and aerosol exposed catalysts are presented in Figure 8.2. From figure it is clear that the coated catalysts are showing large deviation in relative activity (K_{coat}/K_{ref}). HY-12 and HY-60 are showing around 0.94. Fly ash, Nb, and WO_3-ZrO_2 are showing a relative activity of 0.83-0.89. Calcium phosphate and 15%Mg-5%Si are showing a relative activity of 0.748 and 0.60, respectively.

The relative activity of the aerosol exposed catalysts to that corresponding fresh coated catalyst is shown in Figure 8.2. The reference catalyst showed a relative activity (K_{expo}/K_{ref}) of 0.115. Among all the coated catalysts 15%Mg-5%Si and HY-12 are performing well with relative activity (K_{expo}/K_{coat}) of 0.821 and 0.31, respectively. As reported in the previous chapters Mg coated catalysts are always superior. HY-12 zeolite activity cannot be compared with other zeolites like HZSM5-15 and HMOR-10. The rate of deactivation can also depend on zeolite pore size/structure other than acidity as also reported by Reddy et al. [48, 64]. Irrespective of the pore size and structure zeolites with Si/Al around 10-20 are showing high alkali resistivity compared other zeolite formulations. Rest of the coatings showed relative activity around 0.2.
15%Mg-5%Si and HY-12 coated catalysts showed overall activity (K_{expo}/K_{ref}) of 0.4918 and 0.29145, respectively. It again showed that Mg coated catalysts are most promising candidates for the alkali resistive SCR process.

8.4 Conclusions

A comparison is made in Table 8.2 from Chapter 4 to 8 with 3 best performing catalysts from each batch. Among all the catalysts Mg coated catalysts are generally working well, though it is not the case for the batch related in Chapter 5. Such a variation is due to very thin or film Mg coating. 2nd best candidates are zeolite family materials like HZSM5-15, HMOR-10 and HBEA-25. All these materials fall under the broad classification mentioned in chapter 2.

Table 8.2 Comparison of overall relative activity (K_{expo}/K_{ref}) of the coating materials.

	1st choice	2nd choice	3rd choice
Chapter 4	Mg (0.59)	Mn (0.34)	Ti (0.32)
Chapter 5	HBEA-25 (0.45)	Mg (0.29)	-----
Chapter 6	HZSM5-15 (0.49)	HMOR-10 (0.49)	Mg (0.46)
Chapter 7	Coat 2 (0.46)	Coat 3 (0.44)	Coat 4 (0.2365)
Chapter 8	Mg (0.4918)	HY-12 (0.2914)	Cal-Phos (0.24)

1. Coating materials based on physical blocking (Ti and Mn)
   a. Slightly basic substances to block the potassium (Mg)
2. Coating materials based on chemically reactive compounds to potassium
   a. Acidic substances for hosting the potassium on surface (Zeolites)

From the broad classification with materials it can be further concluded that Mg coated compounds are the ultimate choice. Even if we imagine the long life of the second best choice coated materials like zeolites lose the surface acidic sites and become like a physical blocking materials. Then the potassium can easily penetrate through the wall of the catalyst. Ultimate success of the coating technique lies on the slightly basic substances since, they are the only materials which are not depending on acidic nature and effectively counter the potassium poisons not to penetrate through the wall. The lack of acidic Brønsted sites makes it difficult for the potassium to diffuse into the catalyst wall. With this typical comparison and coating strategy to counter the potassium poisons Mg coating is chosen for the long term exposure in comparison with the reference catalyst.

Chapter 9

Long term testing of Mg-coated catalysts

9.1 Coating material

For the long term experimentation Mg-Si coating material is selected.
Magnesium oxide with Silica gel: Mg Supplier**:** Sigma Aldrich; Silica gel supplier: Haldor Topsøe.

9.2 Particle size distribution

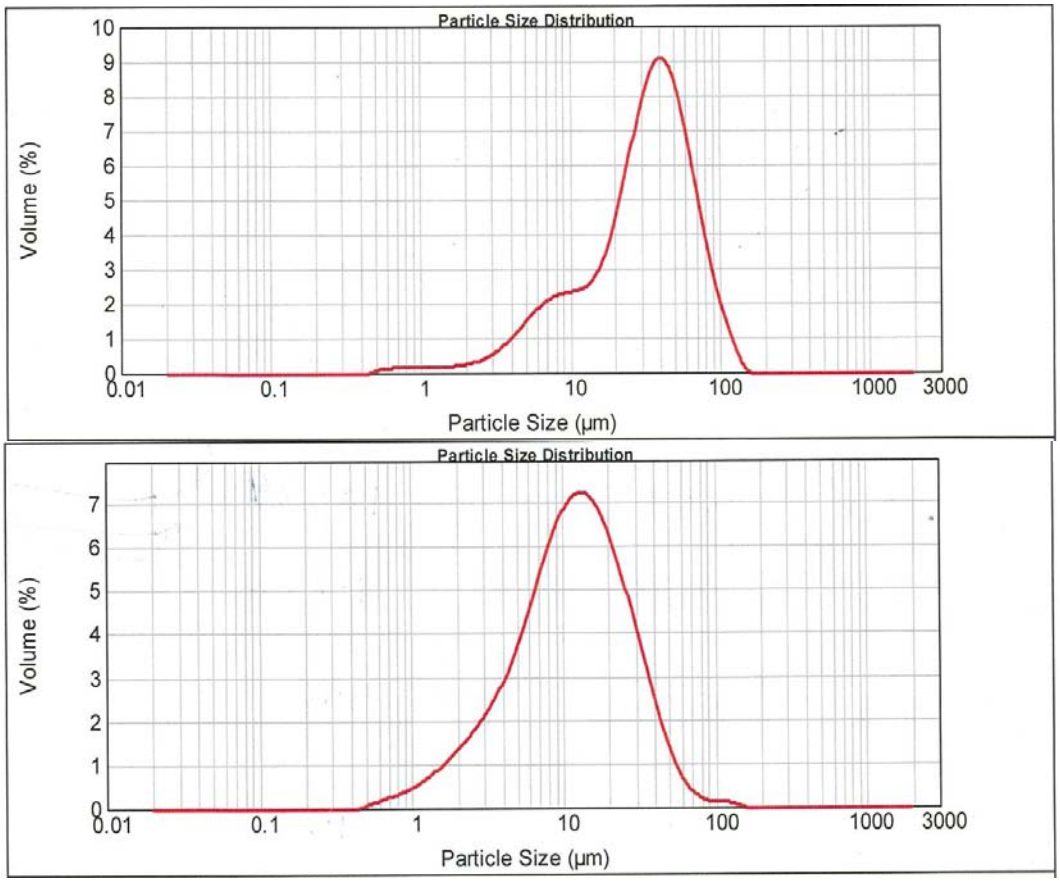

Figure 9.1 Particle size distribution of Mg-Si before crushing (top); after crushing (bottom).

Particle size distribution of Mg-Si aqueous suspension before and after the crushing is showed in Figure 9.1. Mg-Si coating before crushing showed uneven distribution of particle size between 8-40 µm. Particle size distribution around 8 µm is due to Si and that of 40 µm could be due to Mg. After crushing the aqueous suspension with 2-3 mm glass beads in a fluid shaking machine the average

particle size is decreased from 35 μm to 11 μm with uniform distribution. Thus, it is very important to decrease the particle size of the coating materials for better adhesion purpose.

9.3 SO_2 influence on Mg-Si coating

Co-firing of biomass and coal also results 100-200 ppm of SO_2 along with NO_x in the flue gases. It was known that the V_2O_5-WO_3/TiO_2 catalysts can with stand the poisonous SO_2 gas [37, 61]. In the present investigation an attempt is made to test the SO_2 influence on both reference and Mg coated catalysts. SO_2 could react with coated Mg and can form Mg sulfate, which is inactive for the alkali resistivity. Reference and Mg coated catalysts were exposed to 1000 ppm SO_2 gas balanced in N_2 gas at 350 ^oC for 7 days continuously. SO_2 exposed catalysts were tested on the same day to study the SCR reactivity. Fresh reference and Mg coated catalysts showed a rate constant value of 0.043 and 0.030 m/s, respectively. SO_2 exposed reference and Mg coated catalysts showed a rate constant value of 0.039 and 0.037 m/s, respectively. Reference catalyst losing around 9% of the initial activity and Mg coated catalyst gaining 20% of the initial activity after SO_2 exposure. Thus, the presence of SO_2 in real flue gas does not seem to be a problem.

9.4 Long term aerosol exposure with time

A set of experiments were planned for long term aerosol exposure as shown in matrix (Table 9.1). Total exposure time was 50 days with 10 days of interval for each exposure. After every 10 days of exposure one reference and one coated catalyst was removed and replaced with 2 fresh catalysts. X represent first batch of exposed catalyst and # represent 2nd batch of replaced catalyst. In this way repeatability of the experiments can be done along with long exposure time. With 10 days interval the rate of deactivation can also be measure for both reference and coated catalysts. After the exposure the catalysts were stored in decicator to avoid further deactivation with atmospheric moisture.

Table 9.1 Design of experiments for long term aerosol exposure.

	Ref -1	Ref -2	Ref -3	Ref -4	Ref- 5	Mg-1	Mg-2	Mg-3	Mg-4	Mg-5
10 Days	X	X	X	X	X	X	X	X	X	X
20 Days	#	X	X	X	X	#	X	X	X	X
30 Days	#	#	X	X	X	#	#	X	X	X
40 Days	#	#	#	X	X	#	#	#	X	X
50 Days	#	#	#	#	X	#	#	#	#	X
	Ref-6	Ref-7	Ref-8	Ref-9	Ref-5	Mg-6	Mg-7	Mg-8	Mg-9	Mg-5

9.5 SCR activity of reference catalyst

The relative activity (K_{expo}/K_{ref}) of the aerosol exposed catalyst to corresponding fresh reference catalyst is shown in Figure 9.2. Reference catalysts showed decrease in activity with exposure time. These reported values are average measurements along the length of the exposed plates. After 10 days of exposure reference catalysts showed a relative value of 0.71 in both batches. 10-40 days of exposed catalysts in both batches showed maximum deviation of 5% could indicate that the experimental data can be validated. Almost complete loss of activity can be seen after 50 days of exposure. In the previous chapters the reference catalyst showed a relative value of 0.20-0.25 after 850 hours of operation, that data is fitting well into the observed deactivation trend line in this long term experiments. From Figure 9.2 an average deactivation rate of 20%/every10 days can be observed. Such a high rate of deactivation reveals that the potassium aerosol exposure is very intense.

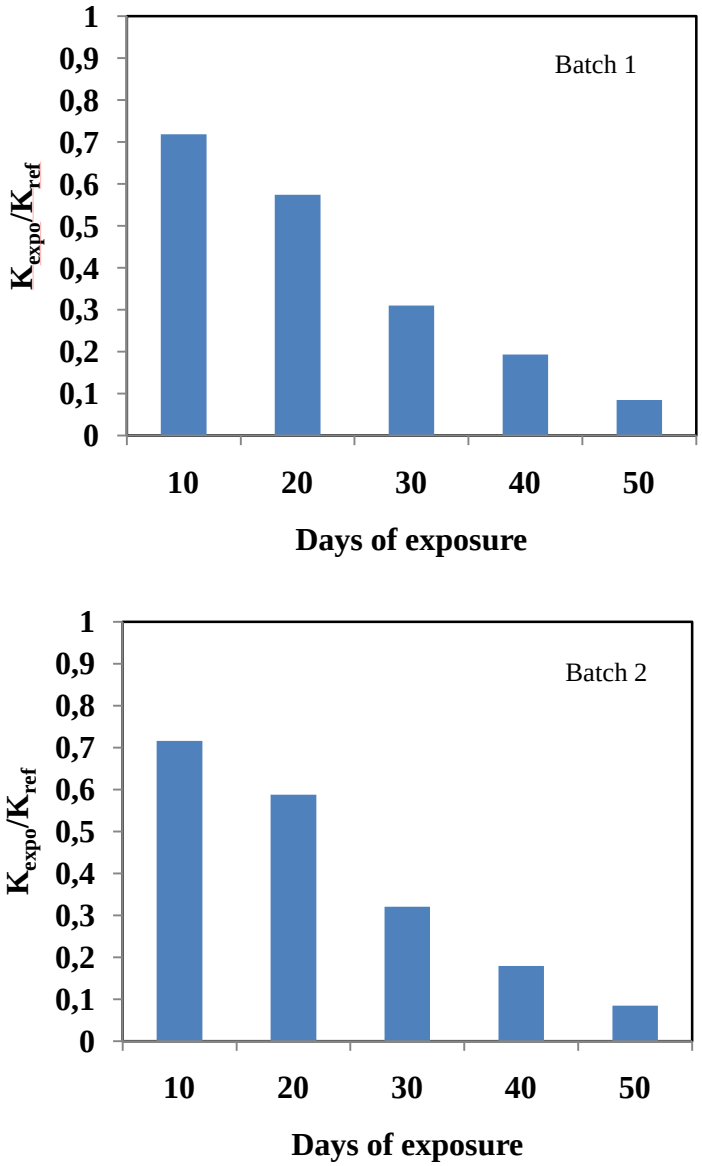

Figure 9.2 Relative activity (K_{expo}/K_{ref}) of reference catalysts with aerosol exposure time at 350°C.

9.6 SCR activity of Mg-Si coated catalyst

The relative activity (K_{coat}/K_{ref}) of Mg coated catalysts is shown in Figure 9.3. From figure it is clear that the coated catalysts are showing large deviation in relative activity ranging from 0.75 to 0.55 could be due to slight variation in coating time form plate to plate. After measuring the relative activity, the position of the catalysts was arranged for aerosol exposure in decreasing relative value with increasing days of exposure. It was anticipated that Mg with thicker coating can withstand the potassium aerosols in an effective manner for the long term experimental purpose.

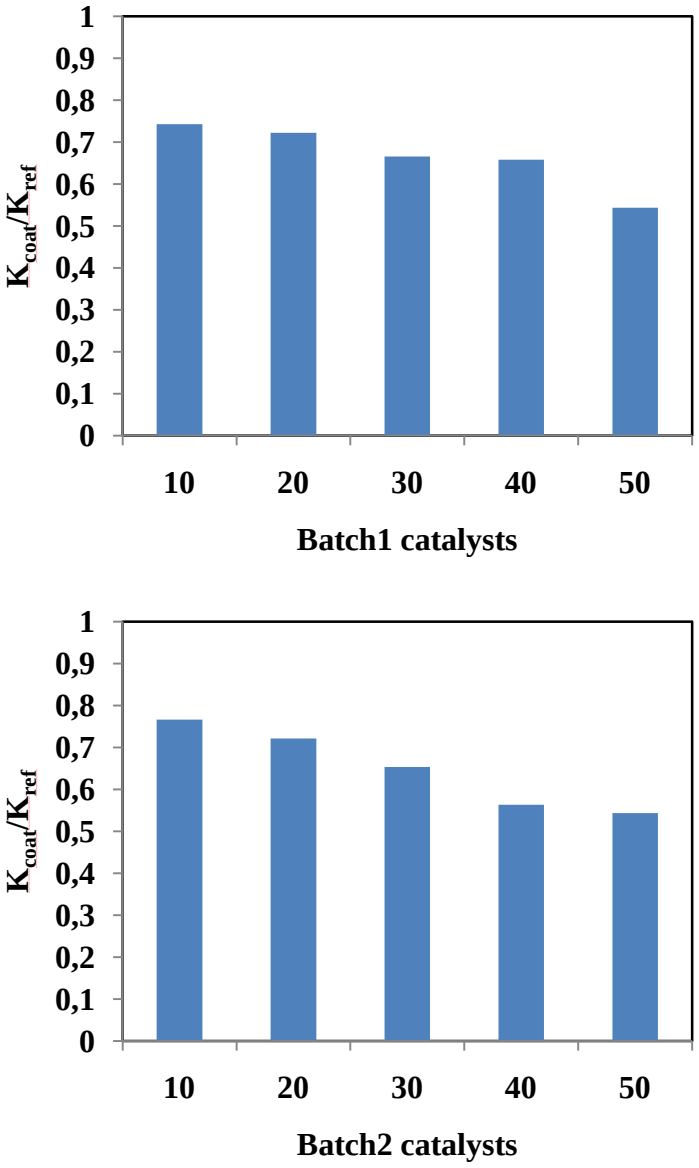

Figure 9.3 Relative activity (K_{coat}/K_{ref}) of Mg coated catalysts at 350°C.

The relative activity (K_{expo}/K_{coat}) of Mg coated catalysts along with exposure time is shown in Figure 9.4. Mg coated catalysts showed decrease in activity with exposure time. After 10 days of exposure Mg coated catalysts showed a relative value of ≈0.84 in both batches. 10 -40 days of exposed catalysts in both batches showed maximum deviation of 5-7% could indicate that the Mg coated catalysts are slightly deviating in repeatability compared to the reference catalysts. Mg

coated catalysts showed a relative value of 0.60 after 50 days of exposure while that of reference catalyst almost completely deactivated. From Figure 9.4 an average deactivation rate of 5%/every10 days can be observed. The slow rate of deactivation under similar conditions could reveal Mg is acting as a protecting layer to prevent alkali aerosols to reach the vanadium catalyst interior.

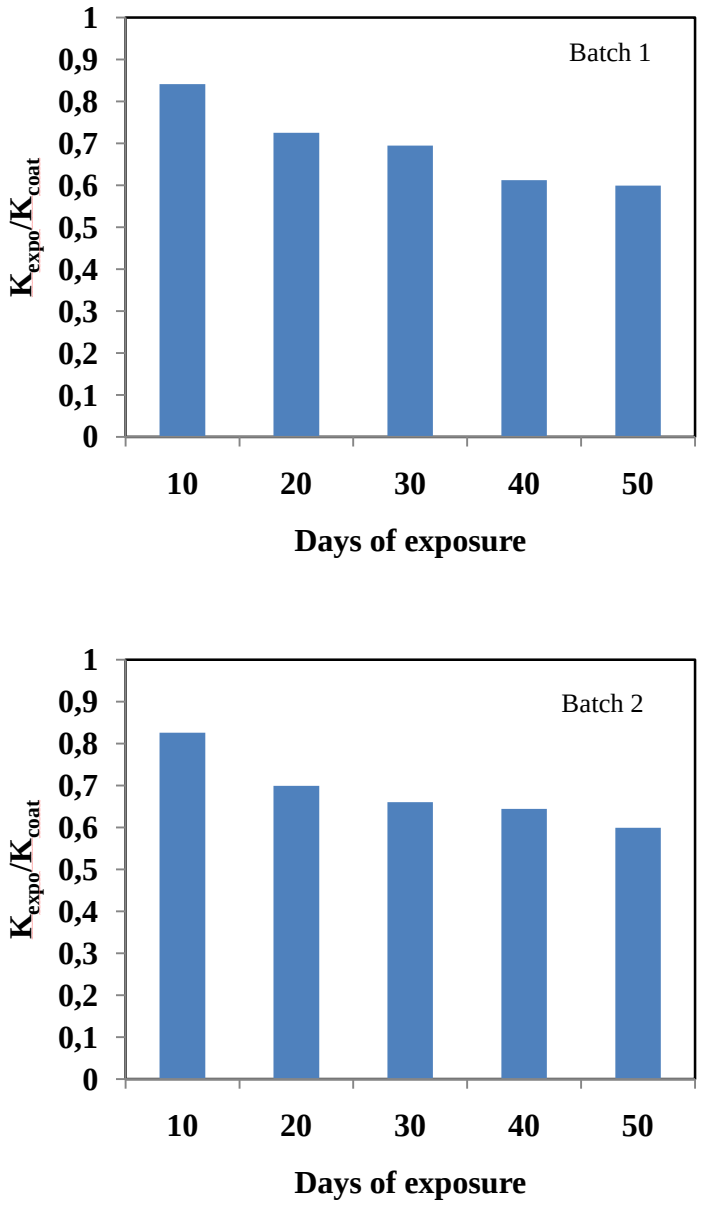

Figure 9.4 Relative activity (K_{expo}/K_{coat}) of Mg coated catalysts with aerosol exposure time at 350°C.

Overall relative activity (K_{expo}/K_{ref}) of Mg exposed catalysts to fresh reference catalyst is shown in Figure 9.5. Overall relative activity includes loss of activity due to coating barrier and potassium aerosol deactivation. Overall relative values can give more information and direct comparison can be possible with the reference catalyst. Mg coated catalysts showed a rate of deactivation of 6-7%/every 10 days. Mg coated catalysts showed a relative value of 0.32 and that of reference catalyst showed 0.08 after 50 days of aerosol exposure. The 50 days exposed Mg catalyst showed 40% loss

of activity due to coating (actually change with thickness of coating) and 28% due to alkali aerosol exposure. Uncoated reference catalyst showed loss of 92% only due to alkali aerosol exposure. Thus, Mg appears to be a good choice of coating material to protect the commercial vanadium catalyst from alkali poisons in biomass fired SCR applications.

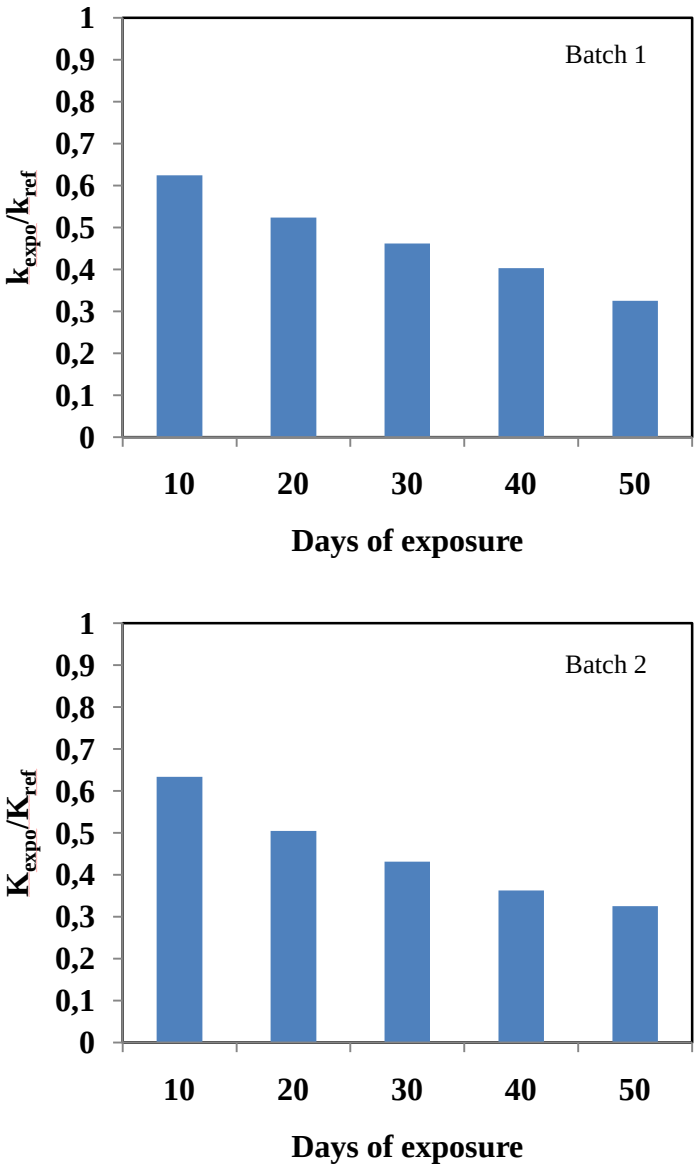

Figure 9.5 Overall relative activity (K_{expo}/K_{ref}) of Mg coated catalysts with aerosol exposure time at 350°C.

9.7 Conclusions

To limit the high rate of alkali deactivation, a novel protective coating technique has been developed and tested using a range of different candidate materials. Among all the tested catalysts slightly basic nature of Mg coated catalysts are generally working well. Mg is acting like a barrier repelling the potassium with basic-basic nature on the surface. Further design of experiments on

reference and Mg coated catalysts for long term exposure gave more insight about the rate of deactivation and consistency of results. 50 days of alkali aerosol exposure reveals that the reference catalyst is losing 92% of the initial activity only due to alkali and that of the Mg coated catalyst is losing 40% due to coating barrier and only 28% due to alkali. Thus, severe rate of deactivation due to alkali poisons can be avoided by coating the vanadium catalyst with Mg.

Chapter 10

10.0 Final conclusions and recommendations

Biomass like straw has become an increasingly important energy source over the last two decades in Denmark and the application of straw on power plants makes a significant contribution to the reduction of CO_2 emissions. However, co-firing coal with straw has created some technical challenges due to the ash composition of straw. Compared with coal, straw has high contents of potassium (0.2–1.9 wt.% on dry base) and chlorine (0.1–1.1 wt.% on dry base). In the combustion of pure biofuels and co-combustion of 10-15% (on an energy basis) straw with bituminous coal, alkali is present as aerosols as the flue gas cools to the SCR temperature. Alkali in the ash from biofuels causes severe deactivation for SCR catalyst. To limit the high rate of alkali deactivation, protective coating technique is better approach.

Overall the protective coating of SCR catalysts developed in the project seems promising. Further research and industrial prototype tests are recommended. Intellectual protection of the investigation has been initiated through patent application entitled 'Protective surface coating for DeNO$_x$ catalyst' and the innovation is transferred to Haldor Topsøe A/S. The results of the present research have not been published because of the patent issues, once the patent is issued publications can be initiated in the near term.

Bibliography

[1] http://www.nordicenergy.net/bioenergy
[2] N.H. Afgan, M.G. Carvalho, M. Jovanovic, Int. Journal of Sustainable Energy, 26 (2007) 179.
[3] Å. Kling, C. Andersson, Å. Myringer, D. Eskilsson, S. G. Järås, Appl. Catal. B, 69 (2007) 240.
[4] Y. Zheng, P. A. Jensen, A. D. Jensen, B. Sander, H. Junker, Fuel, 86 (2007) 1008.
[5] Jensen-Holm, J. R. Thøgersen, P. Lindenhoff, Presented at Power-Gen Europe, Germany (2009).
[6] B Gugele, M Ritter, Annual European Community CLRTAP Emission Inventory 2000, Technical Report 91, European Environment Agency, (2000) 28.
[7] Y.A. Zeldovich, Acta Physicochimica USSR 21 (1947) 557.
[8] R.J. Heinsohn, R.L. Kabel, Sources and Control of Air Pollution, Prentice-Hall (1990) 308.
[9] N deNevers, Air Pollution Control Engineering, McGraw-Hill (1995) 378.
[10] H.N. Soud, K. Fukasawa, Developments in the NO_x abatement and control, IEA Coal Research, London, United Kingdom (1996).
[11] R. Rodenhausen, Environmental Progress,18 (1999) 260.
[12] S. Khan, G. Shroff, J. Tarpara, R. Srivastava, Scr applications: addressing coal characteristic concerns, EPRI-DOE-EPA (1997).
[13] P. Forzatti, Appl. Catal. A, 222(2001) 221.
[14] M. Kleemann, M. Elsener, M. Koebel, A.Wokaun, Appl. Catal., 27(2000) 231.
[15] G. Busca, L. Lietti, G. Ramis, F. Berti, Appl. Catal. B, 18 (1998) 1.
[16] G. Ramis, G. Busca, F. Bregani, P. Forzatti, Appl. Catal., 64 (1990) 259.
[17] S. Soyer, A. Uzun, S. Senkan, I. Onal, Catal. Today., 118 (2006) 268.
[18] N. Topsøe, "Infrared spectroscopic investigations of enviromental denox and hydrotreating catalysts," 1998. Doctoral Thesis.
[19] N. Topsøe, H. Topsøe, J. A. Dumesic, J. Catal., 151 (1995) 226.
[20] N.-Y. Topsøe, J. Catal., 128 (1991) 499.
[21] N.-Y. Topsøe, H. Topsøe, Catal. Today, 9 (1991) 77.
[22] N. Topsøe, H. Topsøe, J. A. Dumesic, J. Catal., 151 (1995) 241.
[23] V. Tufano, M. Turco, Appl. Catal. B, 2 (1993) 9.
[24] J. A. Dumesic, N. Topsøe, H. Topsøe, Y. Chen, T. Slabiak, J. Catal.,163 (1996) 409.
[25] G.T. Went, L. Leu, A.T. Bell, J. Catal., 134 (1992) 492.
[26] J.P. Chen, R.T. Yang, J. Catal., 139 (1993) 277.
[27] H. Gutberlet, B. Schallert, Catal. Today, 16 (1993) 206.
[28] H. Gutberlet, VGB Kraftwerkstechnik 74 (1994) 54.
[29] I. Nova, L. Dall'Acqua, L. Lietti, E. Giamello, P. Forzatti, Appl. Catal. B. 35 (2001) 31.
[30] H. Bosch, F. Janssen, Catal. Today 2 (1988) 369.
[31] J. P. Chen,M. A. Buzanowski, R. T. Yang, J. E. Cichanowicz, J. Air Waste Manage. Assoc. 40 (1990) 1403.
[32] H. Kamata, K. Takahashi, C. U. I. Odenbrand, J. Mol. Catal. A. 139 (1999) 189.
[33] J. P. Chen, R. T. Yang, J. Catal. 125 (1990) 411.
[34] J. P. Chen, R. T. Yang, Appl. Catal. A. 80 (1992) 135.
[35] R. Khodayari, C. U. I. Odenbrand, Appl. Catal. B 33 (2001) 277.
[36] A. L. Kustov, M. Yu Kustova, R. Fehrmann, P. Simonsen, Appl. Catal. B. 58 (2005) 97.
[37] Y. Zheng, A. D. Jensen, J. E. Johnsson, Appl. Catal. B. 60 (2005) 253.
[38] B. Sander, Cofiring Workshop, 2nd World Biomass Conference, Rome, Italy, May 2004.
[39] H. Kamata, K. Takahashi, C. U. I. Odenbrandt, J. Catal., 185 (1999) 106.
[40] L. Lietti, P. Forzatti, G. Ramis, G. Busca, F. Bregani, Appl. Catal. B, 3 (1993) 13.
[41] D. Nicosia, I. Czekaj, O. Kröcher, Appl. Catal. B, 77 (2008) 228
[42] Y. Zheng, A. D. Jensen, J. E. Johnsson, Ind. Eng. Chem. Res., 43 (2004) 941.
[43] J.A. Moulijn, A.E. van Diepen, F. Kapteijn, Appl. Catal A: 212 (2001) 3.
[44] M. Crespi, M. Porle, A.-C. Larsson, R. La Civita, A. R. Nielsen, The influence of biomass burning in the design of an SCR installation, Power-Gen Europe (2008).
[45] R. Khodayari, C.U.I. Odenbrand, Appl. Catal. B 30 (2001) 87.
[46] J. Due-Hansen, S. Boghosian, A. Kustov, P. Fristrup, G. Tsilomelekis, K. Ståhl, C.H. Christensen, R. Fehrmann, J. Catal. 251 (2007) 459.
[47] G. Qi, R.T. Yang, R. Chang, S. Cardoso, R.A. Smith, Appl. Catal. A 275 (2004) 207.
[48] S.S.R. Putluru, A. Riisager, R. Fehrmann, Appl. Catal. B (Press).
[49] A.J. Kruse, S.B. Kristensen, A. Riisager, R. Fehrmann, J Mater Sci 44 (2009) 323.

[50] B. Jørgensen, S.B. Kristensen, A.J. Kruse, R. Fehrmann, C.H. Christensen, A. Riisager, Top Catal 52 (2009) 253.
[51] T.K. Li, D.A. Hirschfeld, J.L. Brown, J Mater Sci 32 (1997) 4455.
[52] P. Gabrielsson, H. Guldberg Pedersen, Volume 5, Handbook of Heterogeneous catalysis.
[53] M. Kang, T.H. Yeon, E.D. Park, J.E. Yie, J.M. Kim, Catal. Lett 106 (2006) 77.
[54] P.R. Ettireddy, N. Ettireddy, S. Mamedov, P. Boolchand, P.G. Smirniotis, Appl. Catal. B. 76 (2007) 123.
[55] Z.B. Wu, B.Q. Jiang, Y. Liu, Appl. Catal. B. 79 (2008) 347.
[56] B.Q. Jiang, Y. Liu, Z.B. Wu, Mater.162 (2009) 1249.
[57] W.S. Kijlstra, D.S. Brands, E.K. Poels, and A. Bliek, J. Catal. 171 (1997) 208.
[58] K. Arata, Appl. Catal. 143 (1996) 3.
[59] Suzuki, Motoyuki: Adsorption engineering, 1990.
[60] H.H. Huang, X. Jiang, H.L. Siew, W.S. Chin, G.Q. Xu, Surface Science 418 (1998) 320.
[61] Y. Zheng, A.D. Jensen, J.E. Johnsson, J.R. Thøgersen, Appl. Catal. B 83 (2008) 186.
[62] P. Kern, M. Klimczak, T. Heinzelmann, M. Lucas, P. Claus, Appl. Catal. B 95 (2010) 48.
[63] S.B. Rasmussen, J. Due-Hansen, M. Yates, M. Villaroel, F. Llambias, R. Fehrmann, P. Avila, Stud. Surf. Sci. Catal. 175 (2010) 739.
[64] S.S.R. Putluru, A. Riisager, R. Fehrmann, Appl. Catal. B 97 (2010) 333.

Appendix-Chapter 4

Al coating particle size distribution, surface and cross section images after exposure.

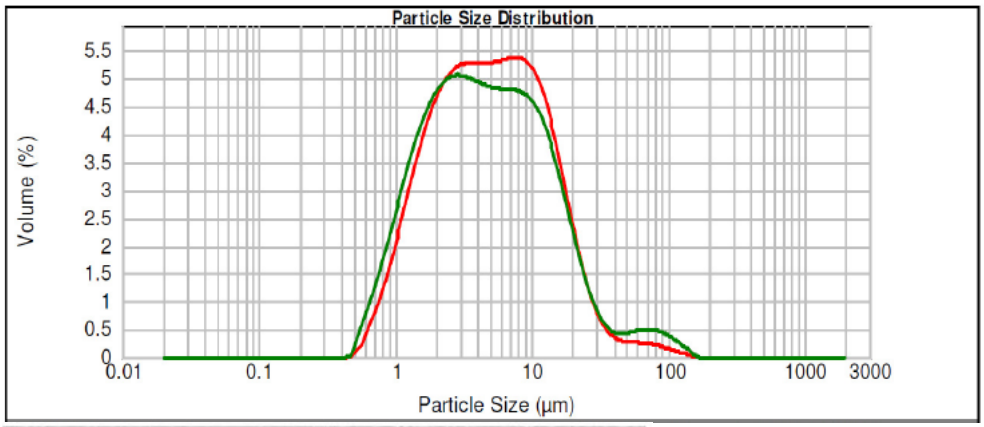

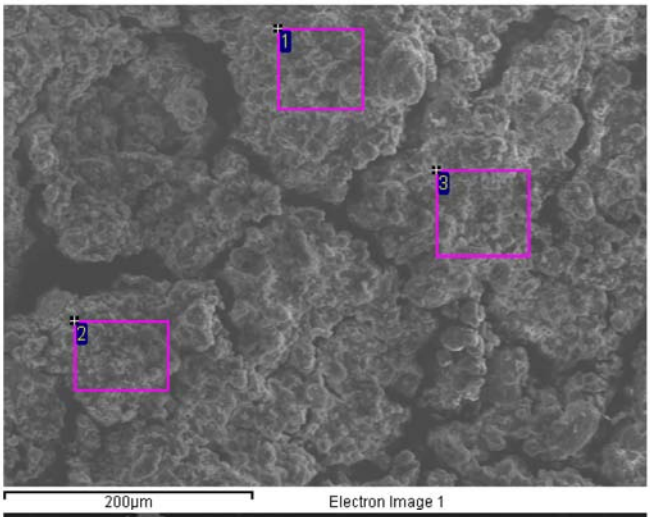

Spectrum	In stats.	O	Al	Si	S	Cl	K	Ti	Mn	Total
1	Yes	18.7	54.3	1.1	7.3	0.8	16.4	1.4		100.0
2	Yes	18.2	58.5	1.0	6.3	0.9	13.4	1.1	0.7	100.0
3	Yes	18.4	72.9		2.7	2.1	2.6	1.3		100.0

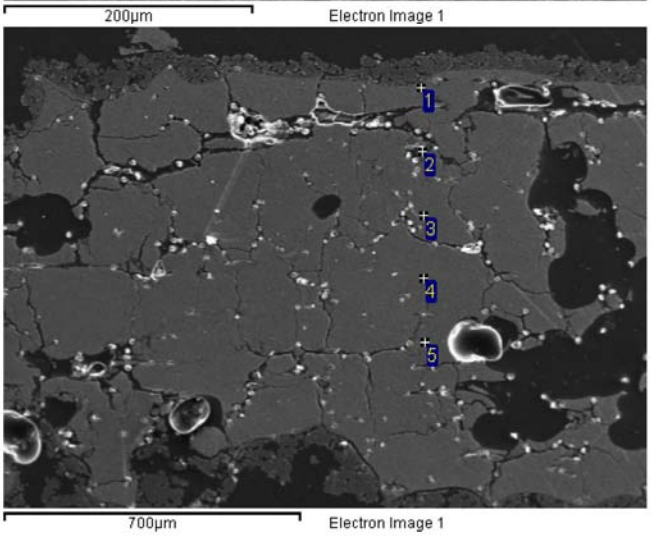

Spectrum	In stats.	O	Al	Si	S	Cl	K	Ca	Ti	V	W	Total
1	Yes	10.14		1.71	0.48	0.77	1.29		78.08	1.43	6.10	100.00
2	Yes	25.30	3.77	16.04	1.51	6.26	0.61	7.54	38.97			100.00
3	Yes	9.45		1.43		0.83	0.59		80.93		6.77	100.00
4	Yes	8.49		1.42		0.96	0.73		79.22	1.19	7.99	100.00
5	Yes	10.53		1.08		0.85	0.57		76.97	1.75	8.25	100.00

Ti coating particle size distribution, surface and cross section images after exposure.

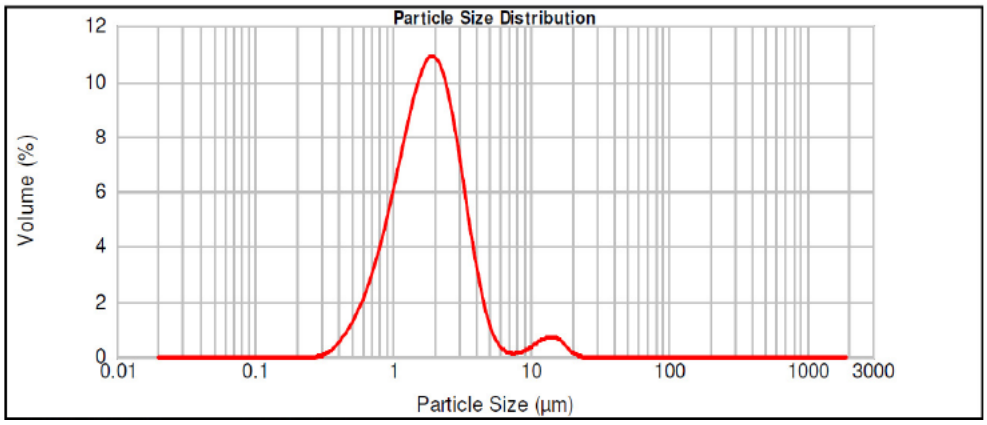

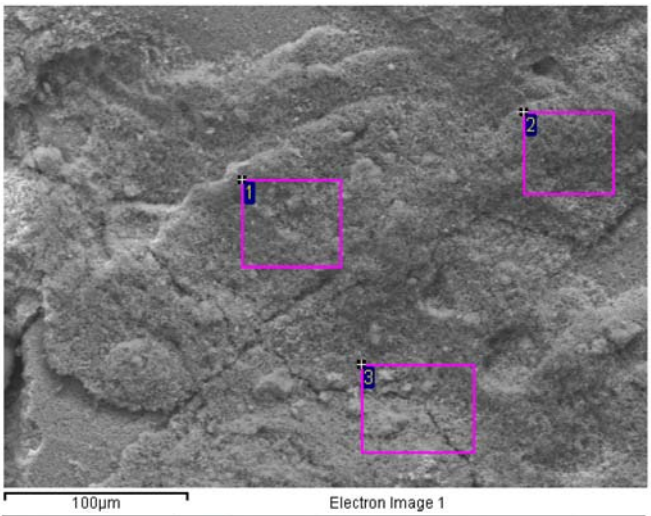

Spectrum	In stats.	C	O	Si	S	K	Ti	V	Total
1	Yes		12.2	2.8	1.2	2.3	81.5		100.0
2	Yes	6.0	8.1	1.8	2.3	4.9	75.5	1.3	100.0
3	Yes		15.5	2.3	1.4	2.4	78.5		100.0

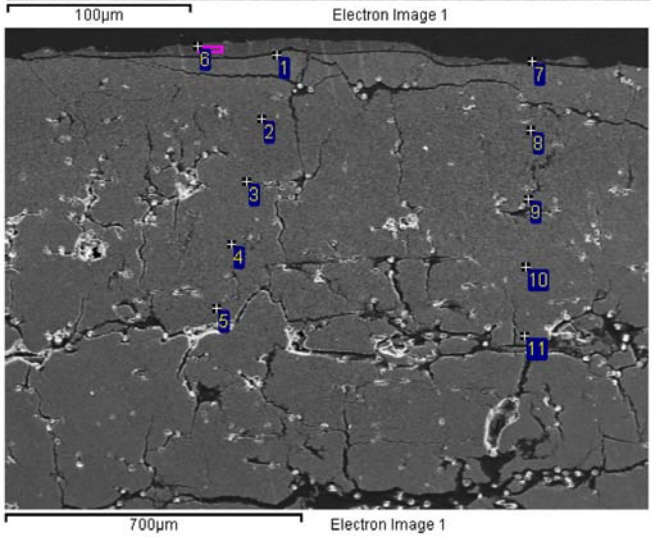

Spectrum	In stats.	O	Si	S	Cl	K	Ti	V	W	Total
1	Yes	8.65	0.62		0.93	0.46	77.30	1.44	10.60	100.00
2	Yes	7.62	0.91		0.86	0.32	74.47	2.36	13.45	100.00
3	Yes	9.65	1.57		0.80	0.26	74.54	1.82	11.36	100.00
4	Yes	7.52	1.60		0.83	0.30	78.41	1.52	9.83	100.00
5	Yes	5.14	1.44		1.08	0.23	82.26	1.74	8.11	100.00
6	Yes	14.30	1.71	0.69	1.40	0.36	81.54			100.00
7	Yes	40.65	2.86	4.94	47.49	0.91	3.14			100.00
8	Yes	8.85	1.20		0.92	0.33	75.85	1.91	10.94	100.00
9	Yes	14.53	1.45	0.72	2.82	0.17	69.20	1.72	9.38	100.00

Sul-Zr coating particle size distribution, surface and cross section images after exposure.

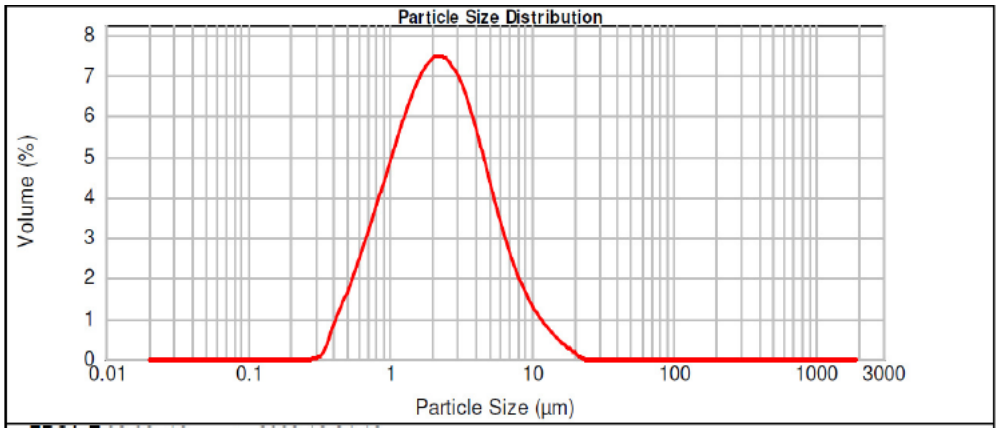

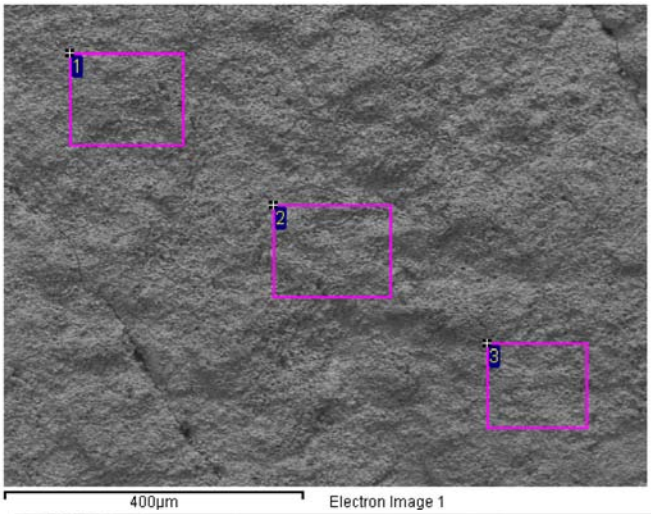

Spectrum	In stats.	O	Si	S	K	Ti	V	Zr	W	Total
1	Yes	6.7	1.6	9.8	25.1	0.8		55.8		100.0
2	Yes	6.5	2.0	8.7	22.0	1.0		59.8		100.0
3	Yes	7.2	2.2	8.5	22.1	1.6	0.6	55.8	2.0	100.0

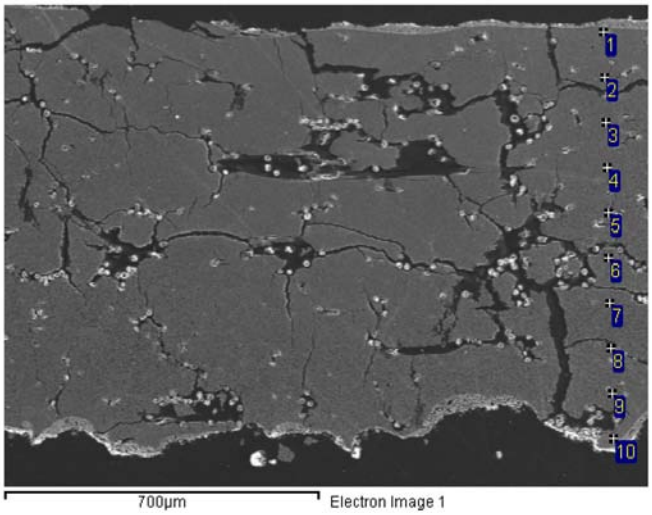

Spectrum	In stats.	O	Si	S	Cl	K	Ca	Ti	V	W	Total
1	Yes	8.41		1.65	0.72	4.96		69.87	1.57	12.83	100.00
2	Yes	9.20	0.73		0.85	0.91		71.53	1.96	14.83	100.00
3	Yes	7.26	0.70		0.55	0.79		73.64	2.51	14.54	100.00
4	Yes	7.91	1.15	0.37	0.96	0.58		74.69	1.86	12.47	100.00
5	Yes	7.70	2.97	1.20	4.58	0.41		72.37		10.77	100.00
6	Yes	6.18	1.24		0.99	0.58		79.36	1.87	9.77	100.00
7	Yes	4.36	1.08	0.44	1.33	0.59		79.97	1.84	10.40	100.00
8	Yes	6.98	1.64		1.00	0.70		76.58	1.20	11.90	100.00
9	Yes	8.31	1.96		0.98	0.72	0.69	73.68	1.97	11.68	100.00

Mn coating particle size distribution, surface and cross section images after exposure.

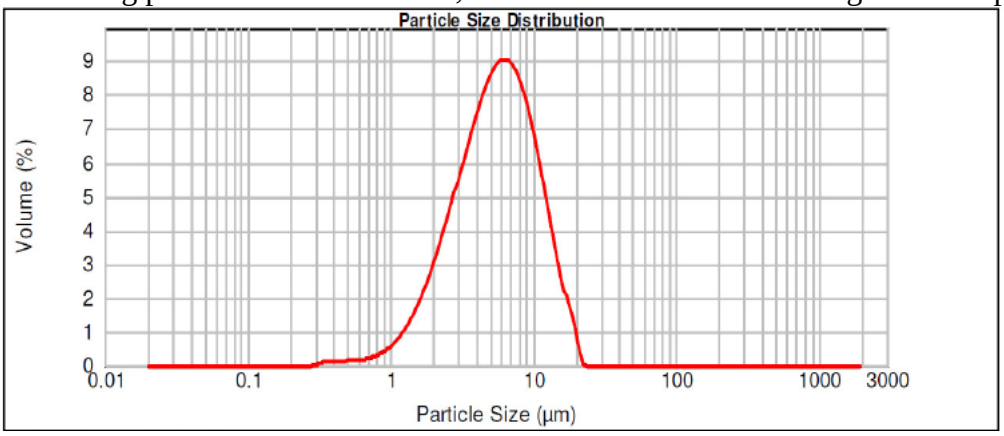

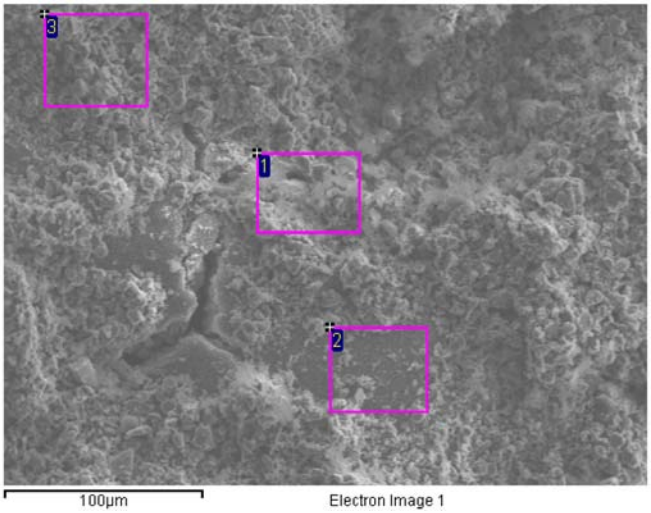

Spectrum	In stats.	O	Al	Si	P	S	Cl	K	Ti	V	Mn	W	Total
1	Yes	5.3	0.8	0.6	0.3	4.0	4.6	13.0	12.5		58.9		100.0
2	Yes	8.1		1.1		1.2		3.2	59.7	0.8	23.1	2.8	100.0
3	Yes	2.8		0.3		1.8		3.8	2.2		89.2		100.0

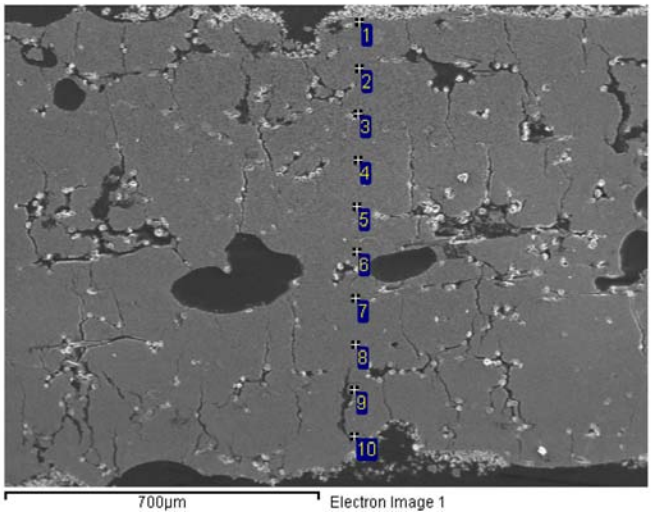

Spectrum	In stats.	O	Si	S	Cl	K	Ca	Ti	V	Mn	W	Total
1	Yes	7.09	1.52		1.01	0.70		80.44	1.11	1.62	6.51	100.00
2	Yes	9.01	1.48		0.90	0.33		80.20	1.30		6.79	100.00
3	Yes			5.11	75.71			13.46			5.73	100.00
4	Yes	9.01	1.83		0.83	0.35		79.61	1.21		7.16	100.00
5	Yes	9.54	2.49		0.87		0.76	79.17	1.10		6.08	100.00
6	Yes	8.73	1.63		0.78	0.22		80.36	1.13		7.14	100.00
7	Yes	9.62	1.50		0.97	0.16		80.22			7.55	100.00
8	Yes	8.44	1.68		0.83	0.33		79.90	1.20		7.61	100.00
9	Yes	9.43	2.07		0.59	0.44		80.87			6.60	100.00

Si coated surface and cross section images after exposure.

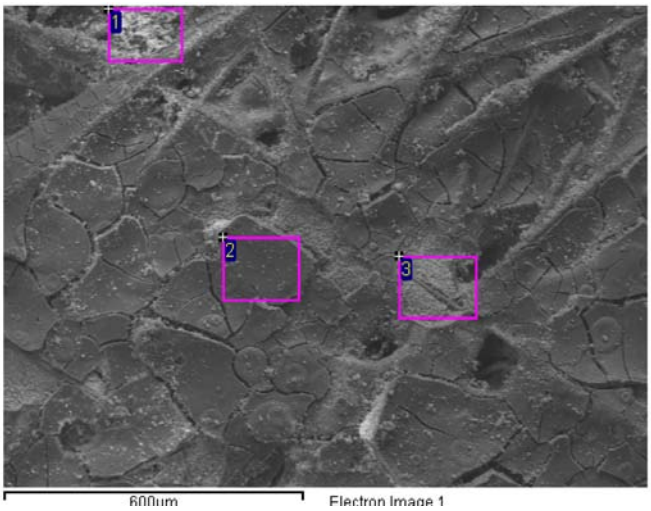

Spectrum	In stats.	O	Na	Al	Si	S	Cl	K	Ca	Ti	V	W	Total
1	Yes	9.5	0.5	0.7	10.9	2.4	30.2	34.1		8.7	0.5	2.7	100.0
2	Yes	13.8	0.5		59.0	5.4	3.9	14.2		3.1			100.0
3	Yes	13.1	0.6	1.3	9.4	2.9	3.0	8.0	2.6	53.5	1.0	4.8	100.0

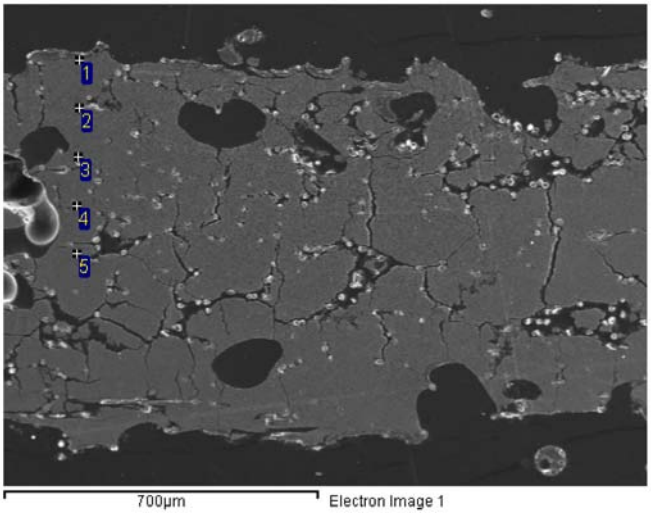

Spectrum	In stats.	O	Mg	Al	Si	Cl	K	Ca	Ti	V	W	Total
1	Yes	9.93			15.64	0.39	0.58		65.82	1.04	6.60	100.00
2	Yes	8.75	1.04	6.45	30.43	0.57	0.36	18.89	29.63		3.89	100.00
3	Yes	10.25			1.73	0.80	0.57		78.86		7.79	100.00
4	Yes	8.21			1.42	0.86	0.43		79.67	1.31	8.11	100.00
5	Yes	7.89			1.38	0.87	0.37		79.48	1.63	8.38	100.00

Appendix-Chapter 5

HBEA-25 coating particle size distribution.

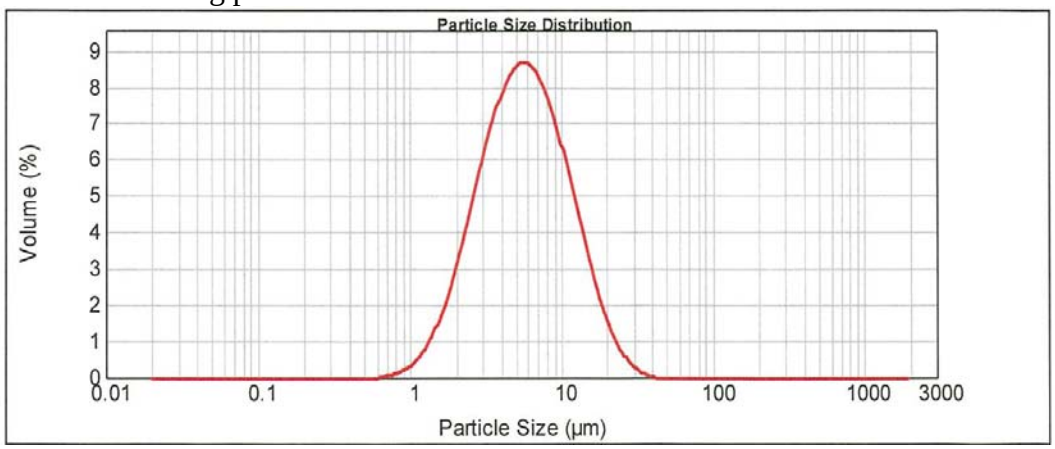

K-10 coating particle size distribution.

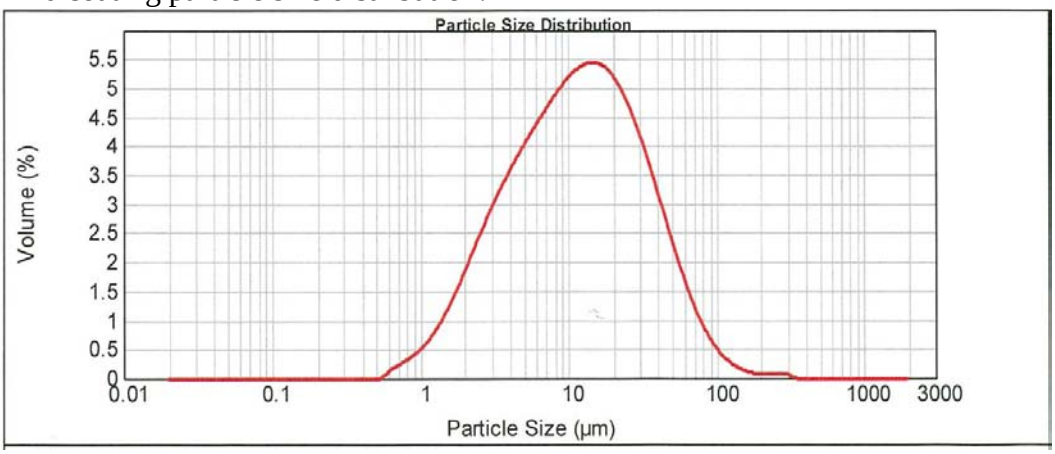

Sul-Zr coating particle size distribution.

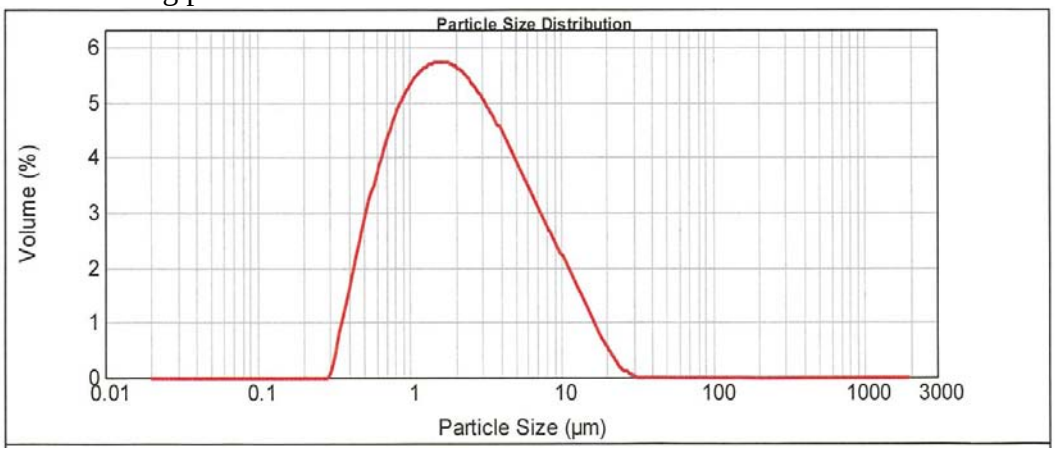

Mg-2 coated catalyst: cross section image

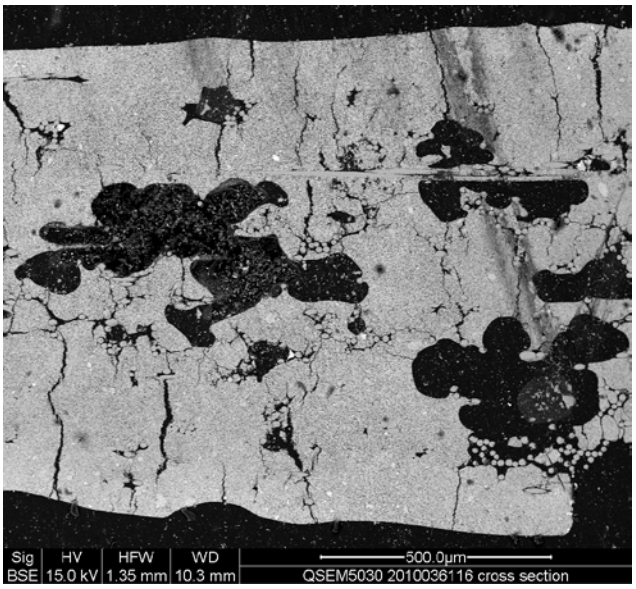

Appendix-Chapter 6

Reference catalyst: Potassium concentration profile across the cross section.

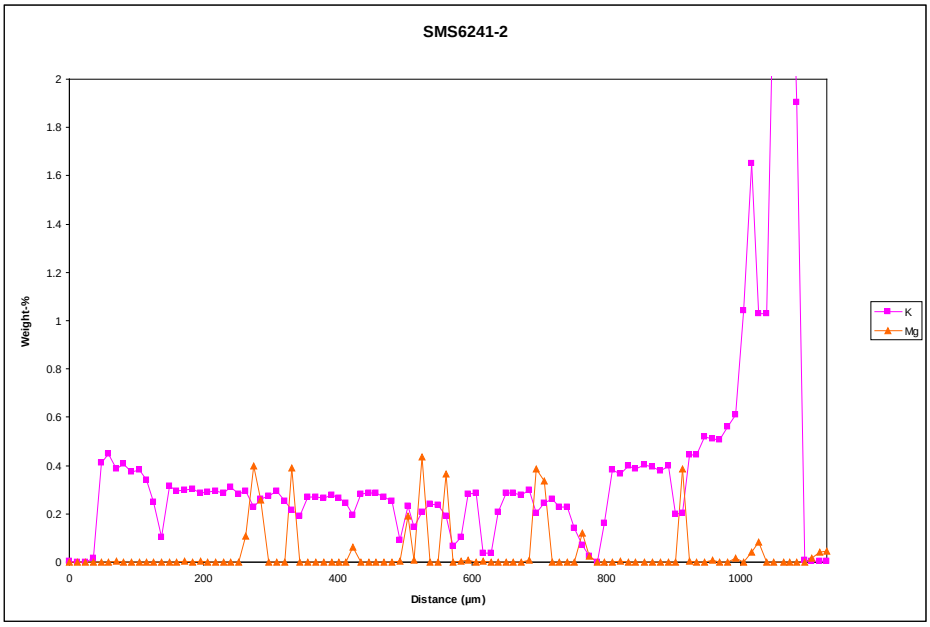

5% Mg coated catalyst: Potassium concentration profile across the cross section.

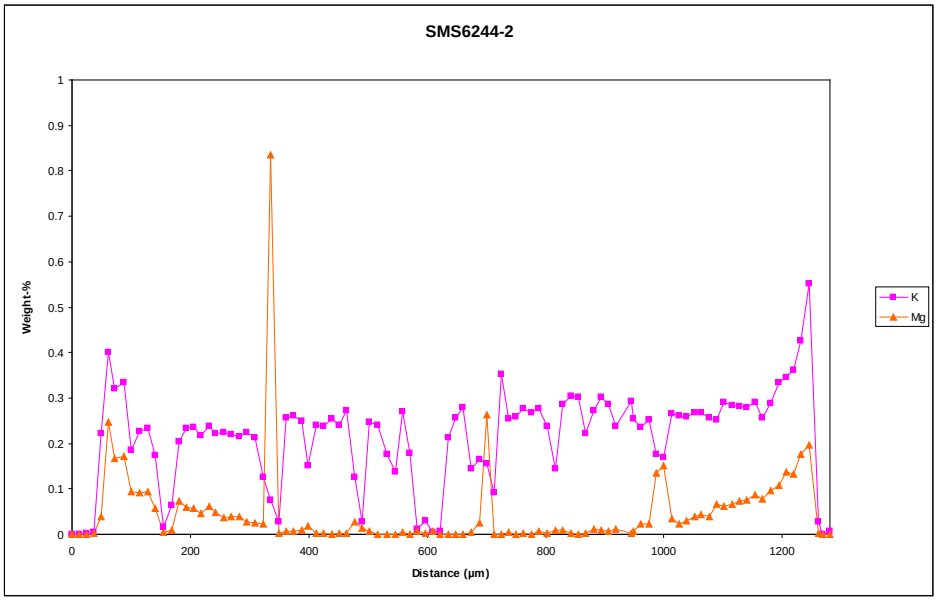

15% Mg coated catalyst: Potassium concentration profile across the cross section.

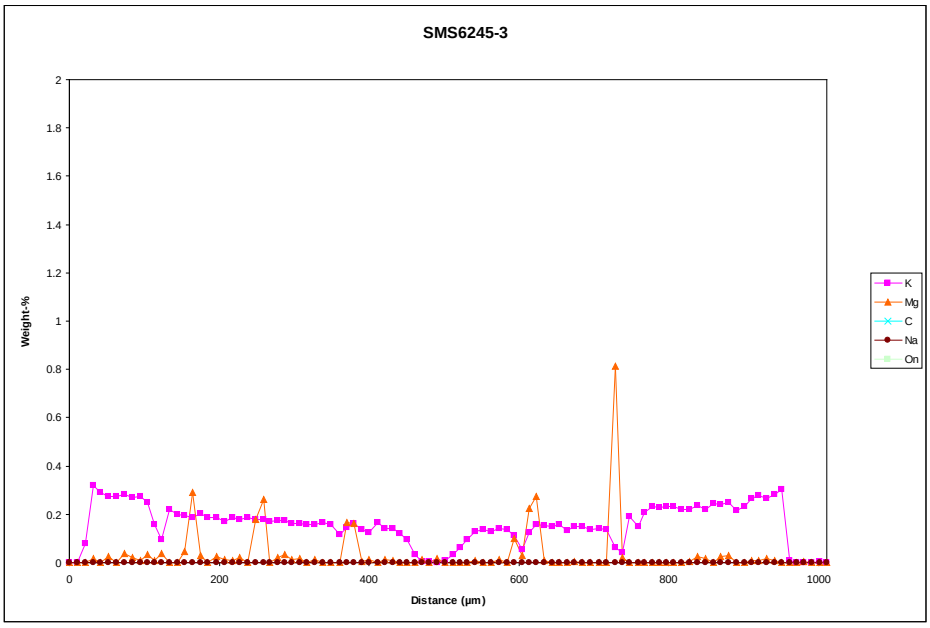

HZSM5-140 coating particle size distribution.

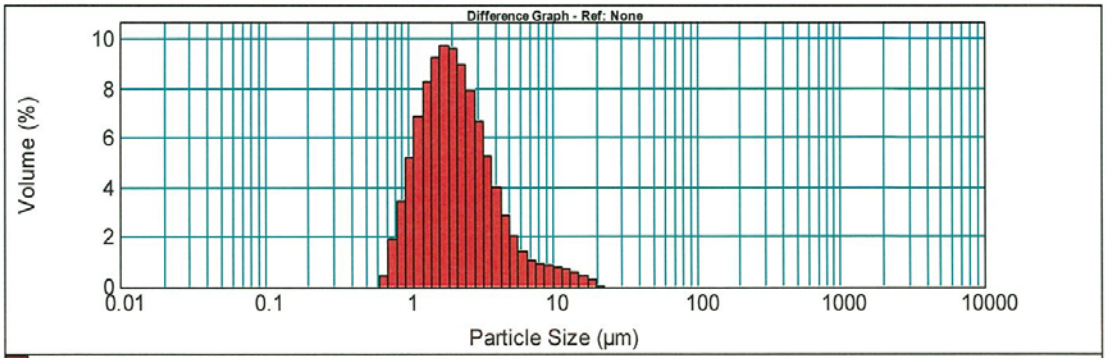

HZSM5-15 coated catalyst particle size distribution and potassium concentration profile across the cross section.

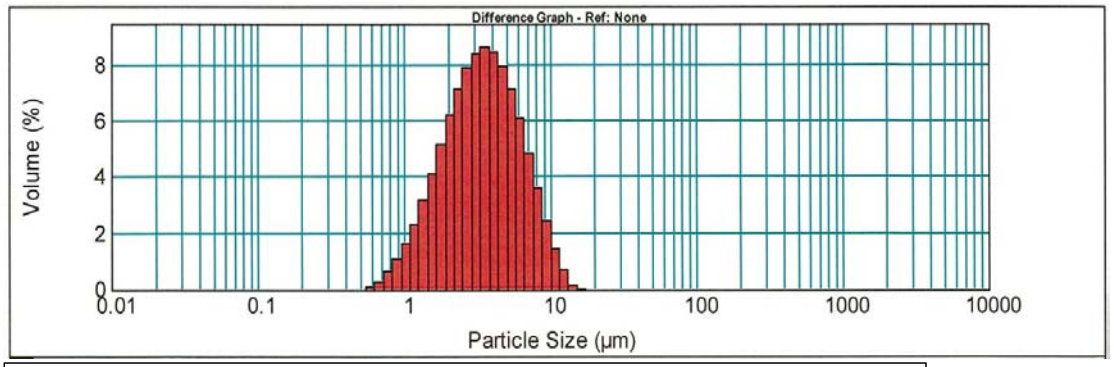

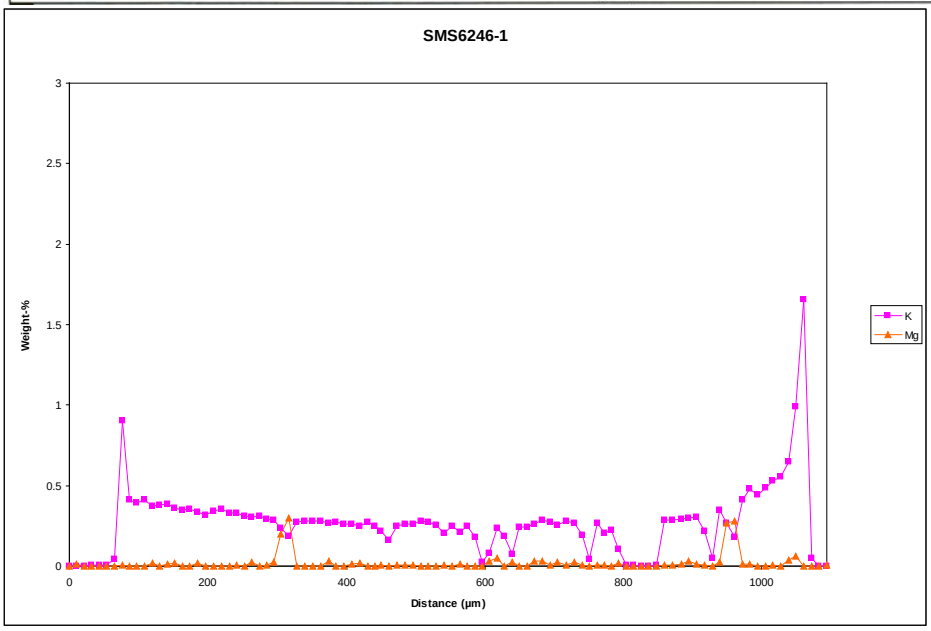

5%Mg-1%Si coated catalyst particle size distribution and potassium concentration profile across the cross section.

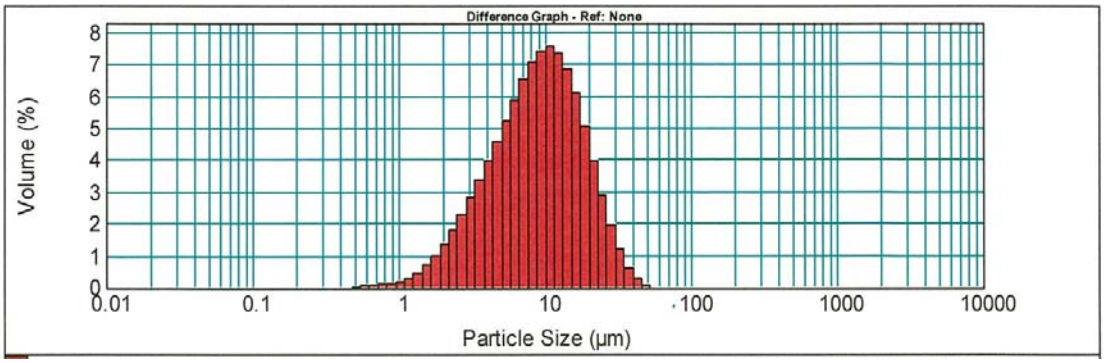

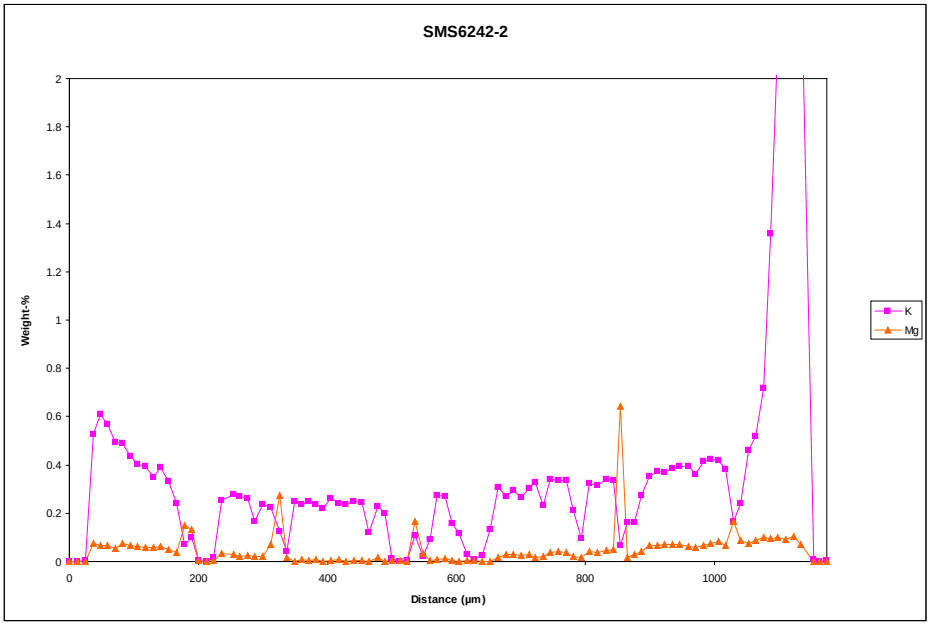

5%Mg-5%Si coated catalyst particle size distribution and potassium concentration profile across the cross section.

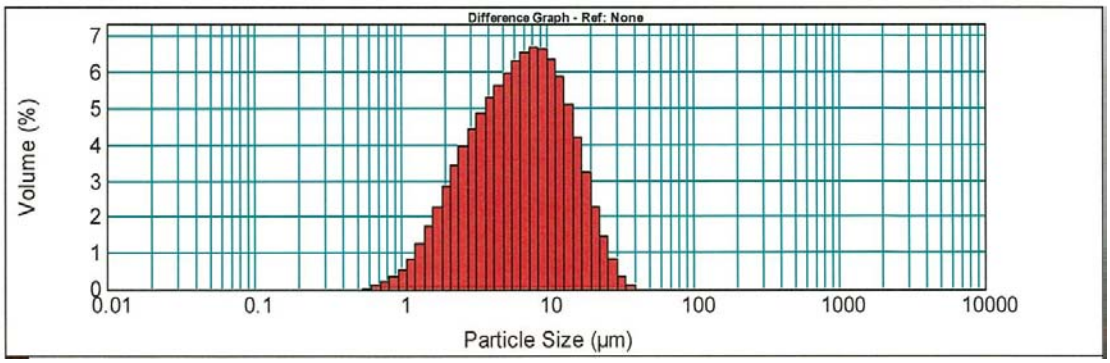

HMOR-10 coated catalyst particle size distribution and potassium concentration profile across the cross section.

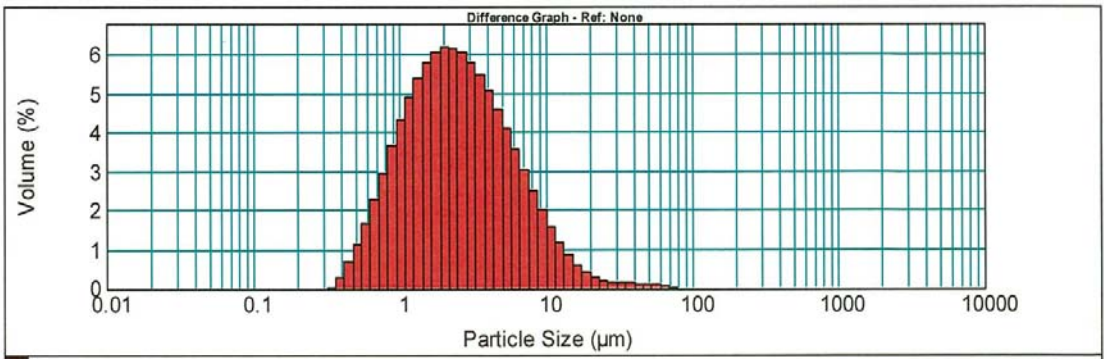

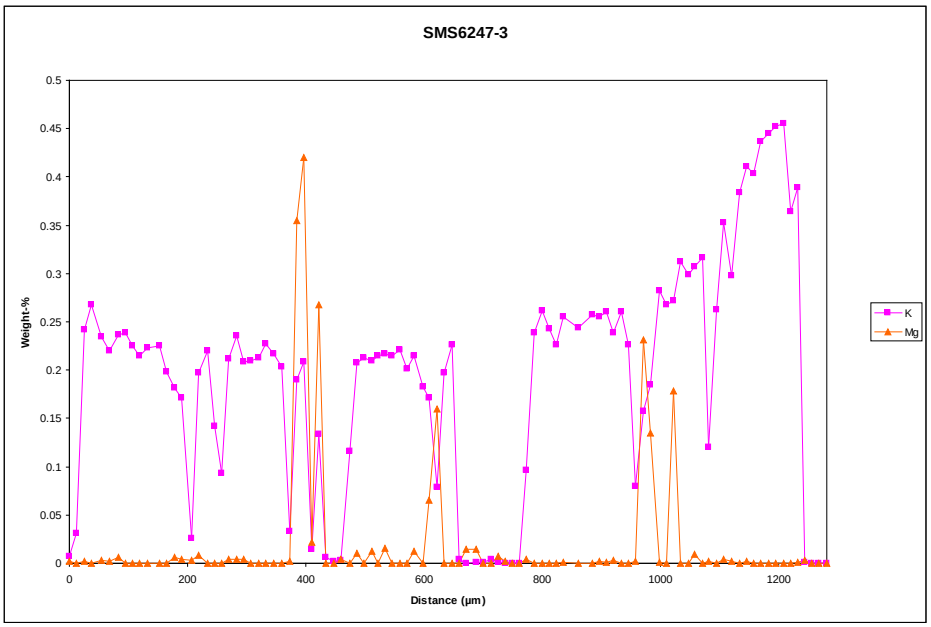

Appendix-Chapter 7

Coat 1 particle size distribution.

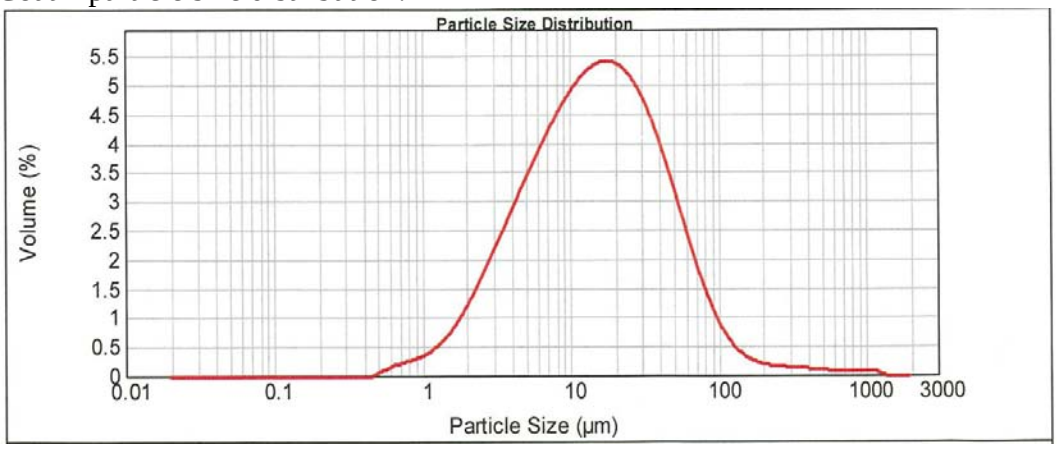

Coat 3 catalyst particle size distribution and potassium concentration profile across the cross section.

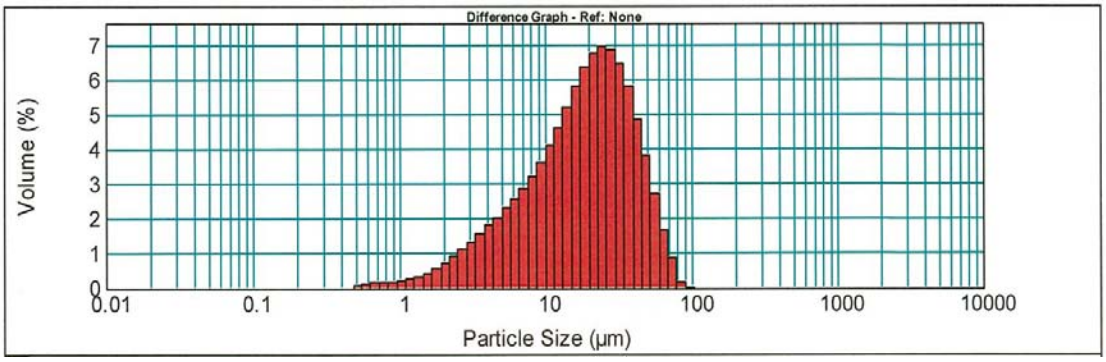

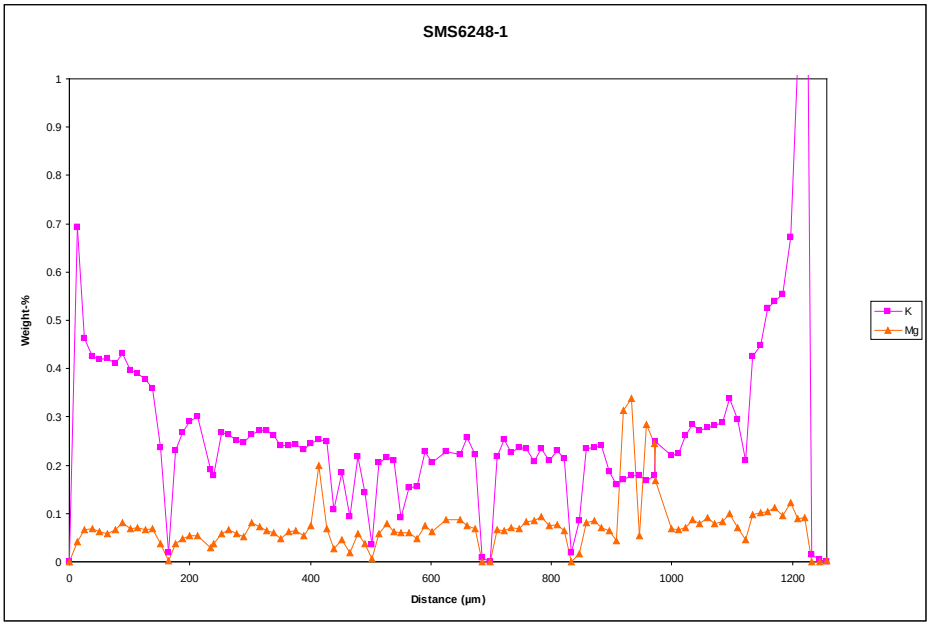

Coat 4 particle size distribution.

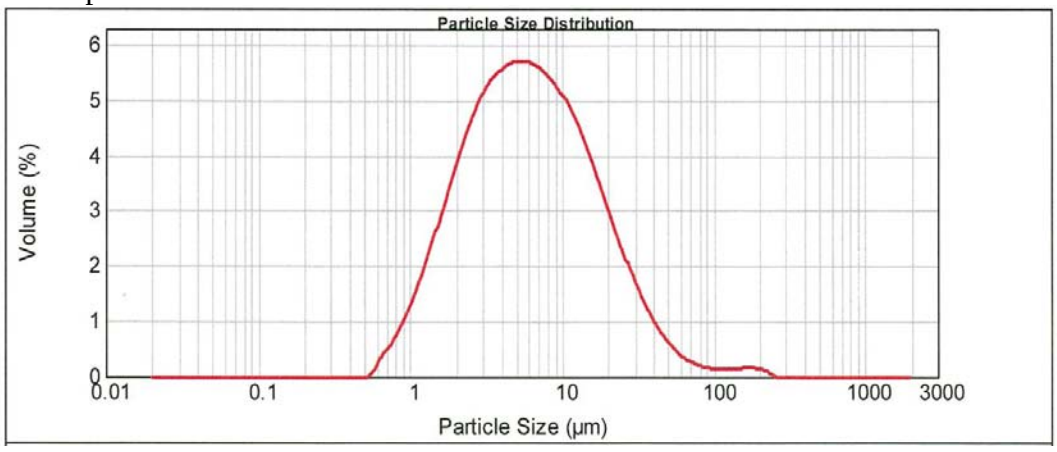

Appendix-Chapter 8

15%Mg-5%Si coating particle size distribution.

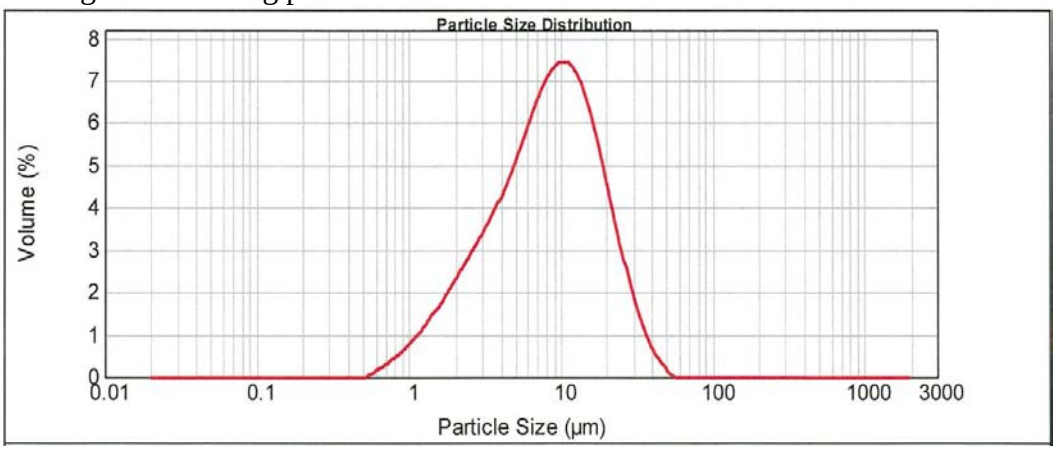

Cal-Phos coating particle size distribution.

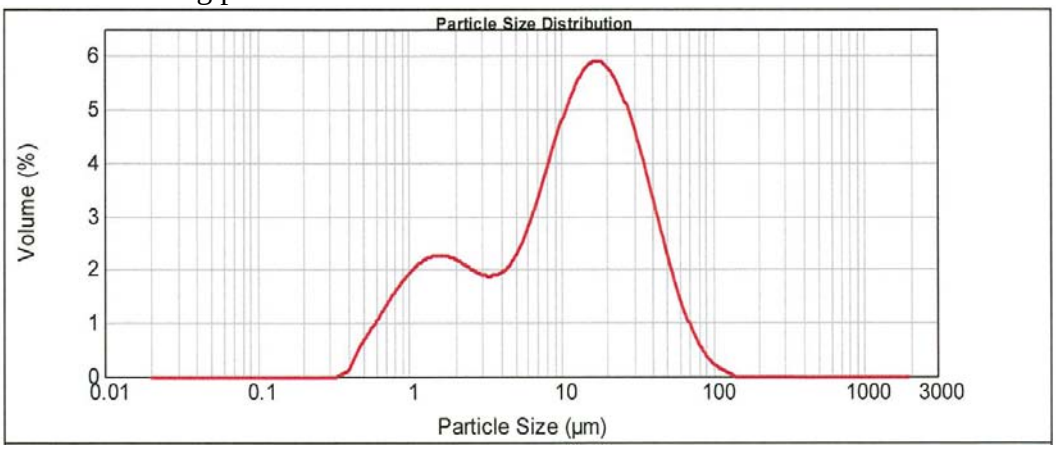

Fly ash coating particle size distribution.

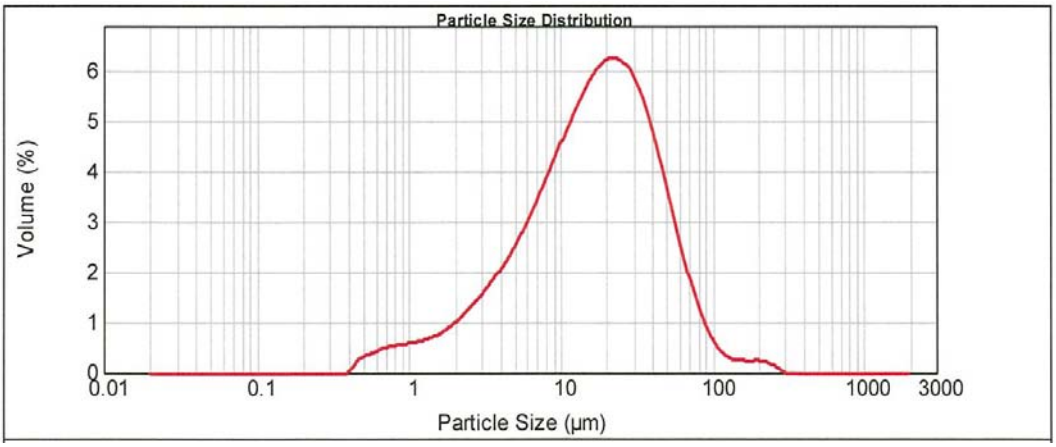

HY-60 coating particle size distribution.

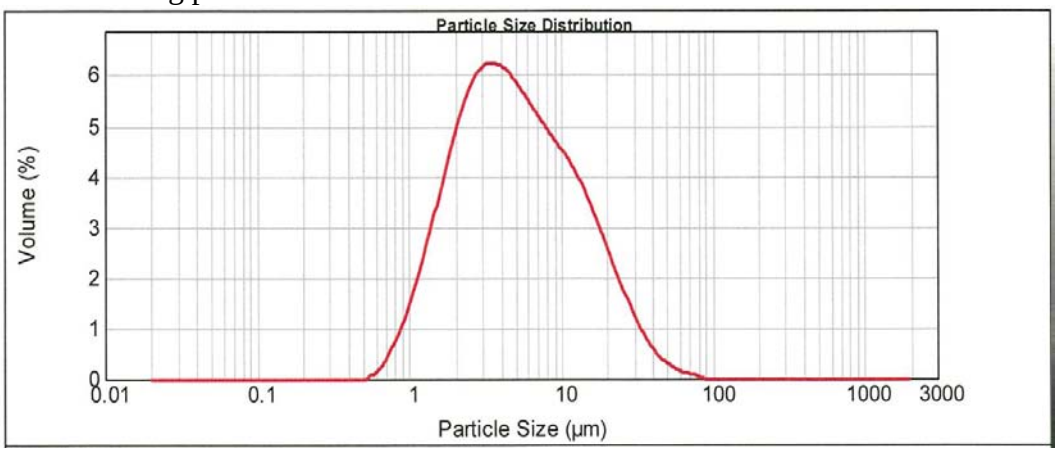

HY-12 coating particle size distribution.

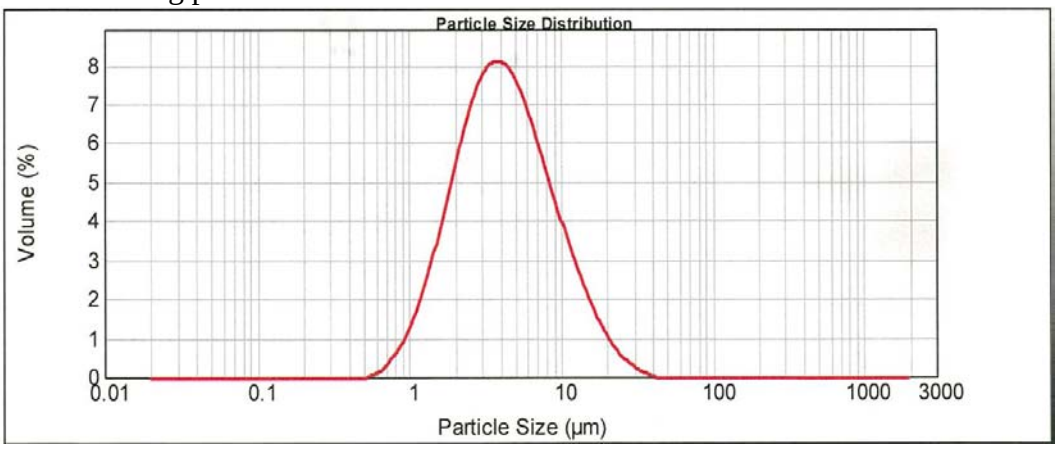

Nb coating particle size distribution.